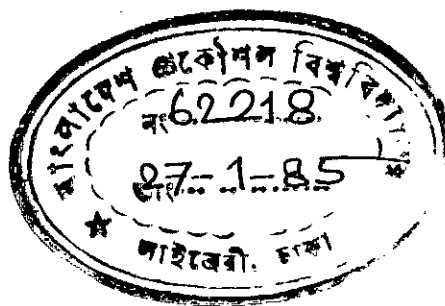


NUMERICAL COMPUTATION FOR VELOCITY AND TEMPERATURE  
WITHIN THE AXISYMMETRIC TURBULENT JETS  
IN MOVING SURROUNDINGS

by  
Md. Abdul Azim

A thesis  
submitted to the Department of Mechanical Engineering  
in partial fulfilment of the requirements  
for M.Sc.Engg. (ME) degree.



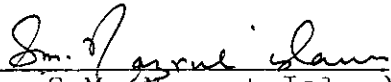
Bangladesh University of Engineering & Technology, Dhaka.

December, 1984

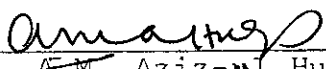


#62218#

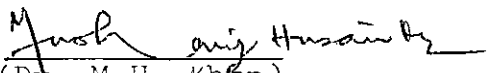
Approved as to Style and Contents by:

  
(Dr. S.M. Nazrul Islam)  
Professor  
Department of Mechanical Engineering  
BUET, Dhaka.

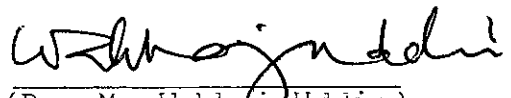
Chairman

  
(Dr. A.M. Aziz-ul Huq)  
Professor and Head  
Department of Mechanical Engineering  
BUET, Dhaka.

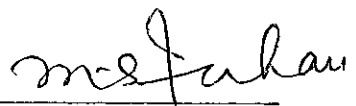
Member

  
(Dr. M.H. Khan)  
Professor  
Department of Mechanical Engineering  
BUET, Dhaka.

Member

  
(Dr. M. Wahhaj Uddin)  
Associate Professor  
Department of Mechanical Engineering  
BUET, Dhaka.

Member

  
(Dr. M. Shahjahan)  
Professor  
Dept. of Water Resources Engineering  
BUET, Dhaka.

Member

December, 1984

ABSTRACT

Theoretical investigation has been carried out for flows in the developing region of coflowing axisymmetric turbulent jets. The surrounding fluid was taken to be moving at various speeds. The equations for mass, momentum and energy conservation for turbulent flow were solved numerically by using appropriate boundary conditions. DuFort-Frankel type explicit finite difference scheme was used to obtain the finite difference form of the above equations. The calculations were performed for velocity ratios of  $\lambda = 0.0, 0.1$  and  $0.25$ . A temperature ratio of  $0.3$  was taken for each value of  $\lambda$ . The exit velocity and temperature profiles were assumed to be flat for each case. Prandtl's mixing length was expressed as a function of shear layer thickness and it was used for modelling turbulent shear stress. But this turbulent shear stress model was not applicable to the transition region. So Schetz model with intermittency was used for this region to express the turbulent shear stress.

A length scale,  $b$ , was identified to be an appropriate scale to express the mean velocity in a self-preserving plot for the initial region. But this scale was not applicable for the transition region for this purpose. Similarly a length scale,  $b_t$ , was defined to study the self-preserving nature of mean temperature both in the initial and transition

regions. But the temperature profile was not self-preserving both for the initial and transition regions.

The calculated results have been compared with the existing experimental measurements and with the results obtained by others by integral methods.

## ACKNOWLEDGEMENTS

With deep sincerity, the author expresses his profound indebtedness to Professor S.M. Nazrul Islam for his guidance, constant encouragement and invaluable suggestion in achieving every minute detail of this thesis.

The author is highly grateful to Professor M.H. Khan, Professor A.M. Azizul Huq, Dr. M. Wahhaj Uddin and Professor M. Shahjahan for their suggestions and help.

The author is also indebted to Computer Center, Bangladesh University of Engineering and Technology, for providing facilities without which this computational work would not have been possible.

Thanks are due to Mr. Abdus Salam for drafting the figures and Mr. M. Abdul Malek for typing the thesis.

## CONTENTS

	<u>Page</u>
ABSTRACT	iii
ACKNOWLEDGEMENTS	v
NOMENCLATURE	viii
LIST OF FIGURES	xi
LIST OF APPENDICES	xiii
CHAPTER I INTRODUCTION	
1.0 General	1
1.1 Axisymmetric Turbulent Jet	1
1.2 Scope of Application	4
1.3 Statement of the Problem	5
CHAPTER II LITERATURE SURVEY	
2.0 General	6
2.1 Developed Region	8
2.2 Initial and Transition Region	9
2.3 Relevant Works	17
CHAPTER III THEORY	
3.0 General	20
3.1 Governing Equations	21
3.2 Boundary Conditions	24
3.3 Solution of the Equations	24
3.3.1 DuFort-Frankel Scheme	24
3.3.2 Calculation Technique	25

	<u>Page</u>
CHAPTER IV RESULTS AND DISCUSSION	
4.0 General	26
4.1 Mean Velocity	26
4.1.1 Initial Region	26
4.1.2 Transition Region	31
4.2 Jet Geometry and Scale for Velocity	32
4.2.1 Jet Geometry	32
4.2.2 Scale	34
4.3 Mean Temperature	36
4.3.1 Initial Region	36
4.4 Jet Geometry and Scale for Temperature	38
4.4.1 Jet Geometry	38
4.4.2 Scale	39
CHAPTER V CONCLUSION	40
REFERENCES	42
FIGURES	47
APPENDICES	70

## NOMENCLATURE

$a_t$	Tollmien Constant for Similarity Variable
$b$	Length Scale for the Self-preserving Variable for Velocity
$b_t$	Length Scale for the Self-preserving Variable for Temperature
$b_1$	Width of the Shear Layer
$b_m$	Mean Width of the Shear Layer
$C_1$	Mixing Length Constant
$C_a, C_k, C_s, C_t$	Constants for Different Mean Velocity Model for the Developed Region
$C_p$	Specific Heat at Constant Pressure
$C_v$	Specific Heat at Constant Volume
$C_\mu$	Viscosity Constant
$D$	Diameter of the nozzle
$K$	Turbulent Kinetic Energy
$k$	Thermal Conductivity
$\ell$	Mixing Length
$N$	Dimensionless Total Effective Kinematic Viscosity
$N_H$	Dimensionless Total Effective Diffusivity for Heat
$p$	Mean Static Pressure
$p'$	Fluctuating Pressure
$p^o$	Instantaneous Pressure
$P_r$	Prandtl Number
$q$	Heat Flux due to Molecular and Turbulent Transport



$r_0$	Radius of Nozzle
$r_1$	Radius of Potential Core
$r_2$	Outer Radius of Jet
$r_m$	Mean Radius of Jet
$r_{\frac{1}{2}}$	Radial Distance at Half-velocity, $(u-u_e)/(u_c-u_e)=0.5$
$r_{t\frac{1}{2}}$	Radial Distance at Half-Temperature, $(t-t_e)/(t_c-t_e)=0.5$
$R$	Dimensionless Radial Distance from Jet Center Line, $ru_0/\nu$
$r, x, \theta$	An Axisymmetric Co-ordinate System
$t$	Time
$\bar{t}$	Mean Temperature
$t'$	Fluctuating Temperature
$t^0$	Instantaneous Temperature
$T$	Non-dimensional Mean Temperature, $\bar{t}/t_0$
$u^0, v^0, w^0$	Instantaneous velocities in x, r and $\theta$ -direction
$u', v', w'$	Fluctuating Velocities in x, r and $\theta$ -direction.
$u$	Axial Mean Velocity
$v$	Radial Mean Velocity
$\hat{U}$	Internal Energy
$U$	Non-dimensional Mean Axial Velocity, $u/u_0$
$\hat{V}$	Volume
$V$	Non-dimensional Mean Radial Velocity, $v/u_0$
$\vec{V}$	Velocity Vector
$x_t$	Laminar Transition Length
$X$	Dimensionless Axial Distance, $xu_0/\nu$
$\alpha$	Thermal Diffusivity

$\beta$	A Constant in the Intermittency Equation
$\gamma$	Intermittency Factor
$\delta$	Shear Layer Thickness
$\Delta$	Difference
$\nu$	Molecular Diffusivity
$\theta_0$	Momentum Thickness at the Exit
$\sigma$	Standard Deviation
$\epsilon$	Dissipation of Turbulent Energy
$\rho$	Density
$\tau$	Shear Stress
$\phi$	Viscous Dissipation
$\eta_1$	Self-preserving Variable for Velocity
$\eta_{t1}$	Self-preserving Variable for Temperature
$\eta_2$	Self-preserving Variable for Velocity
$\eta_{t2}$	Self-preserving Variable for Temperature
$\Phi$	Potential Energy
$\mu$	Viscosity
$\lambda$	Velocity Ratio, $u_e/u_0$

#### Subscripts

c	Evaluated at the Center Line of Jet
e	Evaluated at the Outer-edge of Jet
o	Value at the Exit
t	Value at the Transition or for the Temperature
T	Turbulent Flow Quantity
i, j	Grid Indices Corresponding to X, R Directions Respectively
RMS	Root Mean Square
max	Maximum Value
min	Minimum Value

## LIST OF FIGURES

<u>Figure</u>		<u>Page</u>
1.1	Jet Geometry and Nomenclature	47
3.1	Co-ordinate System and Finite-Difference Grid	48
4.1(a)	Center Line Velocity	49
4.1(b)	Center Line Temperature	50
4.2(a)	Mean Axial Velocity Distribution in the Initial Region	51
4.2(b)	Mean Axial Temperature Distribution in the initial Region	52
4.3(a)	Self-preserving Velocity Profiles against $\eta_1$ in the Initial Region	53
4.3(b)	Self-preserving Temperature Profiles against $\eta_{t1}$ in the Initial Region	54
4.4(a)	Self-preserving velocity Profiles against $\eta_2$ in the Initial Region	55
4.5	Mean Radial Velocity in the Initial Region	56
4.6(a)	Iso-velocity Lines in Initial Region	57
4.6(b)	Iso-temperature Lines in Initial Region	58
4.7(a)	Mean Axial Velocity Distribution in the Transition Region	59
4.7(b)	Mean Axial Temperature Distribution in the Transition Region	60
4.8(a)	Self-preserving Velocity Profiles against $\eta_1$ in the Transition Region	61
4.8(b)	Self-preserving Temperature Profiles against $\eta_{t1}$ in the Transition Region	62
4.9(a)	Self-preserving Velocity Profiles against $\eta_2$ in the Transition Region	63
4.9(b)	Self-preserving Temperature Profiles against $\eta_{t2}$ in the Transition Region	64

	<u>Page</u>
4.10(a) Growth of Half-Radii for Velocity	65
4.10(b) Growth of Half-Radii for Temperature	66
4.11(a) Length Scale, $b/r_0$ against $x/r_0$	67
4.11(b) Length Scale, $b_t/r_0$ against $x/r_0$	68
4.12 Calculated Values of the Ratio, $\ell/b$ against $x/r_0$	69

LIST OF APPENDICES

<u>Appendix</u>		<u>Page</u>
A	Derivation of Equations	70
B	Finite-Difference Formulation	77
C	Stability Analysis of Momentum Equation	75
D	Computer Program	89

CHAPTER I  
INTRODUCTION



1.0 General

A jet is formed when a fluid discharges through an opening or a nozzle from a container under high pressure into a region of lower pressure. The ambient fluid surrounding the jet may itself be in motion or at rest. Jets are of three kinds: 1) bounded, 2) wall, and 3) free jets. Flow of bounded jets are confined by solid boundaries. Wall jets flow over solid surfaces. Free jets flow without contacting solid surfaces. When free jets formed by discharging fluid through a circular nozzle or an orifice are known as axisymmetric jets.

1.1 Axisymmetric Turbulent Jet

The formation of a boundary layer within the nozzle and its separation at the exit is the initiation of a shear layer in the free jet flow. Turbulence originates as instabilities in laminar flow when the Reynolds number exceeds some critical value. Using flow visualization technique [48]<sup>\*</sup> it has been shown that these instabilities, due to interaction of viscous terms and non-linear inertia terms in the equation of motion, generate waves. These waves starting from the nozzle outlet grow with unstable amplitude within two to three wave lengths from the exit. The wave crest in contact with the ambient fluid folds back into the following trough. This folding engulfs the surrounding fluid and forms a ring vortex core

---

\* Number in the parenthesis indicates reference at p-42.

which rolls downstream. After one or two revolutions, the vortices interact strongly with the waves behind and break down into turbulent eddies. The interactions (like vortex pairing) of turbulent eddies cause large scale vortical motions. Small scale vortical motions also evolve through breakdown of large eddies.

A free shear layer resulting from an initially turbulent boundary layer can also roll up into an organized vortical structure from which large and small scale motions evolve. This kind of jet flow is shown in Fig. 1.1 with three distinguishable layers: 1) Shear, 2) Ambient, and 3) Potential core.

For convenient analysis, the turbulent jet flow is divided into three principal regions: 1) Initial region, 2) Transition region, and 3) Developed region. The initial region of a jet has a potential core of uniform velocity initiating from the exit. The transition region starts after the initial region. Further downstream, the developed region exists where the flow variables i.e mean velocity, turbulent intensity etc. become approximately self-preserving. The combined initial and transition region is called the developing region of the jet.

A continuous transfer of momentum and energy takes place from the jet fluid to the surrounding fluid. A difference in velocity between a jet and the region into which it is

discharged forms a high degree of instability due to intensive shearing action of the peripheral fluid of jet with the ambient fluid. The shearing action initially occurs over a small lateral region and the fluid near the axis remains unshered. For turbulent jets, the shearing phenomena steadily converts kinetic energy of oncoming mean flow into kinetic energy of turbulence and the latter decays through viscous shear. Such a conversion of energy occurs throughout the jet flow. On the other hand, the reduction of kinetic energy of the mean flow represents a decrease in the flow velocity. The elementary consideration of continuity indicates that the area of flow cross-section must increase in order to accommodate the flow as the flow velocity decreases. This phenomena flattens the velocity profile in the shear layer and reduces centerline velocity after the potential core region. Energy transfer in a turbulent flow field depends on the interaction of eddies, and correlations between various quantities of the turbulence and the mean motion. For simplicity, turbulence may be considered to consist mainly of eddies of two kinds, depending on scale: 1) large eddies; and 2) small eddies. The large eddies are energy containing eddies, and they are strained by both the mean and the turbulent stresses present in the flow field. The small eddies contain less energy and they are invariant to mean and turbulent stresses in the flow field. The small scale eddies exist in the field of large scale eddies and



dissipate turbulent energy to heat. The initial and boundary conditions play an important role and influence the flow, momentum transfer and energy transfer in the initial region. The boundary conditions are related to the shape of the nozzle and the space surrounding the shear layer. The initial conditions for steady jets are the flow properties at the exit plane of the nozzle which depend on the boundary layer thickness inside and outside the nozzle. The flow variables in the initial region are dominated by the large scale structure which can be expected to achieve independence of the initial conditions in a finite flow length and the flow become self-preserving depending on the boundary conditions.

## 1.2 Scope of Application

The informations of the mean quantities within a jet is relevant to many problems of diffusion, discharge of pumps, aircraft design, combustion in a chamber, fluid amplifiers and driers. The diffusion phenomena in free jets is associated with flows in the exhausts of rocket engines, atomized fuel injection sprays and waste disposal plumes. The results of analysis of discharge from jet is useful in designing the discharge pit of pumps. Free jets in the exhausts of rocket engines create aerodynamic noise which in many cases is objectionable and should be controlled. The aerodynamic noise is generated by Reynolds stresses associated with either subsonic or supersonic flows. So to design the exhausts of

rocket engines, a better understanding and detailed knowledge of the Reynolds stresses is necessary. The results of the present study is applicable to the incompressible flow cases and also can be applied to the compressible flow cases as a first approximation.

### 1.3 Statement of the Problems

The flow within the Axisymmetric Incompressible Turbulent Jets for initial and transition regions has been studied by developing computer simulation. Jets studied here were of three different velocity ratios,  $\lambda = 0.0, 0.1$  and  $0.25$  with a flat velocity and a flat temperature profiles in each case. The objectives of the present study are:

1. Finite-difference formulation of the equations, governing the flow, and development of computer program in order to solve those equations for mean velocity and mean temperature with given boundary conditions.
2. Comparison of the results obtained by present calculation with the existing experimental measurements.
3. Study of the behavior and applicability of a length scale  $[17]$ ,  $b$ , both for initial and transition regions.
4. Study of the self-preservation of the mean velocity and mean temperature in the developing region.

CHAPTER II  
LITERATURE SURVEY

2.0 General

The increasing availability of faster and more economical digital computers has stimulated the development of effective differential methods. These methods predict quite accurately the most important features of many turbulent flows. The success in the case of wall boundary layers is most striking. For this case a single mixing length or eddy viscosity model has led to predictions which agree well with experimental data over a wide range of conditions.

The prediction of <sup>properties in</sup> free shear flows was for a long time most commonly done by integral methods. But now the differential methods have become the center of interest with most researchers. A comparison of the Proceedings of the 1968 Stanford Conference on Computation of Turbulent Boundary Layers, the Proceedings of the 1972 Langley Working Conference on Free Turbulent Shear Flows and the Proceedings of the 1979 Imperial College Second Symposium on Turbulent Shear Flows will provide an indication of the shift in emphasis.

Turbulent flows can be expressed mathematically by the conservation of mass equation and the Navier-Stokes equations. Since the Navier-Stokes equations are non-linear, solution for each individual flow pattern has certain unique characteristics that are associated with its initial and boundary conditions. The equations have been analysed by researchers for various flow

patterns. But it is still not possible to make quantitative predictions concerning turbulent quantities without relying greatly on empirical data. The reason is that in the time-averaged turbulent equations, there are more unknown dependent variables than there are equations. In order to obtain a useful set of closed equations, it is necessary to make appropriate assumptions concerning the flow. These assumptions are based on physical concepts developed from experimental data and experience. In this way, many authors have developed empirical and semi-empirical equations to obtain a set of closed equations. Progress in this line of research, as related to axisymmetric jets, is presented in this chapter.

Flow of axisymmetric jets is free shear flow. In the far downstream of developed region of axisymmetric jets, initial conditions influence the flow pattern insignificantly. It may be thought that different natures of disturbances which are introduced by initial conditions try to achieve the characteristics of small scale flow at the initiation of developed region and in the further downstream. Much work has been done both theoretically and experimentally in this region by Wygnanski [45], Heskestad [13], Newman [30], Townsend [43], Rotta [36], Launder [24], Roshko [35] and others. On the other hand, much less work is available in initial and transition regions except lately in relation to noise by Bradshaw et al [3], Ko and Davies [19], Lau [23].

and others. In the recent years, some investigations have been done on the Large-scale Coherent Structures of free shear flows. In 1977, Chassing [7] in a detailed literature review stated that the free turbulent jet has been investigated extensively by several experimentalists and it is well known for a long time that some region of 'universal' self preserving profiles can be reached at a typical distance from the exit. This review reveals that the influence of the inlet conditions does not emerge after that typical distance. So it is not worth to investigate in that universal self-preserving region to get some numerical information regarding the influence of initial conditions.

## 2.1 Developed Region

In 1925, Prandtl [33] enunciated the concept of mixing length for free shear flow. It was used by Tollmien [42] in 1926 to calculate mean velocities in an axisymmetric jet. In this calculation he did not consider the region of the jet close to the nozzle. The investigation was based on the assumptions that: (a) the effective force was the tangential shear expressed in terms of the lateral momentum transport and mixing length, (b) the mixing length varied as the first power of the axial distance from the efflux section, (c) turbulence velocity was proportional to the mixing length and mean velocity gradient. Tollmien [42] established a series solution for mean velocity with variable,  $\eta_t = r/(a_t x)$  and the Prandtl's mixing length  $l = C_t x$  where  $a_t$  and  $C_t$  are empirical constants. The series

solution agreed fairly well with his measurements for the developed region of jets. In 1930, Schlichting [39] used Prandtl's hypothesis to express turbulent shear stress,  $\tau/\rho = C_s \delta (U_{\max} - U_{\min}) \left( \frac{\partial u}{\partial r} \right)$  where  $C_s$  is an empirical constant and  $\delta$  is the width of shear layer, and solved the same problem as Tollmien [42] did in 1926 making similar assumptions. The solution shows satisfactory agreement with measurements except in the region of low velocity near the jet boundary. The local turbulence level at the edges of jet flow are high that makes the measurements extremely difficult.

## 2.2 Initial and Transition Regions

In the initial region of a jet issuing from a nozzle, the solution given by Tollmien [42] and Schlichting [39] are not applicable. This is due to the presence of the potential core and the effects of initial conditions, although Prandtl's mixing length is approximately linear for this region.

Kuethé [21], in 1935, applied Prandtl's mixing length to the initial and transition regions and worked out an approximate method for computing the mean velocity for a round jet. He assumed Prandtl's mixing length to be proportional to the width of shear layer and expressed shear stress as:

$$\overline{u'v'} = \ell^2 \left| \frac{\partial u}{\partial r} \right| \frac{\partial u}{\partial r} \quad 2.1$$

where  $\ell = C_1 \delta$  and  $C_1$  is an empirical constant determined by experiment. The theoretical calculations

of the mean velocity for both initial and transition regions showed agreement with experimental results from pitot tube measurements.

In 1944, Squire and Trouncer [41] developed a mean velocity model for the initial and transition regions of coflowing jets with assumptions similar to those that Kuethe [21] used for jets in still air. The Reynolds shear stress was expressed by Prandtl's mixing length hypothesis given by equation 2.1. The empirical constant,  $C_1$  used to determine the mixing length was found to be different from that predicted by Kuethe [21]. As a special case, the length of the potential core was calculated to be  $x/r_0 = 7.75$  for jets in still air. This value does not agree with that of Kuethe [21].

Albertson et al [2], in 1948, measured mean axial velocities for both axisymmetric and two-dimensional jets, and their measurements of mean velocity in the initial and transition regions were found to follow the normal probability function;  $u/u_c = e^{-(r^2/2\sigma^2)}$ , where  $\sigma = C_a x$ ;  $C_a$  is an empirical constant which has two values, one for the initial region and the other for the transition region. This model of mean axial velocity showed satisfactory agreement for the two dimensional case, but somewhat in less agreement for the axisymmetric case.

Landis and Shapiro [22] in 1951 investigated Co-flowing Gas Jets experimentally and found the initial region to be

extended upto  $x/r_0 = 12$  for velocity ratio  $\lambda = 0.25$  and  $x/r_0 = 16$  for  $\lambda = 0.46$ .

In 1957, Miller and Comings [27] used Prandtl's mixing length hypothesis for a two-dimensional jet flow and developed a self-preserving empirical model for mean axial velocity in the transition region after  $x/r_0 = 10$ :  
 $u/u_c = \exp[-(\pi/\theta)(r/b_m)^2]$  where  $b_m$  was defined by  
 $b_m = \int_0^{\infty} (u/u_c) dr$ . The measured values of  $b_m$  showed a linear relationship with axial distance.

Many experimentalists, without identifying initial conditions, showed self-preservation of the mean velocity in the initial and transition regions of the turbulent jets. Some empirical equations for the initial region are:

$$\text{Abramovich [1] in 1963 : } u/u_c = (1 - \eta^{3/2})^2$$

$$\text{Simson [40] in 1964 : } u/u_c = (1 - \eta^{7/4})^2$$

where  $\eta = r/b_1$  and  $b_1$  was chosen in between  $u/u_c = 1$  and  $u/u_c = 0$ .

$$\text{Nayer et al [29] in 1969 : } u/u_c = e^{-1.415(\eta + 0.7)}$$

where  $\eta = (r - r_{1/2})/b_1$  and  $b_1$  was chosen in between  $u/u_c = 0.99$  and  $u/u_c = 0.01$ .

Nayer's definition is realistic, but this model does not apply to the initial region. Though these models are developed from similar experimental data, they do not agree with each other, probably because of different initial conditions.



In 1968, Kirshner [18] used a constant viscosity model for the transition region and solved the momentum integral equation in the same way as for laminar flow. The expression for the mean axial velocity of the turbulent jet was the same as that for the laminar jet with the molecular diffusivity replaced by constant eddy diffusivity. The constant eddy diffusivity was defined by:  $v_T = C_k b_1 u_c$ , where  $C_k$  is an empirical constant. The result of the solution agreed with the measurements of Kirshner [18] for the transition region. Though this model is simple to use, the turbulent diffusivity is not constant throughout the jet flow, specially in the intermittent regions.

Peters [32] in 1972 solved the integral form of equations using shear stress model  $C_1 K$  where  $C_1$  is constant and  $K$  is the turbulent kinetic energy. He assumed a cosine velocity profile at the inlet. In the same year Harsha [11] solved the conservation equations using the same model for transition and developed regions.

Morgenthaler and Zelazny [28] in 1972, presented a model for initial region of coflowing streams in the Langley Working Conference on Turbulent Free Shear Flows. This model, in fact, is application of transition model i.e.  $v_T \text{ core} = 0.4 v_T \text{ transition}$  and was far more successful than anticipated.

Hatta and Nozaki [12] in 1975, developed a model for mean axial velocity by an approximate solution of the axial

momentum integral equation for the initial and transition regions. Turbulent diffusivity,  $\nu_T$  was defined by  $\nu_T \propto (r_m - r_1)u_c$  where  $r_m$  is the mean radius of the jet expressed by :

$$u_o r_m^2 = u_o r_1^2 + 2 \int_{r_1}^{r_2} u r dr.$$

Neglecting the pressure gradient in the momentum equation, a model for the axial mean velocity was established:  $u/u_c = (1 - \eta)^4(1 + 4\eta)$  where  $\eta = r/b_1$ . This investigation also derived expressions for  $b_m$ ,  $b_1$  and  $r_1$  as linear functions of axial distance. Though this approximate model showed agreement with Hatta and Nozaki's [12] measurements but it is not in complete agreement with the Bradshaw et al [3], Sami et al [37] and VonFrank [44] measurements. This discrepancy likely comes from the initial conditions which were not documented by the authors.

Madni and Pletcher [26] in 1975 calculated the mean velocity of co-flowing jets by an explicit finite difference method from the differential forms of mass and momentum conservation equations derived by using boundary layer approximations. Reynolds shear stress was defined by Equation 3.8 for the initial region and by Equation 3.10 and 3.11 for the transition region. The calculation started with uniform exit velocity and showed agreement with measurements for the main portion of the shear layer. This model underpredicts the mean velocity of the outer region where velocity is low.

Davies et al [8] measured the axial mean velocity and showed self-preservation against the independent variable,  $(r-r_0)/x$  in the initial and transition regions. Measurements of Bradshaw et al [4], Von-Frank [44], Sami et al [37], Laurence [25], Lau [23], Kolpin [20] and others showed that the mean axial velocity is self-preserving when it is plotted against the variable  $(r-r_{\frac{1}{2}})/b_1$ . These measurements did not show wholly self-preservation against the variable,  $(r-r_0)/x$ . Yau et al [47] used a polynomial form as an empirical model for the axial velocity in the initial and transition regions with independent variable  $(r-r_1)/x$ , where  $r_1$  is potential core radius. This model did not show satisfactory agreement with measurements in the initial region, but it was fairly applicable to the developed region.

Recently, Bradshaw [5], Crow and Champagne [6], Yule [46] and Hussain and Zedan [15] published some experimental works for jet flow, identifying the initial conditions. Bradshaw [4] studied the effects of exit boundary layer on turbulence with boundary layer untripped or tripped by concentric rings. Experimental results have shown that the shear layer becomes fully turbulent at an approximate distance  $x_t = 7 \times 10^5 \left( \frac{v}{u_0} \right)$  from the exit for any boundary layer thickness used in the experiment.

In 1977, Yule [46] studied the jet flow for a wide range of Reynolds numbers ( $9 \times 10^3 - 10^5$ ) by using flow visualization

and hot wire techniques. He found the shear layer fully turbulent at an approximate distance  $x_t = 1.2 \times 10^5 \left( \frac{v}{u_0} \right)$  from the nozzle exit which is different from Bradshaw's [4] results. This work did not specify the exit boundary layer thickness and turbulence level. In the same year Habib & Whitelaw [10] worked on coaxial jets for both initial and transition region. They used K -  $\epsilon$  model and  $C_\mu \frac{k^2}{\epsilon} \left( \frac{\partial u}{\partial r} \right)$  as the shear stress model. The exit condition was fully developed turbulent profile and obtained numerical solutions that were in close agreement with the experimental results.

In 1978 Hussain and Zedan [15] measured mean velocity and determined the jet boundaries, varying both the laminar and turbulent boundary layer thickness, and controlling the turbulence at the nozzle exit. Experimental results showed the mean velocity to be self-preserving at a distance from the exit which varies with the initial turbulence level and the boundary layer thickness. For a turbulent boundary layer at the nozzle exit the virtual origin was found to be very close to the geometric origin at the nozzle exit. This investigation was carried out over a range of Reynolds numbers ( $6 \times 10^4 - 1.4 \times 10^5$ ) with maximum momentum thickness  $\theta_0 / r_0 = 0.011$  at the exit plane.

Large-scale coherent structure in turbulent shear flows was apparent for a long time. The current upsurge in research in this area has been triggered by the recent discovery of quasi-deterministic structures (Crow and Champagne 1971,

Brown and Roshko 1974, Winant & Browand 1974, Hussain & Zaman 1975). In 1978, Yule claimed that the axisymmetric turbulent mixing-layer structure is three-dimensional, but the outside is diffused and disorganised while the inner side of the eddies possess a reasonable degree of spatial and temporal coherence. Another motive for this study stemmed from the recent hypothesis profounded by Lau in the same year. He stated that the near field of a circular jet consists of two coaxial streets of toroidal vortex rings bifurcating at  $x/D \cong 1.5$  from a single upstream street; "the main vortex street accelerating and converging on the jet axis constitutes the potential core and the branch vortex street decelerating and diverging from the jet axis". This provocative suggestion, even though inferred from extensive data, and intended to explain the large radial variation in structure passage frequency (Kg & Davies 1971, Lau & Fisher 1975, Bruun 1977, Clark 1979), appeared to be quite unconvincing and in need of investigation.

Sufficiently close to the jet lip i.e.  $x/D \leq 1$ , the axisymmetric mixing layer characteristics should not be different from those of the plane mixing layer provided that  $\theta_0/D \leq 1$ ,  $\theta_0$  is the exit shear layer momentum thickness. Thus comparison with the plane mixing layer is strictly meaningful only for  $x/D \leq 1$ . However, in 1980, Hussain and Husain [14] compared some integral measures of axisymmetric mixing layer with

those of the plane mixing layer. They justified such a comparison giving two reasons : (i) the latter flow has been more extensively studied while available data in the axisymmetric mixing layer are extremely limited and (ii) there is an amazing similarity between the average measures of the axisymmetric layer until the end of the potential core and the plane mixing layer.

### 2.3 Relevant Works

The development of both theoretical and experimental works on free shear flows are detailed chronologically in Table 2.1.

Table 2.1 Relevant Works on Axisymmetric Turbulent Jets

	Authors	Equations	Shear Stress Model	$\lambda$	Remarks
1	Squire [41] (1944)	Integral Form a) Mass b) Momentum	$\lambda^2 \left( \frac{\partial u}{\partial r} \right)^2$ $\lambda = C_1 b_1$	0.0 0.125 0.5	Assumed a cosine velocity profile and determined jets boundary. Shear width, $b_1$ , was assumed between $u/u_c = 0.0$ and $u/u_c = 1.0$
2	Albertson et al [2] (1948)	Experimental	-	0.0	Measured mean axial velocities found to follow the distribution $u/u_c = \exp(-r^2/2\sigma^2)$ . This model showed satisfactory agreement for two dimensional case.
3	Landis & Shapiro [22] (1951)	Experimental	-	0.25 0.46	Found core length to be $x/r_0 = 8$ for $\lambda = 0.25$ and $x/r_0 = 16$ for $\lambda = 0.46$ .
4	Simson [40] (1964)	Experimental	-	0.0	In the initial region for mean axial velocity $u/u_c = (1 - \eta^{7/4})^2$
5	Nayer et al [29] (1969)	Experimental	-	0.0	In the initial region for mean axial velocity $u/u_c = \exp[-1.415(\eta + 0.7)]$ where $\eta = (r - r_{1/2})/b_1$ and $b_1$ is the shear width.
6	Harsha [11] (1972)	Diff. Form a) Mass b) Momentum c) Turbulent K.E.	$C_1 b_1$	0.0	Calculation was performed for the transition and developed region.
7	Morgenthaler & Zelazny [28] (1972)	Diff. Form a) Mass b) Momentum c) Turbulent K.E.	$C_1 b_1$		Used a core model similar to transition model as $v_{Tcore} = 0.4 v_{Ttransition}$ , more successful than anticipated.

Table 2.1 (Contd..) Relevant Works on Axisymmetric Turbulent Jets

	Authors	Equations	Shear Stress Model	$\lambda$	Remarks
8	Lauder [24] (1974,1977)	Diff. Form a) Mass b) Momentum c) Turbulent K.E. d) Dissipation	$C_{\mu} \frac{k^2}{\epsilon} \left( \frac{\partial u}{\partial r} \right)$	0.0	Used two equation model.
9	Hatta & Nozaki [12] (1975)	Diff. Form a) Mass b) Momentum c) Energy	$v_T \sim (r_m - r_1) u_c$	0.0	Obtained a polynomial form velocity profile. Linear jet boundaries were calculated. Length scale is $b_1$ .
10	Madni & Pletcher [26] (1975)	Diff. Form a) Mass b) Momentum c) Energy	$\ell^2 \left( \frac{\partial u}{\partial r} \right)^2$ $\ell = C_1 b_1$	0.0 0.25 0.5	Used different shear stress model for transition region. Flat mean velocity and flat mean temperature profile at the exit.
11	Habib & Whitelaw [10] (1977)	Diff. Form a) Mass b) Momentum c) Turbulent K.E. d) Dissipation	$C_{\mu} \frac{k^2}{\epsilon} \left( \frac{\partial u}{\partial r} \right)$	1.0 3.0	Used fully developed turbulent profile at the exit. Numerical solution was in close agreement with experimental results.
12	Hussain & Zedan [15] (1978)	Experimental	-	0.0	For turbulent boundary layer at the nozzle exit the virtual origin was found to be very close to the geometric origin at the nozzle exit.



## CHAPTER III

### THEORY

#### 3.0 General

Turbulent motion is governed by the Navier-Stokes differential equations. The mathematics of the non-linear Navier-Stokes eqns. has not been developed to a point where general solution can be obtained. In order to apply Navier-Stokes equations to practical cases, hypothesis and empirical assumptions have to be introduced for obtaining a set of closed equations with time averaged dependent variables. The early theoretical work uses Boussinesq's eddy viscosity hypothesis and Prandtl's mixing length equation as empirical quantities to calculate mean velocities. The assumptions, necessary to build the empirical relations depend on the boundary conditions of the flow field and have to be readjusted for each particular flow case.

Theoretical work on Free Shear Flows can be developed in any of the following three classes of turbulent model: 1) turbulent viscosity models in which the length scale of turbulence is found by way of algebraic formulae, 2) turbulent viscosity models in which the length scale of turbulence is found from a partial differential transport equation, and 3) models in which the shear stress itself is the dependent variable of a partial differential conservation equation.

Studies with the models of class-2 has commanded the major part of the group's attention. The models of class-3 have not yet been refined sufficiently to achieve the level of

universality of which they are believed to be capable.

Therefore, engineering calculations of turbulent flows are confined to models of class-1 and class-2 for the immediate future.

Theoretical analyses with models of class-1 and class-2 are most simply explained as attempts to close the exact Reynolds stress transport equations for  $-\rho \overline{u_i' u_j'}$ .

### 3.1 Governing Equations

Assuming steady, incompressible flow without contacting any solid surface, constant fluid properties and boundary layer approximation, the equation for mean motion are derived in Appendix-A.

The mass conservation equation is:

$$\frac{\partial(u_r)}{\partial x} + \frac{\partial(v_r)}{\partial r} = 0 \quad 3.1$$

The momentum conservation equation is:

$$u \frac{\partial u}{\partial x} + v \frac{\partial u}{\partial r} = \frac{1}{r} \frac{\partial}{\partial r} (r \tau / \rho) \quad 3.2$$

where  $\tau$  is the shear stress and  $\rho$  is the density of the fluid.

The energy equation is:

$$u \frac{\partial t}{\partial x} + v \frac{\partial t}{\partial r} = \frac{1}{\rho C_p r} \frac{\partial}{\partial r} (-r q) \quad 3.3$$

The flow configuration and co-ordinate system are shown in Fig. 3.1. The shear stress,  $\tau$  includes both viscous and turbulent contributions and it is written as:

$$\tau/\rho = \nu \frac{\partial u}{\partial r} - \overline{u'v'} \quad 3.4$$

where  $\nu$  is the molecular diffusivity. The turbulent part of shear stress is  $-\overline{u'v'}$  and it is usually expressed by Boussinesq's hypothesis:

$$-\overline{u'v'} = \rho \nu_T \frac{\partial u}{\partial r} \quad 3.5$$

where  $\nu_T$  is the turbulent diffusivity. For the initial region of turbulent jets, the diffusivity,  $\nu_T$  is expressed in terms of Prandtl's mixing length,  $l$  and mean velocity gradient,  $\frac{\partial u}{\partial r}$ .

Likewise, the heat flux,  $q$  includes both molecular and turbulent transport and is written as:

$$q = -k \frac{\partial t}{\partial r} + \rho C_p \overline{v't'} = -\rho C_p (\alpha + \alpha_T) \frac{\partial t}{\partial r} \quad 3.6$$

Turbulent diffusivities for heat and momentum are assumed to be related through:

$$\alpha_T = \frac{\nu_T}{Pr_T} \quad 3.7$$

where  $Pr_T$  is the turbulent Prandtl number which was set equal to a constant value of 0.7 for air by Madni and Pletcher [26].

$$\text{For initial region: } v_T = \lambda^2 \frac{\partial u}{\partial r} \quad ; \quad \lambda = 0.07626 \quad 3.8$$

where  $\lambda$  is Pandtl's mixing length and  $\delta$  is the width of the mixing layer. This model is not applicable to the transition region. Schetz's [38] and Madni-Pletcher's models [26] are combined for calculating mean flow properties in the transition region.

Madni-Pletcher's model is :

$$v_T = \frac{0.03}{r_0} \int_r^\infty u r \partial r \quad 3.9$$

Schetz's model is:

$$v_T = \frac{0.024\gamma}{r_0} \int_0^\infty u r \partial r \quad 3.10$$

where  $\gamma$  is an intermittency factor and the expression for  $\gamma$  is as follows:

$$\begin{aligned} \gamma &= 1.0; \quad 0 < r/r_{\frac{1}{2}} < 0.8 \\ \gamma &= (0.5)^\beta; \quad r/r_{\frac{1}{2}} > 0.8 \end{aligned} \quad 3.11$$

where  $\beta = (r/r_{\frac{1}{2}} - 0.8)^{2.5}$

A variable  $\eta_2 = (r - r_{\frac{1}{2}})/b$  is used first by Islam [17] as self preserving variable for the initial region, where the scale,

$$b = - \frac{r_0}{\left[ \frac{\partial (u/u_c)}{\partial (r/r_0)} \right]_{r=r_{\frac{1}{2}}}} \quad 3.12$$

### 3.2 Boundary Conditions

Basic differential equations 3.1, 3.2 and 3.3 governing the mean flow were solved numerically incorporating the shear stress equation 3.5. The turbulent diffusivity,  $\nu_T$  was expressed by equation 3.8, for the initial region and by a combination of equations 3.10 and 3.11, for the transition region. The appropriate boundary conditions applicable to equations 3.1, 3.2 and 3.3 are:

$$\frac{\partial u}{\partial r}(x,0) = \frac{\partial t}{\partial r}(x,0) = 0, \quad v(x,0) = 0$$

$u(x,r) = u_e(x)$  for  $r > b_2$  where  $b_2$  is the outer shear layer distance from center line.

$$t(x,r) = t_e(x), \quad \text{for } r > b_2$$

Initial distributions of  $u$  and  $t$  were flat and the turbulence level was very low.

### 3.3 Solution of the Equations

An explicit finite difference scheme of the DuFort-Frankel [9] type was used to solve the conservation equations 3.1, 3.2 and 3.3.

#### 3.3.1 DuFort-Frankel Scheme

The DuFort-Frankel Scheme is a three level formula since it requires information from the first level and the second level

to evaluate an unknown at the third level. In this scheme, truncation error is of the order  $|(\Delta x)^2 + (\Delta r)^2|$  and the central grid point  $(i, j)$  is replaced by its average at the  $(i-1)$  and  $(i+1)$  levels. The parabolic nature of the conservation equations permits the application of DuFort-Frankel scheme to solve those equation where the solution marches in the streamwise direction.

### 3.3.2 Calculation Technique

The method of approximating the derivatives and their truncation errors are given in Appendix-B. The finite difference grid used for the calculation are shown in Fig. 3.1. The computer program developed for this purpose has the capability of handling non-uniform grid spacings in both r-and x-direction. Von Neuman's method of stability analysis [34] with first order error was applied to the momentum equation. It was found that a mild stability constrain results which is given in Appendix-C. For calculating the mean flow properties from the continuity and momentum equations, non-uniform grid spacings were used in x-direction which was restricted by the stability constraint. The grid spacings in the r-direction were chosen to be uniform, dividing the discharge radius  $r_0$  into 50 equal divisions to attain convergence of the solution. The calculation with uniform grid spacings ( $\Delta x/\Delta r < 0.5$ ) in both directions also attain convergence but consumes more computer time.

At starting, first level information is obtained from initial conditions and second level information by a simple finite difference explicit scheme. This scheme requires only the previous step values. Switching of the calculations from the initial to transition region takes place when center line velocity in the initial region decreases by 0.1%.

## CHAPTER IV

RESULTS AND DISCUSSION4.0 General

Mean velocity and mean temperature distributions in the initial and transition regions of axisymmetric jets were determined by numerical simulation. The differential eqns. 3.1, 3.2 & 3.3, governing the flow were solved by using boundary conditions given in Art. 3.2. The investigation was carried out for three different velocity ratios 0.0, 0.1 and 0.25. For all three cases, the same computer program was used with different values of the parameters involved. At the exit, flat velocity and flat temperature profiles were considered.

This chapter presents discussion on the results obtained by present calculation and comparisons of this results with existing experimental measurements in the developing region of the jets.

4.1 Mean Velocity

Mixing length model of shear stress given by Equation 3.8 for initial region and Schetz model [38] with intermittency given by Equation 3.10 for transition region were applied to the equations governing the flow to express the turbulent shear stress.

4.1.1 Initial Region

In Fig. 4.1(a), the non-dimensional center line velocity,  $(u_c - u_e)/(u_0 - u_e)$ , obtained by present simulation is plotted



against  $x/r_0$  for velocity ratios 0.0, 0.1 & 0.25. The experimental results of Landis and Shapiro [22] for  $\lambda = 0.25$  and Albertson et al [2] for  $\lambda = 0.0$  are incorporated in the same figure. Experimental results of Landis and Shapiro [22] and Albertson et al [2] are in satisfactory agreement with the calculated results as shown in the Fig. 4.1(a). The figure shows constant velocity on the center line upto a certain distance from the exit plane. This distance with constant center line velocity is called the potential core of jet. It is also shown in the figure that the core length increases with the increase in  $\lambda$ . Landis and Shapiro [22] experimentally found the potential core to be  $11r_0$  for  $\lambda = 0.25$  and Albertson et al [2] found it to be  $6r_0$  for  $\lambda = 0.0$ . The values for potential core for  $\lambda = 0.0$  is  $7r_0$  and for  $\lambda = 0.25$  is  $14r_0$  obtained by the present calculation deviate from the results of Landis and Shapiro [22] and Albertson et al [2]. These deviations are likely to be due to the difference in initial conditions used in the present simulation with that prevailed in their experimental investigations.

The integral solution of Squire and Truncer [41] is also shown in Fig. 4.1(a) to show a comparison with the present results and also with existing experimental measurements. The results of integral solution do not agree with either experimental data or the present results obtained by calculation. This is due to the assumptions used in simplifying

the governing equations and the use of different model for mixing length. It is a clear indication that the integral method, which is simple in character, is not applicable to the determination of the flow characteristics within the axisymmetric turbulent jet. However, the appropriate determination of empirical velocity profile to be used for such integral solution can give satisfactory results for jets as given in ref. [17] .

The figure also shows small deviation of measurements [2,22] with calculated values at the beginning of the transition region. This may be due to the influence of the initial conditions. But the main reason of such deviation is due to the interaction of shear layer from both sides. At downstream section the calculated values and experimental values agree satisfactorily which indicates that the effects from the interaction of shear layer die down there and the flow may become self-preserving. However, the effects of velocity ratio exist all the time.

The mean axial velocity calculated by present simulation is plotted against the radial distance  $r/r_0$  in Fig. 4.2(a). The measurements of Islam [17] and Sami et al [37] are incorporated in the same figure for comparison. The figure shows that the values obtained by present calculation agree with measurements [17,37] at  $x/r_0 = 4$  and 6 but it shows deviation at  $x/r_0 = 2$ . The deviation is found to follow a particular

pattern which can be explained by the early termination of potential core in the present calculation. In addition, the experimental results at  $x/r_0 = 2$  can not be obtained with much accuracy due to the unstability of the flow close to the nozzle. This phenomena were observed by Bradshaw [4] and Islam [17]. However, except close to the nozzle, present calculation shows satisfactory agreement with measurements.

It is a common practice to plot velocity against self-preserving or similarity variable. The self-preserving independent variable was defined in many different ways by different authors to express the flow to be self-preserving. Schlichting [39], VonFrank [44] and others used,  $\eta_1 = (r - r_{1/2})/x$  as the self-preserving variable for expressing the flow to be self-preserving in the developed region. Many authors used,  $(r - r_{1/2})/\delta$ , as the self-preserving variable to explain the self-preservation character of the flow in the developed region. Islam [17] defined a variable,  $(r - r_{1/2})/b$  and used in the initial region and transition region to explain the flow to be self-preserving. The present results are plotted against both the variable,  $\eta_1 = (r - r_{1/2})/x$  and  $\eta_2 = (r - r_{1/2})/b$ , to identify the applicability of these variables in the developing region. The non-dimensional velocity,  $(u - u_e)/(u_c - u_e)$ , obtained by present calculation are plotted against  $\eta_1$  and  $\eta_2$  in Fig. 4.3(a) and Fig. 4.4(a) respectively. The figures show that the mean axial velocity has an approximate

self-preserving distribution when plotted against the variable,  $\eta_2$  but it does not show self-preservation when plotted against the variable  $\eta_1$ . Islam's [17] data for  $\lambda = 0.0$  are incorporated in Fig. 4.3(a) and Fig. 4.4(a) to study the self-preserving behavior against  $\eta_1$  and  $\eta_2$  respectively. The data in case of Fig. 4.3(a) do not show self-preservation but in case of Fig. 4.4(a) found to collapse almost on a line showing the self-preservation. This is a clear indication that scale,  $b$  is non-linear function of  $x$ .

A third order polynomial profile for mean axial velocity in the initial region, except close to the nozzle, with independent variable  $\eta_2$ , was obtained by curve fitting, based on least square method, as follows.

$$(u-u_e)/(u_c-u_e) = 0.5-0.1 \eta_2 + 0.0024 \eta_2^2 + 0.00045 \eta_2^3 \quad 4.1$$

RMS error for this profile is 0.00528.

Mean radial velocity obtained by present simulation for  $\lambda = 0.0$  is plotted against radial distance  $r/r_0$  in Fig. 4.5. Results from the measurements of Sami et al [37] and solution obtained by integral method [17] are presented in the same figure. The results obtained by present calculation are in good agreement with the experimental results [37]. But integral solution [17] has got slight deviation with both experimental data and present results. This is due to the velocity profile assumed in obtaining the integral solution.

#### 4.1.2 Transition Region

Different empirical turbulent diffusivity models were applied by many authors to express the turbulent shear stress in the governing equations for the transition region. Mixing length model is only applicable to initial region where large scale motion exists and it is associated with a major drawback which is the prediction of zero viscosity on the center line. Small scale motion together with the interaction of shear layer dominates in the transition region. Madni-Pletcher [26] model, Schetz [38] constant viscosity model and Schetz [38] model with intermittency were applied to express turbulent shear stress at different time by different authors. In the present calculation, Schetz [38] model with intermittency is used for transition region.

Trapezoidal rule is used to evaluate the integral Equation 3.10 for turbulent diffusivity,  $\nu_T$ . The switching to calculation with Schetz model from the calculation with mixing length model takes place when central line velocity in the initial region decreases by 0.1%.

The mean axial velocity,  $(u-u_e)/(u_c-u_e)$  for  $\lambda = 0.0$  obtained by present calculation is plotted against the radial distance  $r/r_0$  in Fig. 4.7(a). The experimental measurements of Islam [17] for  $\lambda=0.0$  are incorporated in the same figure for comparison. Slight deviation of measurements [17] with the calculated values is shown in the figure. This deviation can be attributed

to the early occurrence of transition region in the present calculation. Because, early occurrence of transition region makes the spread of jet higher than the measurements [17] at the same axial distance.

Mean axial velocity for transition region obtained by present calculation are plotted against the variable  $\eta_1$  and  $\eta_2$  in Fig. 4.8(a) and Fig. 4.9(a) respectively as done in case of initial region. Experimental results [17] for  $\lambda = 0.0$  are also presented in Fig. 4.9(a). From figures it is found that neither the variable,  $\eta_1$  nor the variable,  $\eta_2$  is a good self-preserving variable for the transition region. The experimental results [17] showed self-preservation in the central part of the shear layer. The deviations from self-preservation likely to come from at inner side due to interaction of shear layers from both sides of center line and at outer side due to intermittency. Fig. 4.9(a) also indicates that the band of experimental values of mean axial velocity is wider at the outer edge than that of at the inner side.

## 4.2 Jet Geometry and Scale for Velocity

### 4.2.1 Jet Geometry

In early time, Prandtl's mixing length was expressed as,  $\ell = C_t x$ , a linear function of axial distance. But it has been found through intensive investigations by different authors at different time that this mixing length model used to express

turbulent shear stress predicts flow properties within the initial region of the jet very poorly. Now it is understood that this mixing length is not a linear function of axial distance. From this understanding, study of jet geometry stemmed which is not a linear function of axial distance rather depends on structure of flow, initial conditions and boundary conditions. The growth of jet boundary and the growth of half-radii along axial distance are important jet or flow geometries. It was found by many researchers that the experimental error is highest at the jet boundary and least at the half-radii. These are due to highest intermittency at the outer edge and least intermittency at the half-radii. The jet geometry in the present investigation is shown in Fig. 4.6(a) and 4.10(a).

Iso-velocity lines with  $\lambda = 0.0$  for three different velocities,  $(u-u_e)/(u_c-u_e) = 0.01, 0.5$  and  $0.99$  are plotted in Fig. 4.6(a) in  $r/r_0$  v.s.  $x/r_0$  plane. Experimental measurements of Islam [17] for  $\lambda = 0.0$  are also presented in this figure for the same iso-velocity lines. It is found in the figure that measurements [17] along iso-velocity line,  $(u-u_e)/(u_c-u_e) = 0.99$  are higher than that of the present calculation near the termination of the core. This is an indication that core length obtained by measurements [17] is higher than that obtained in the present simulation technique. The deviation may be attributed to the use of value of constant in mixing length model. The figure also shows that iso-velocity lines are not

perfectly linear in the initial region and jet spreads at an angle of  $12^\circ$  approximately. Some authors identified the iso-velocity line  $(u-u_e)/(u_c-u_e) = 0.5$  as central region of the mixing zone. But this figure shows that the mixing zone is not symmetric about the iso-velocity line,  $(u-u_e)/(u_c-u_e) = 0.5$  at least for  $\lambda=0.0$

Growth of half radii for velocity for three different velocity ratios 0.0, 0.1 and 0.25 are presented in Fig. 4.10(a) in  $r_{1/2}/r_0$  v.s.  $x/r_0$  plane. Experimental measurements of Landis and Shapiro [22] for  $\lambda = 0.25$  and Albertson et al [2] for  $\lambda = 0.0$  are incorporated in this figure. The values obtained by present calculation for  $\lambda=0.0$  and 0.25 are found to be in slight disagreement with the corresponding values of measurements [22,2]. The figure also indicates the effects of velocity ratio on the jet geometry. The effect is that growth of half-radii for lower velocity ratio is higher than that for high velocity ratio which subsequently indicates that spreading of jet is mainly dominated by the boundary conditions imposed by velocity ratio on the flow of jet.

#### 4.2.2 Scale

Turbulent flow is characterized by the existence of several length scales, some of which play very specific roles in the description and analysis of the flow. Shear stress involved in the equations governing the flow is expressed by a length



scale. The concept of the fundamental diffusive length scale stemmed from the existence of large size eddies in the initial region. This large size eddies are as big as the width of the flow which is the relevant length scale in the analysis of the interaction of the turbulence with the mean flow. The inherent difficulty in the determination of the width of the flow propelled the investigators in seeking new length scale.

In Fig. 4.11(a) a new diffusive length scale [17]  $b$  for initial region for three different velocity ratios 0.0, 0.1 and 0.25 are plotted in  $b/r_0$  v.s.  $x/r_0$  plane. The length scale  $b$  is defined by Equation 3.12. The backward difference formula has been used to determine the mean axial velocity gradient at the half-width. Experimental measurements of Islam [17] for  $\lambda = 0.0$  are presented in the same figure. The slight disagreement of the values calculated by present simulation with the measurements [17] is due to the early occurrence of transition region in the present calculation. The figure indicates that slope of the scale  $b$  against axial distance decreases with increased velocity ratio.

In order to find out the relation between the new length scale,  $b$  and the diffusive length scale given by Equation 3.8; the ratio of  $\ell/b$  is plotted in Fig. 4.12 against  $x/r_0$ . It is worth mentioning that in the present calculation both the scales  $\ell$  and  $b$  are considered as function of axial distance only. The figure shows that the ratio  $\ell/b$  is a

function of  $\lambda$  and is constant along axial distance in the initial region for a particular value of  $\lambda$ . The constant values of the ratio,  $\ell/b$  are 0.957 for  $\lambda = 0.0$ , 0.907 for  $\lambda = 0.1$  and 0.703 for  $\lambda = 0.25$ . This is a clear indication from the figure that the scale,  $bs$  is quite applicable to the initial region of axisymmetric jet flow. So the difficulty in determining the width of the flow may be overcome by using length scale,  $b$ .

#### 4.3 Mean Temperature

Thermal energy equation 3.3 comes into play, in addition to the equations 3.1 and 3.2, governing the flow of non-isothermal axisymmetric jet. The relation given by Equation 3.7 is applied to the thermal energy equation to express the turbulent thermal diffusivity.

##### 4.3.1 Initial Region

In Fig. 4.1(b), the non-dimensional center line temperature,  $(t_c - t_e)/(t_0 - t_e)$ , obtained by present calculation is shown against  $x/r_0$  for velocity ratios 0.0, 0.1 and 0.25 with a temperature ratio of 0.3 for each case. The experimental results of Landis and Shapiro [22] for  $\lambda = 0.25$  are incorporated in the same figure. Close agreement is found at the downstream section. The disagreement of the calculated values with measurements [22] in the transition region is due to the

sever interaction of two thermal shear layer, converging on the center line from two sides.

The figure shows that center line temperature remains constant upto a certain distance axially which increases with the increase of velocity ratio. This distance obtained by present calculation is  $7r_0$  and that obtained in measurements [22] is  $8r_0$ . The deviation is due value of the constant used in mixing length model.

The mean axial temperature calculated by present simulation is plotted against the radial distance  $r/r_0$  in the Fig. 4.2(b).

Self-preservation of mean axial temperature are shown in Fig. 4.3(b) and Fig. 4.4(b) for  $\lambda = 0.0$  plotted against  $\eta_{t1} = (r-r_{t\frac{1}{2}})/x$  and  $\eta_{t2} = (r-r_{t\frac{1}{2}})/b_t$  respectively. Fig. 4.3(b) shows that mean axial temperature is self-preserving only in the central region of the mixing layer. The picture of self-preservation is different in Fig. 4.4(b). The non-self-preservation in the inner part shown in the figure is due to the presence of thermal mixing layer within the velocity potential core and in the outer part is due to the intermittency.

### 4.3.2 Transition Region

Schetz [38] model with intermittency for turbulent momentum diffusivity is used for turbulent thermal diffusivity with a modification. This modification is obtained by using Equation 3.7.

The mean axial temperature,  $(t-t_e)/(t_c-t_e)$ , for  $\lambda = 0.0$  obtained by present finite difference method is plotted against the radial distance  $r/r_0$  in Fig. 4.7(b).

Mean axial temperature for  $\lambda = 0.0$  are plotted in Fig. 4.8(b) and Fig. 4.9(b) against self-preserving variable  $\eta_{t1}$  and  $\eta_{t2}$  respectively. In both of the figures self-preservation was found only in the central region of mixing layer. Prolonged effects of interaction of thermal shear layer from two sides make the mean axial temperature non-self-preserving against  $\eta_{t1}$  in Fig. 4.8(b). It is a clear indication from Fig. 4.9(b) that the scale  $b_t$  is not applicable in the transition region for temperature to be self-preserving against  $\eta_{t2}$ .

## 4.4 Jet Geometry and Scale for Temperature

### 4.4.1 Jet Geometry

Important jet geometries, the growth of thermal boundary and the growth of half-radii for temperature are shown in

Fig. 4.6(b) and Fig. 4.10(b) respectively. Iso-temperature lines with  $\lambda=0.0$  for three different temperatures,  $(t-t_e)/(t_c-t_e) = 0.01, 0.5$  and  $0.99$  are plotted in Fig. 4.6(b) in  $r/r_0$  v.s.  $x/r_0$  plane. The iso-temperature line,  $(t-t_e)/(t_c-t_e) = 0.99$  indicates that length of thermal potential core is less than that of velocity potential core for same value of  $\lambda$ . In fact, this is a consequence of higher value of turbulent thermal diffusivity than turbulent momentum diffusivity.

Growth of half-radii for temperature obtained by present calculation for three different velocity-ratio  $0.0, 0.1$  and  $0.25$  are presented in Fig. 4.10(b) in  $r_{t_{1/2}}/r_0$  v.s.  $x/r_0$  plane. Experimental measurements of Landis and Shapiro [22] for  $\lambda = 0.25$  are incorporated in this figure. Slight disagreement of the present calculated values with the measurements [22] may be due to the late termination of the thermal core in the present calculation or due to the interaction of thermal shear layer from two sides.

#### 4.4.2 Scale

A scale,  $b_t$  for temperature analogous to the scale for velocity is plotted in Fig. 4.11(b) in  $b_t/r_0$  v.s.  $x/r_0$  plane for  $\lambda=0.0, 0.1$  and  $0.25$ . The behavior of the scale,  $b_t$  is similar to the scale,  $b$  for velocity plotted against  $x/r_0$  for each case. Yet mean temperature is not found to be self-preserving against the variable  $\eta_2$ .

CHAPTER V

CONCLUSION

A fast and effective computer program has been developed to solve the finite-difference equations of conservation. The same computer program was used for solution of conservation equations for axisymmetric turbulent jets both in moving and in rest surrounding.

Numerical calculations were performed for mean velocity and mean temperature in the developing region of jets for three different velocity ratios 0.0, 0.1 and 0.25 with a constant temperature ratio 0.3 for each case.

The results obtained by present calculation were compared with existing experimental measurements. The agreement in the comparison indicates that Prandtl's mixing length,  $\ell$ , expresses the turbulent shear stress approximately in the initial region. This mixing length,  $\ell$ , is a simple algebraic equation where shear layer thickness appears as a variable. The thickness of the shear layer is obtained by defining outer boundary at  $(u-u_e)/(u_c-u_e)=0.01$  and inner boundary at  $(u-u_e)/(u_c-u_e) = 0.999$ .

A self-preserving model with shear layer thickness as a length scale is not suitable because the highest experimental uncertainty occurs near the outer boundary where the mean velocity is low. In developing self-preserving model, it is

found most suitable to define length scale on the basis of measurements along half-radius where experimental uncertainty is the lowest. Islam [17] defined a length scale,  $b$  which is inversely proportional to mean velocity gradient at half-radius.

The dependency of length scale,  $\lambda$  on radial distance were considered negligible in the present calculation. The length scale,  $b$  is found to be non-linear in axial distance. A constant value of the ratio,  $\lambda/b$  in the initial region for a particular value of  $\lambda$  indicates the non-linearity of scale,  $\lambda$  and the applicability of scale,  $b$  in that region.

In the initial region, mean velocity is found to be self-preserving against the variable,  $\eta_2$  but mean temperature does not show self-preservation against the variable,  $\eta_{t2}$ . The non-self-preservation of mean temperature at the inner side of mixing layer may be due to the intervening layer between the velocity potential core and the thermal potential core which is in need of intensive experimental investigation.

The polynomial form of mean velocity profile developed for the initial region in the present calculation and given by Equation 4.1 may be applied to integral method of solution.

REFERENCES

1. Abramovich, G.N., "Theory of Turbulent Jets", Translation by Scripts Technica, MIT Press, 1963.
2. Albertson, M.L., Dai, Y.B., Jensen, R.A. and Rouse, H., "Diffusion of Submerged Jets", Proc. Am. Soc. Civil Engrs., Vol. 74, 1948. p. 1751.
3. Bradshaw, P., Ferriss, D.H. and Johnson, R.F., "Turbulence in the Noise-Producing Region of a Circular Jet", Journal of Fluid Mechanics, Vol. 19, 1964, pp. 591-624.
4. Bradshaw, P., "The Effect of Initial Conditions on the Development of a Free Shear Layer", Journal of Fluid Mechanics, Vol. 26, Part 2, 1966, pp. 225-236.
5. Bradshaw, P., "The Understanding and Prediction of Turbulent Flow", Aeronautical Journal, Vol. 76, July 1972, pp. 403-418.
6. Champagne, F.H. and Crow, S.C., "Orderly Structure of Jet Turbulence", Journal of Fluid Mechanics, Vol. 48, Part 3, 1971, pp. 547-591.
7. Chassing, P. and Minh H. Ha, "Some Numerical Predictions of Incompressible Turbulent Flows", Institute de Mecanique des Fluides, L.A. an C.N.R.S., Numerical Methods in Laminar and Turbulent Flow, A Halsted Press Book.
8. Davies, P.O.A.L., Ko, N.W.M and Bose, B., "The Local Pressure Field of Turbulent Jets", Aero Research Conc., London, Current Paper, No. 989, 1968.
9. DuFort, E.C. and Frankel, S.P., "Stability Conditions in the Numerical Treatment of Parabolic Differential Equations", Mathematical Tables Aids Computation, Vol. 7, 1953, pp. 135-152.



10. Habib and Whitelaw, "Velocity Characteristics of Confined Co-axial Jet", ASME Transaction, Vol. 101, Dec.1979.
11. Harsha, P. and Lee, S.C., "Correlation Between Turbulent Stress and Turbulent Energy", AIAA Journal, Vol. 8, No. 8, 1970, pp. 1508-1510.
12. Hatta, K. and Nozaki, T., "Two-dimensional and Axisymmetric Jet Flows With Finite Initial Cross-Sections", Bull. of the J.S.M.E., Vol. 18, No.118, 1975, pp. 349-357.
13. Heskestad, G., "Hot-wire Measurements in a Radial Turbulent Jet, ASME Journal of International Flow, G. Sovran, ed., Elsevier, 1967, pp. 170-201.
14. Hussain, A.K.M.F and Husain Z.D., AIAA Journal Vol.18, p. 1462, 1980.
15. Hussain, A.K.M.F and Zedan, M.F., "Effects of the Initial Condition on the Axisymmetric Free Shear Layer: Effects of the Initial Momentum Thickness", Physics of Fluids, Vol.21, No.7, July 1978, pp. 1100-1112.
16. Hussain, A.K.M.F and Zedan, M.F., "Effects of Initial Condition on the Axisymmetric Free Shear Layer: Effect of the Initial Fluctuation Level", Physics of Fluids, Vol. 21, No.9, Sept. 1978, pp. 1475-1481.
17. Islam, S.M.N., "Prediction and Measurement of Turbulence in the Developing Region of Axisymmetric Isothermal Free Jets", Ph.D. Dissertation, Dept. of Mech. Engg. Univ. of Windsor, Ontario, Canada, 1979.
18. Kirshner, J.M., "Jet Flows", Fluidics Quarterly, Vol.1, No. 3, April 1968, pp. 33-46.
19. Ko, N.W.M. and Davies, P.O.A.L., "The Near Field Within the Potential Core of Subsonic Cold Jets", Journal of Fluid Mechanics, Vol. 50, 1971, pp. 49-78.

20. Kolpin, M.A., "The Flow in the Mixing Region of a Jet",  
Journal of Fluid Mechanics, Vol. 18, 1964, pp.529-548.
21. Kuethe, A., "Investigation of the Turbulent Mixing  
Regions Formed by Jets", Journal of Applied Mechanics,  
Vol. 3, Series A, 1935, p. 87.
22. Landis, F. and Shapiro, A.H., "Momentum and Mass Transfer  
in Co-axial Gas Jets", Heat Transfer and Fluid Mechanics  
Institute, 1951.
23. Lau, J.C. and Fisher, M.H., "The Vortex-Street Structure  
of Turbulent Jets", Part 1, Journal of Fluid Mechanics,  
Vol. 67, Part 2, 1975, pp. 299-337.
24. Launder, B.E., Reece, G.J. and Rodi, W., "Progress in the  
Development of a Reynolds Stress Turbulence Closure",  
Journal of Fluid Mechanics, Vol. 68, Part 2, 1975,  
p. 537.
25. Laurence, J.C., "Intensity, Scale and Spectra of Turbulence  
in the Mixing Region of Free Subsonic Jet", NACA,  
Rep. No. 1292, April 1956.
26. Madni, I. and Pletcher, R.H., "Prediction of Turbulent  
Jets in Coflowing and Quiescent Ambients", ASME Journal  
of Fluid Engineering, Vol. 97, Dec. 1975, pp.558-567.
27. Miller, D.E. and Comings, E.W., "Static Pressure Distri-  
bution in the Free Turbulent Jet", Journal of Fluid  
Mechanics, Vol.3, Part 1, Oct. 1957, pp. 1-15.
28. Morgenthaler, J.H. and Zelazny, S.W., "Predictions of  
Axisymmetric Free Turbulent Shear Flows Using a  
Generalized Eddy-Viscosity Approach", Proceedings of  
Langley Working Conference on Free Turbulent Shear Flows,  
p. 287, 1972.

29. Nayer, B.M., Siddon, T.E. and Chu, W.T., "Properties of the Turbulence in the Transition Region of a Round Jet", Technical Note No. 131, IAS, Univ. of Toronto, Jan. 1969.
30. Newman, B.G., "The Prediction of Turbulent Jets and Wall Jets", Canadian Aeronautics and Space Journal, Vol.15, No. 8, October, pp. 287-305.
31. O' Brien, G.G. Hyman, M.A. and Kaplan, S., "A Study of the Numerical Solution of Partial Differential Equations", Journal of Mathematical Physics, Vol.29, 1951, p. 223.
32. Peters, C.E. and Phares, W.J., "An Integral Turbulent Kinetic Energy Analysis of Free Shear Flows", Proceedings of Langley Shear Flows Conference, NASA SP. 321, Vol.1, July 1972, p. 523.
33. Prandtl, L., "Bericht über Untersuchungen zur ausgebildeten Turbulenz", ZAMM, Vol.5, 1925, p.136.
34. Roache, P.J., "Computational Fluid Dynamics", Hermosa Publishers, 1976.
35. Roshko, A., "Structure of Turbulent Shear Flows: A New Look", AIAA Journal, Vol. 14, No.10, October 1976, pp. 1349-1357.
36. Rotta, J.C., "Turbulent Shear Layer Prediction on the Basis of the Transport Equations for the Reynolds Stresses", Proceedings 13th Congr. Theory Appl. Mech., Moscow, 1972, pp. 295-308.
37. Sami, S., Carmady, T. and Rouse, H., "Jet Diffusion in the Region of Flow Establishment", Journal of Fluid Mech., Vol. 27, Part 2, 1967, pp. 231-252.

38. Schetz, J.A., "Turbulent Mixing of a Jet in a Coflowing Stream", AIAA Journal, Vol. 6, 1968, pp. 2008-2010.
39. Schlichting, H., "Boundary Layer Theory", 6th Ed., McGraw-Hill, New York, N.Y., 1968.
40. Simon, A.K., "Measurement of Velocity in the Establishment Region of a Two-dimensional Jet", ASME Paper, No. 64-WA/Aut-2, 1964.
41. Squire, H.B. and Trouncer, J., "Round Jets in a General Stream", ARC Report No. 1974, Jan. 1944.
42. Tollmien, W., "Berechnung Turbulenter Ausbreitungsvorgänge", ZAMM, Vol.6, Part 6, 1926, p. 468.
43. Townsend, A.A., "The Structure of Turbulent Shear Flow", Cambridge Univ. Press, 1956.
44. Von Frank, E., "Turbulence Characteristics in the Mixing Region of a Perturbed and Unperturbed Round Free Jet", M.S. Thesis, Dept. of Aero. Engg., Penn. State Univ., 1970.
45. Wygnanski, I. and Fiedler, H., "Some Measurements in the Self-preserving Jets", Journal of Fluid Mechanics, Vol. 38, Series E, June 1966, pp. 417-424.
46. Yule, A.J., "Observations of Late Transitional and Turbulent Flow in Round Jets", Proceedings of Symposium on Turbulent Shear Flows, Univ. Park, Penn., April 1977.
47. Yüu, S., Yasukouchi, N., Hiyosawa, Y. and Jotaki, T., "Particle Turbulent Diffusion in a Dust Laden Round Jet", AIChE Journal, Vol. 24, No.3, May 1978, pp.509-519.
48. Beavers, G.S. and Wilson, T.A., "Vortex Growth in Jets", Journal of Fluid Mechanics, Vol. 44, Part 1, April 1970, pp. 97-112.

FIGURES

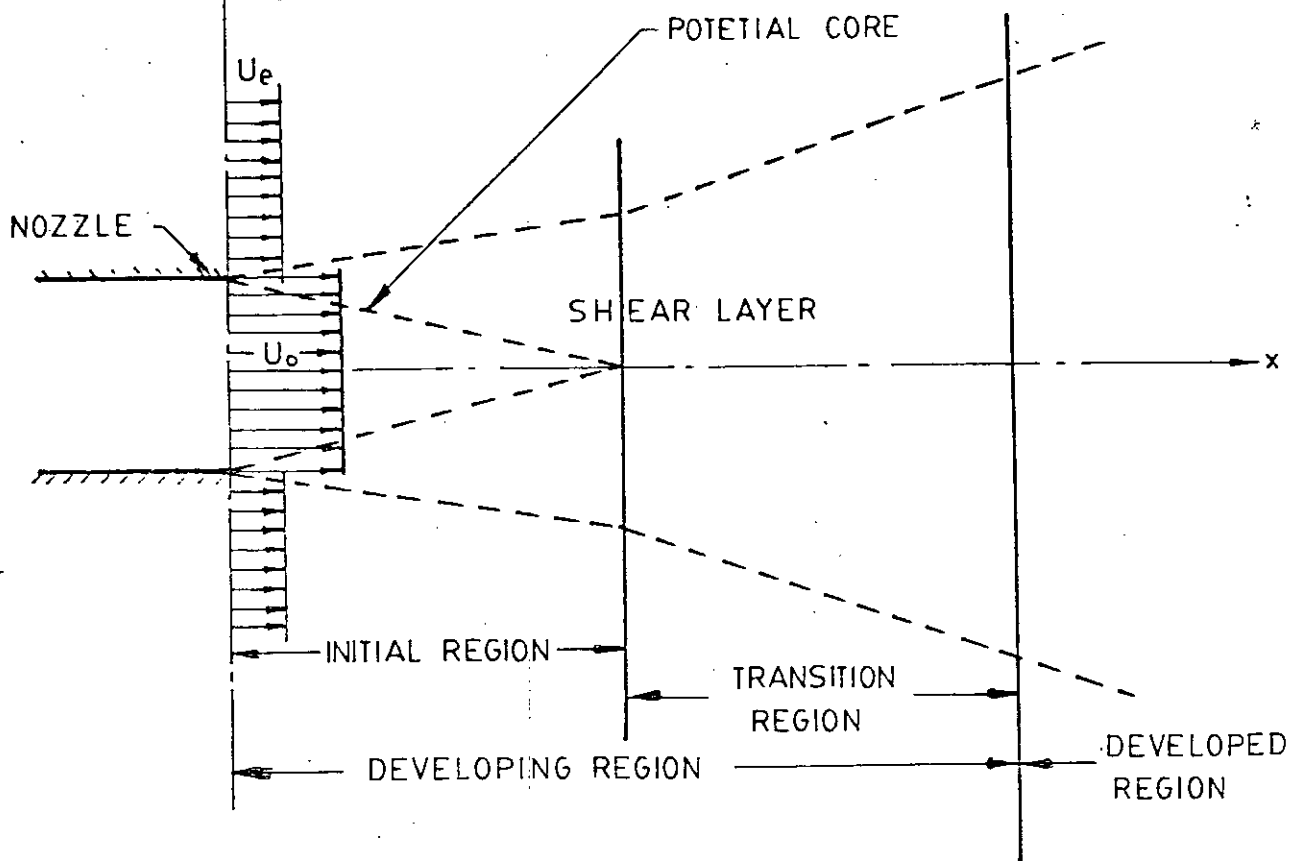


FIG. 1-1 JET GEOMETRY AND NOMENCLATURE

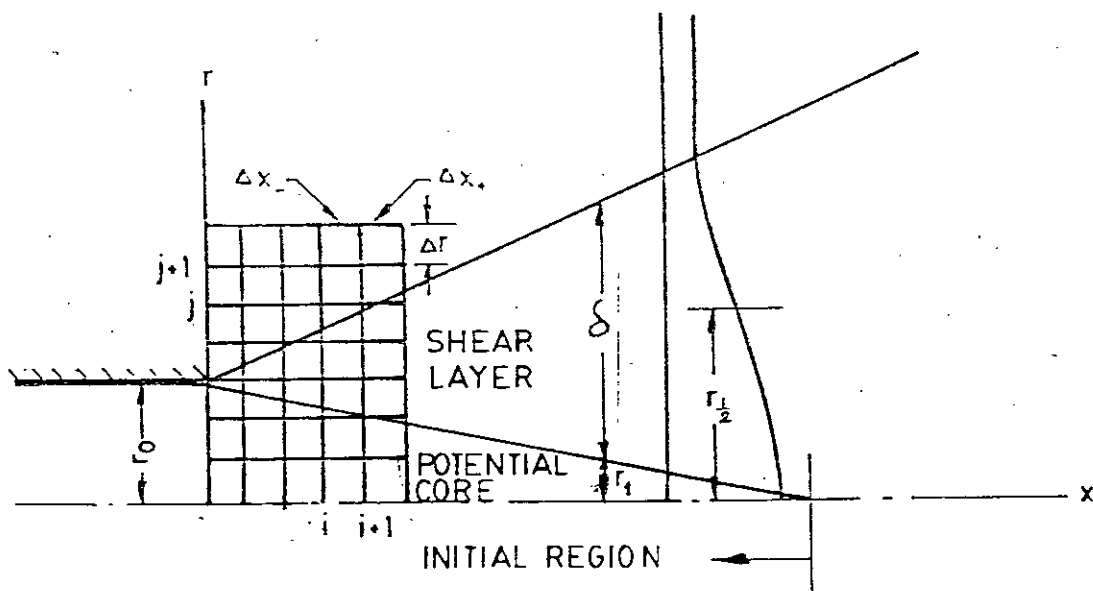


FIG. 3-1 CO-ORDINATE SYSTEM AND FINITE-DIFFERENCE GRID

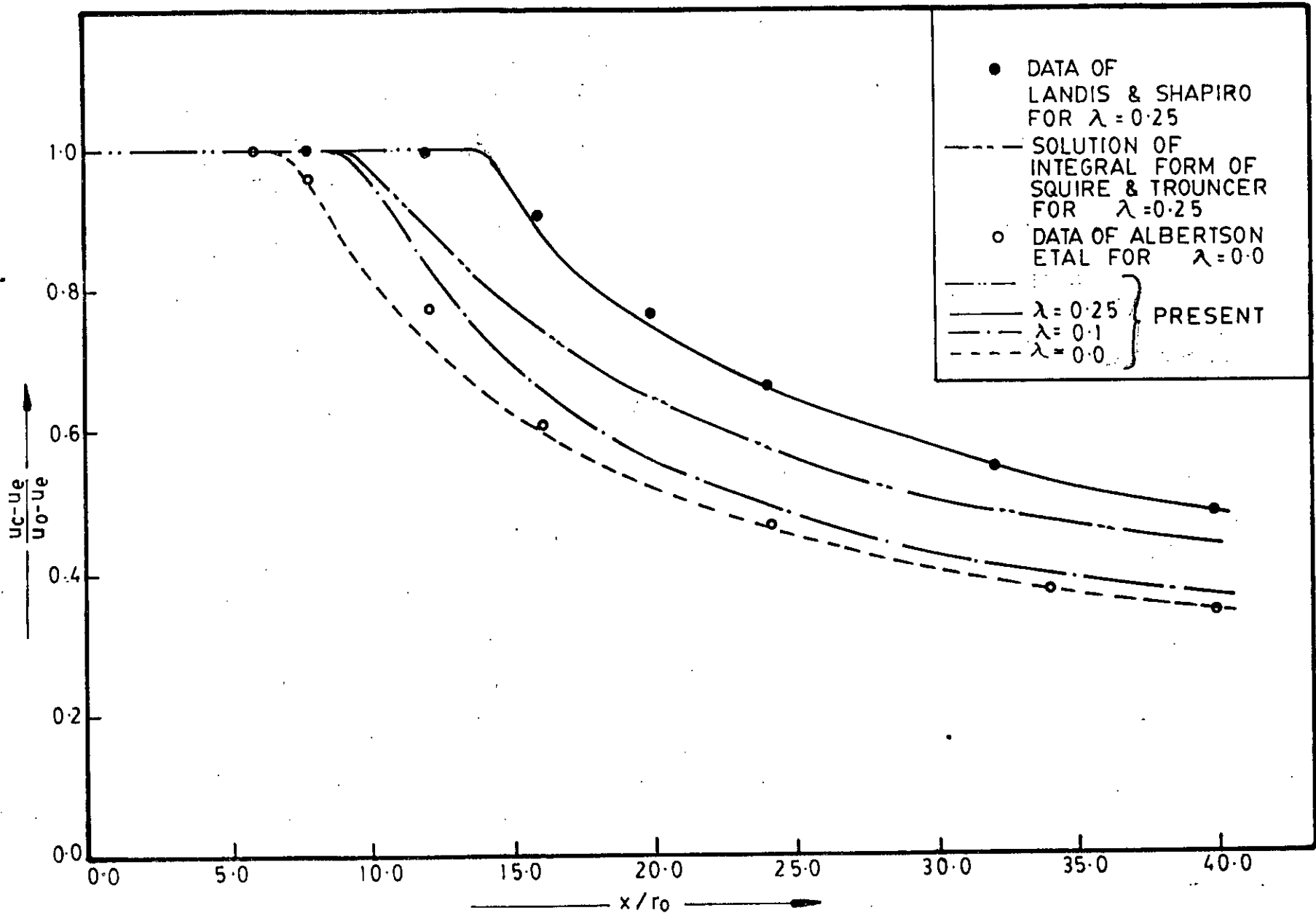


FIG. 41 (a) CENTER LINE VELOCITY

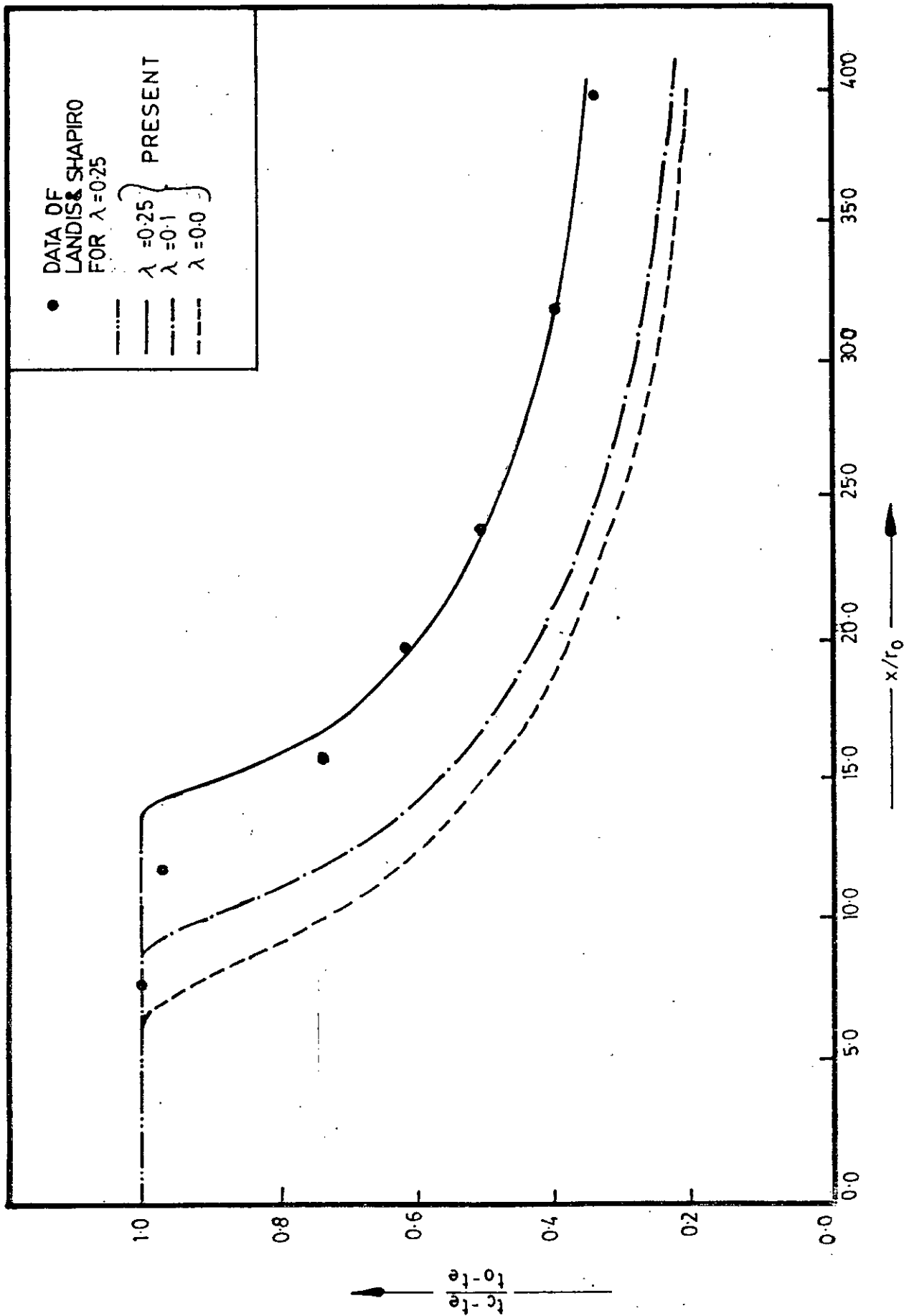


FIG. 4.1 (b) CENTER LINE TEMPERATURE



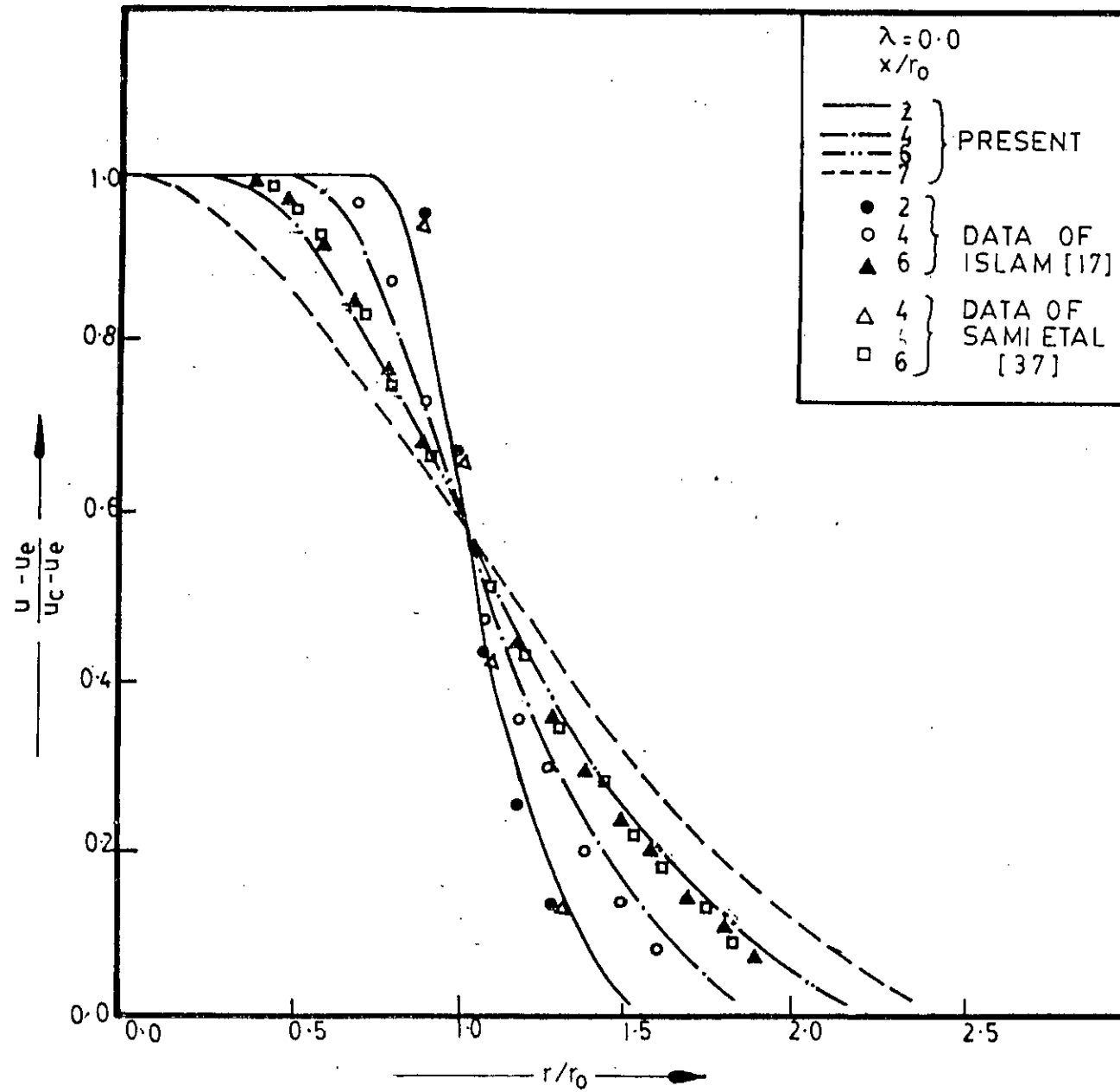


FIG 4.2 (a) MEAN AXIAL VELOCITY DISTRIBUTION

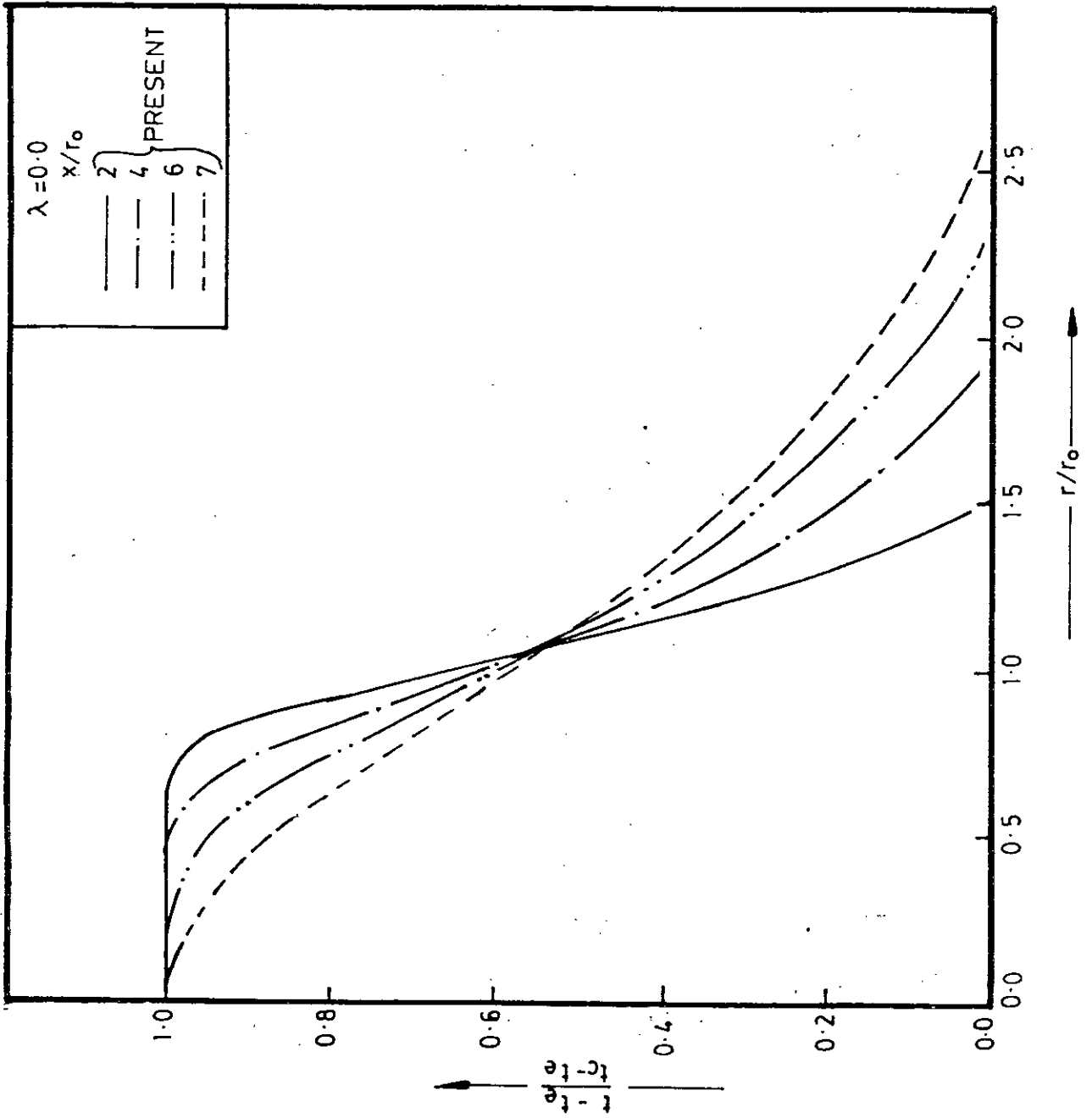


FIG. 4.2 (b) AXIAL MEAN TEMPERATURE DISTRIBUTION

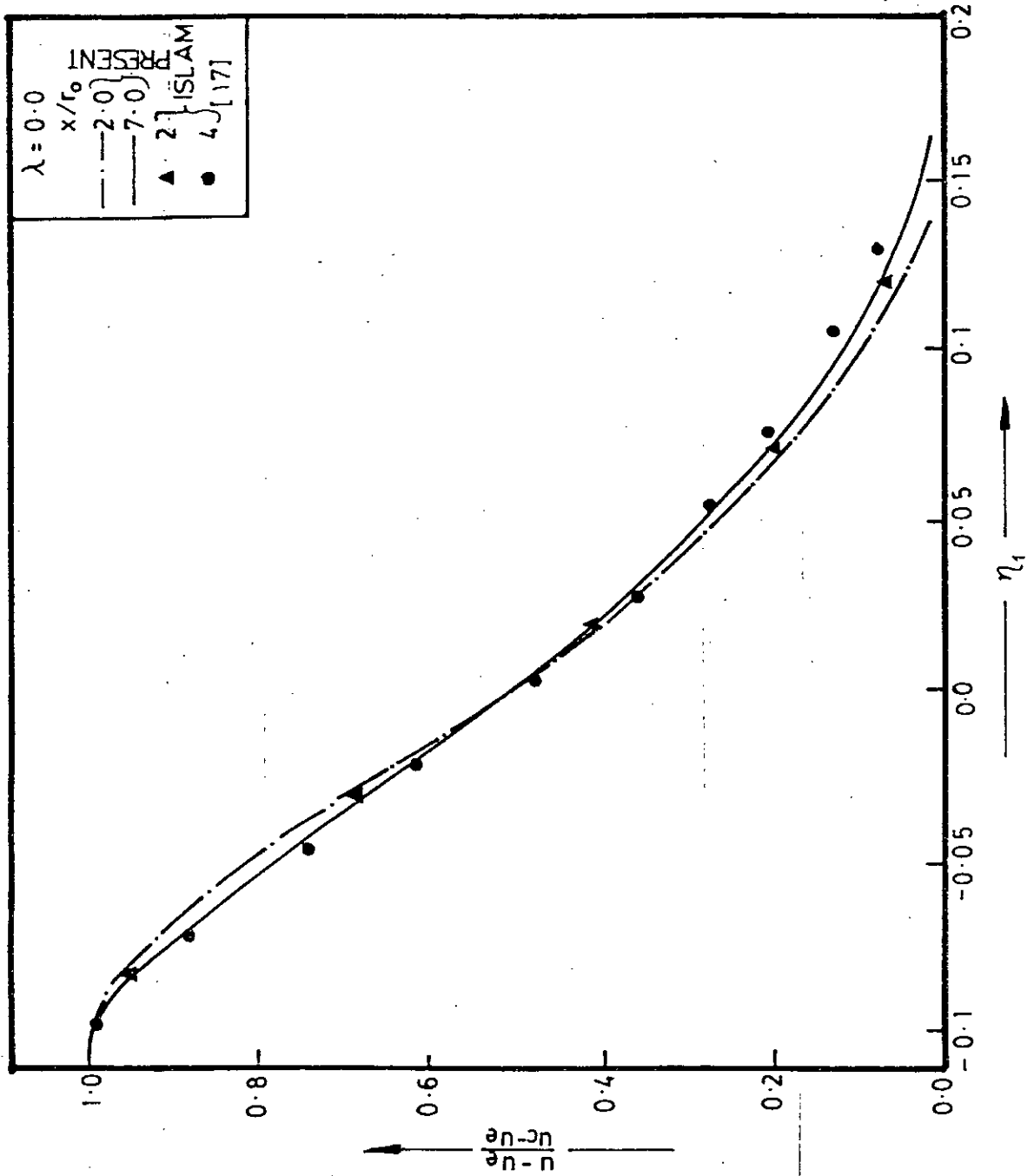


FIG 4.3 (a) MEAN AXIAL VELOCITY DISTRIBUTION

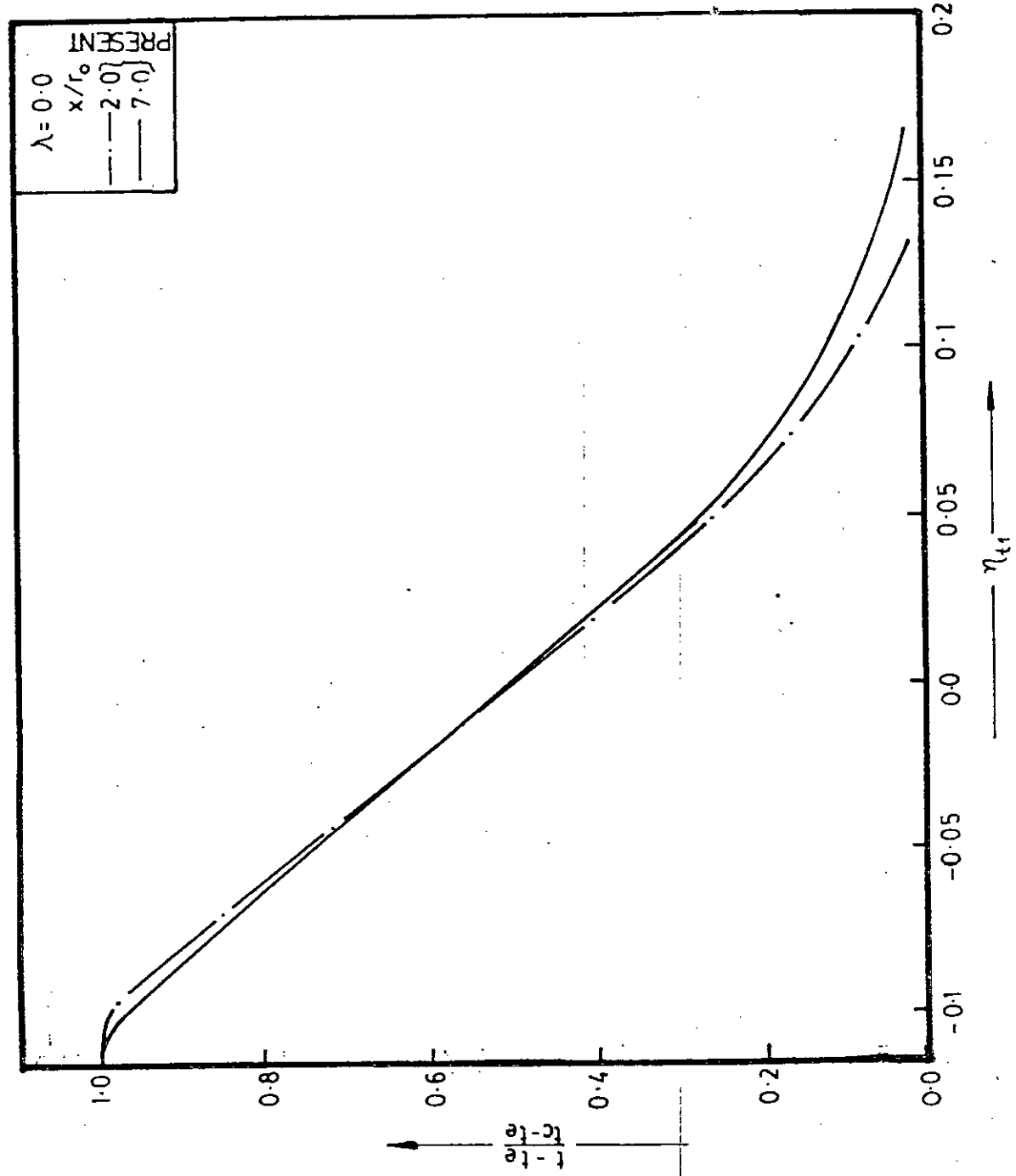


FIG. 4.3 (b) MEAN AXIAL TEMPERATURE DISTRIBUTION

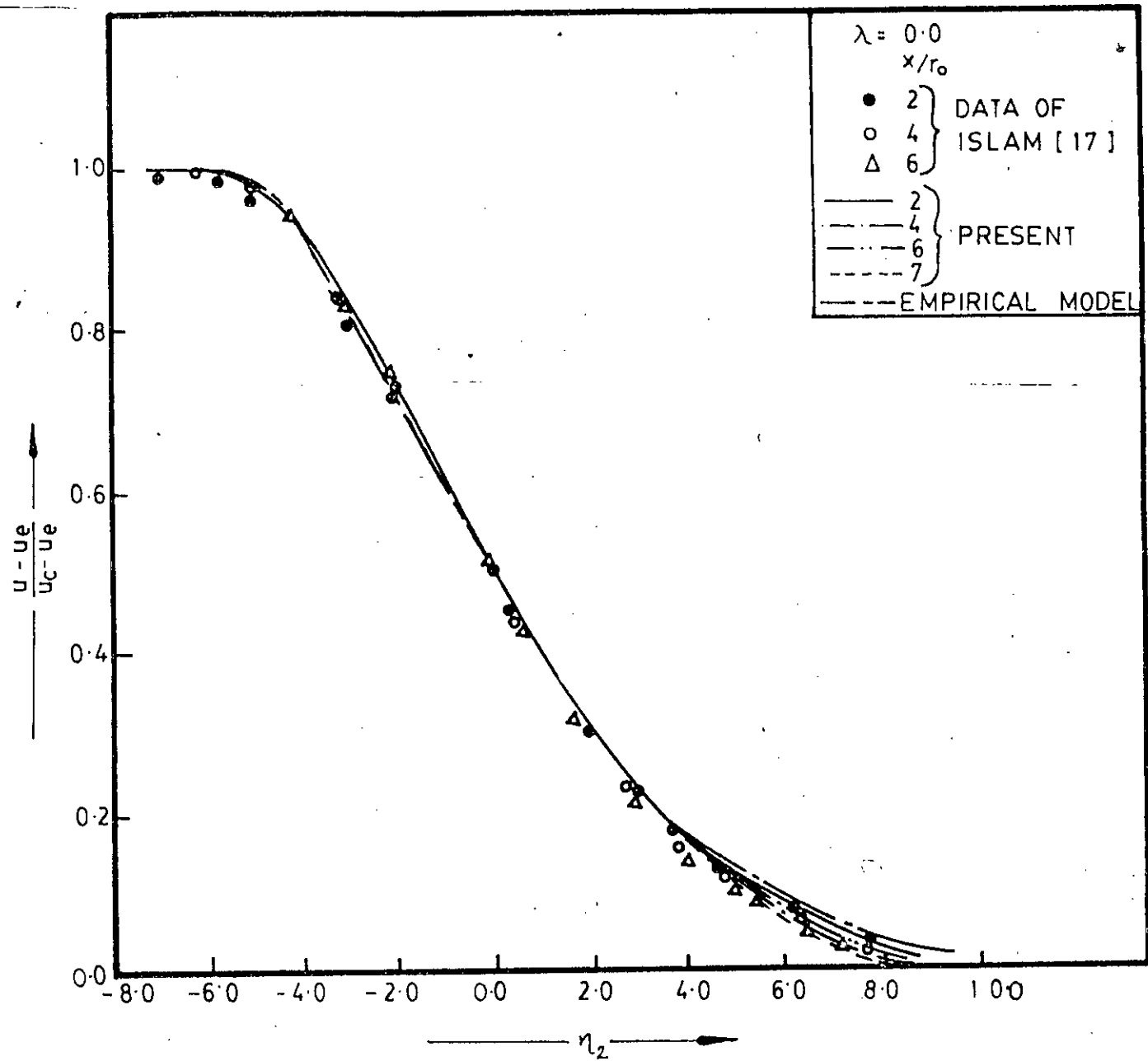


FIG. 4.4 (a) MEAN AXIAL VELOCITY DISTRIBUTION

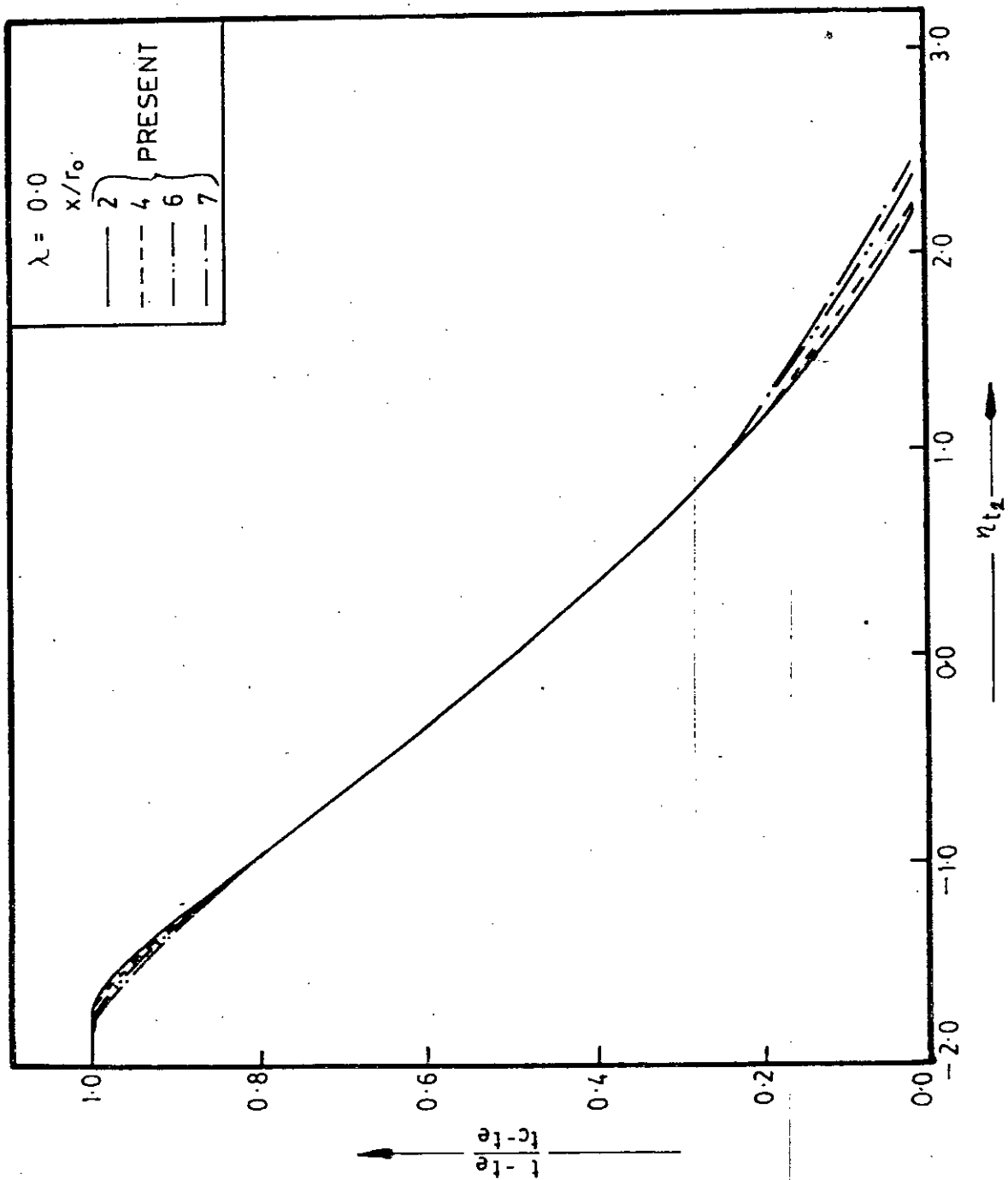


FIG. 4.4 (b) MEAN AXIAL TEMPERATURE DISTRIBUTION

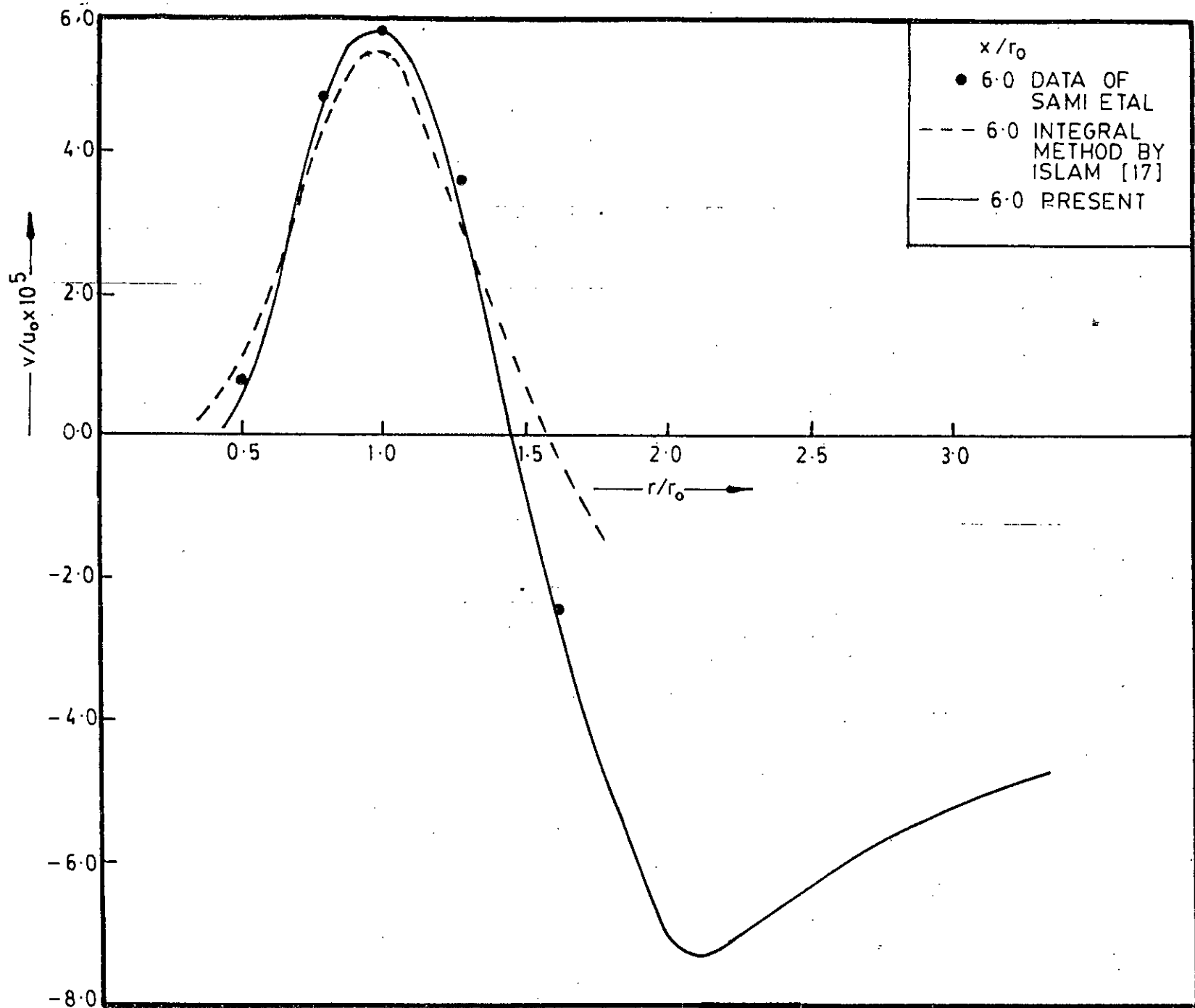


FIG. 4.5 MEAN RADIAL VELOCITY DISTRIBUTION

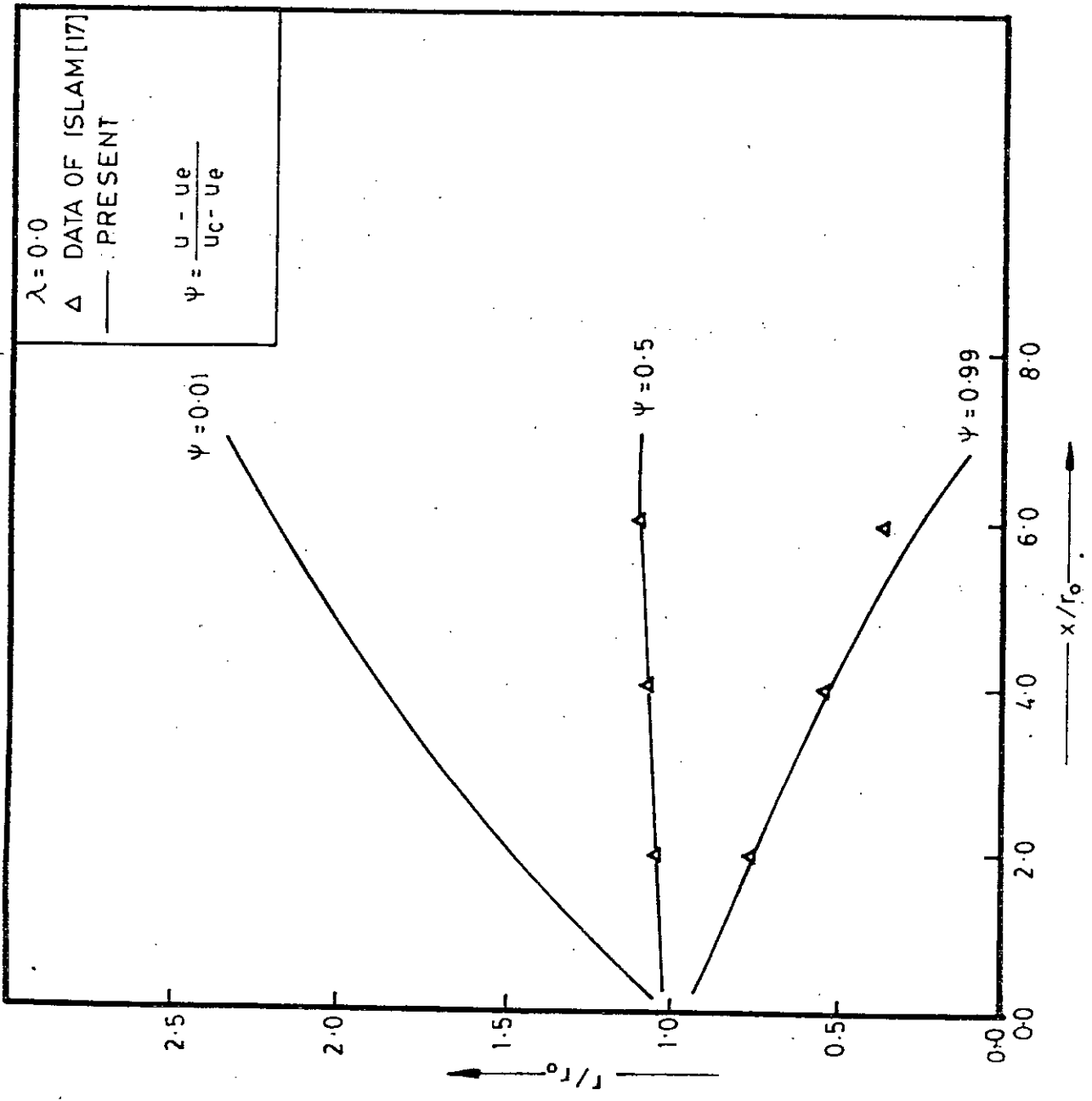


FIG. 4.6 (a) ISO-VELOCITY LINES



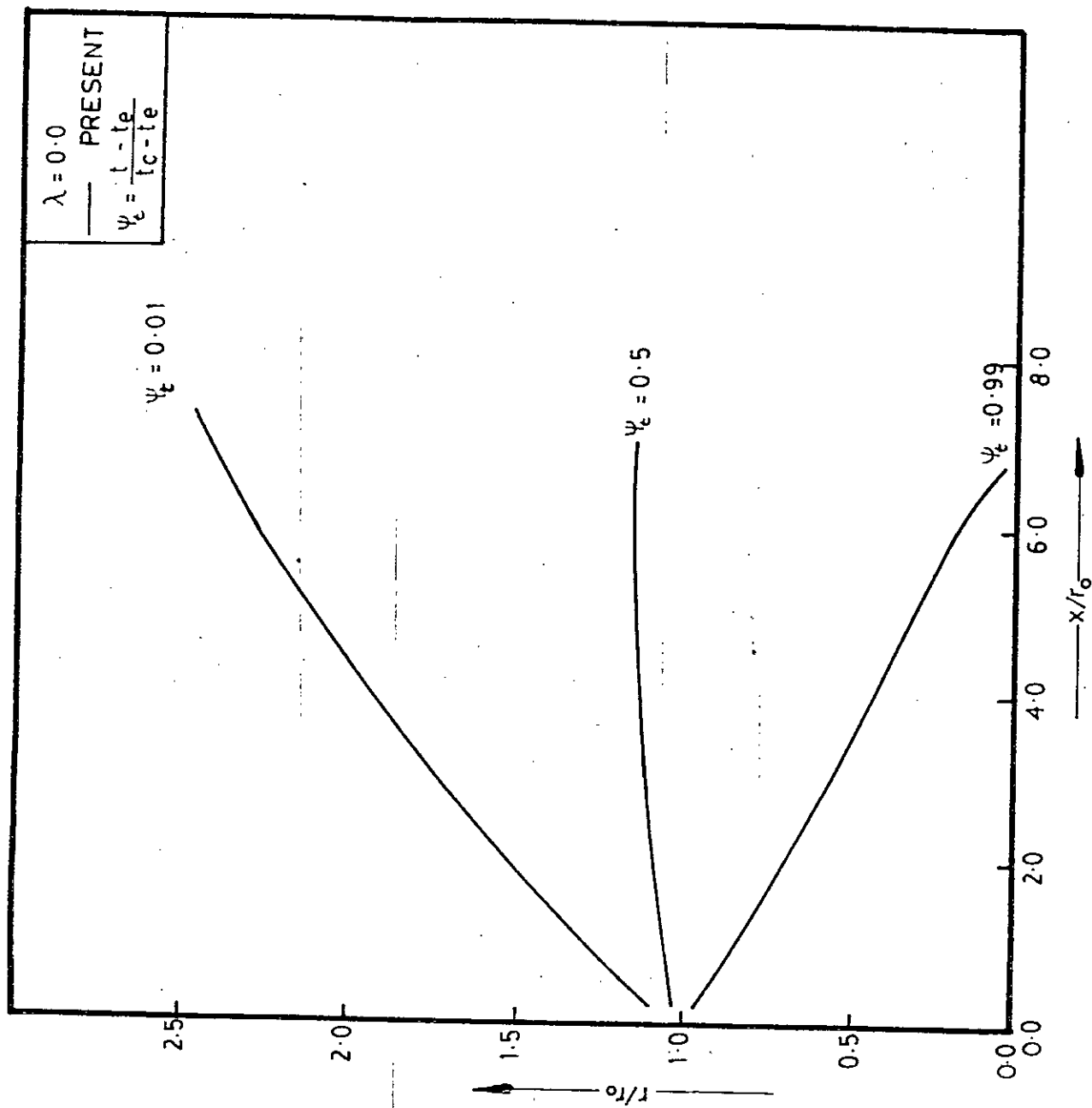


FIG. 4.6 (b) ISO-TEMPERATURE LINES

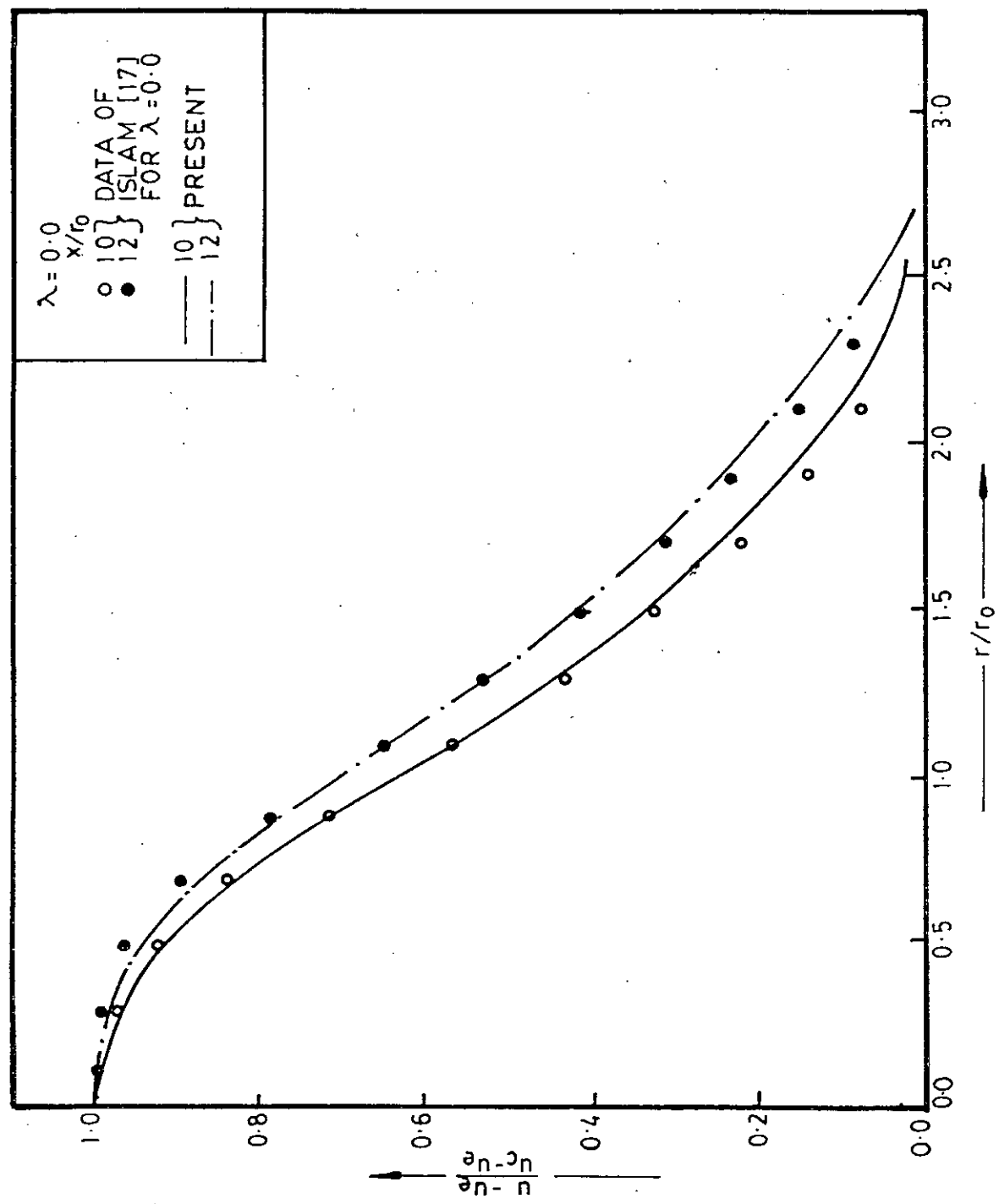


FIG. 4.7 (a) MEAN AXIAL VELOCITY DISTRIBUTION

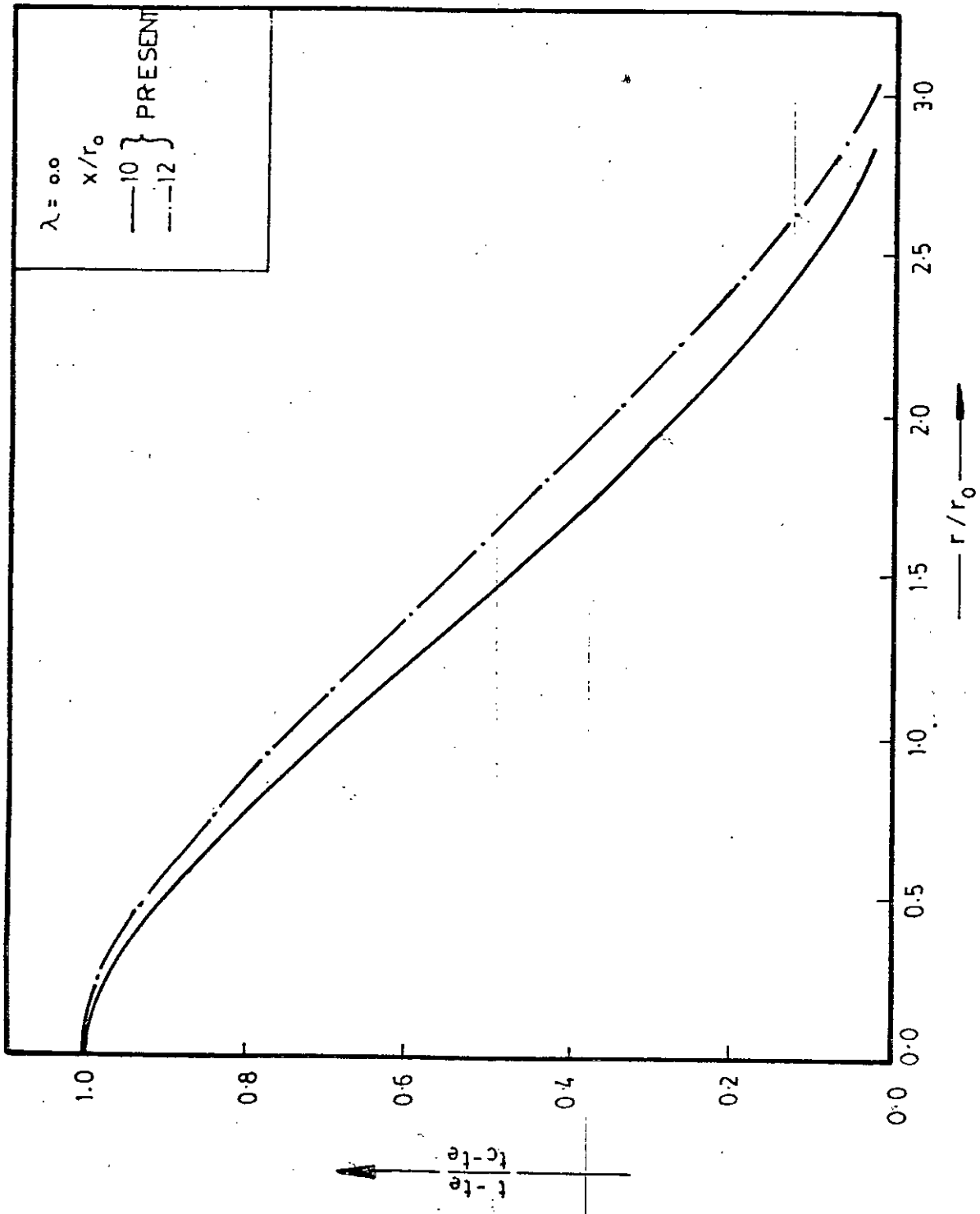


FIG. 4.7 (b) MEAN AXIAL TEMPERATURE DISTRIBUTION

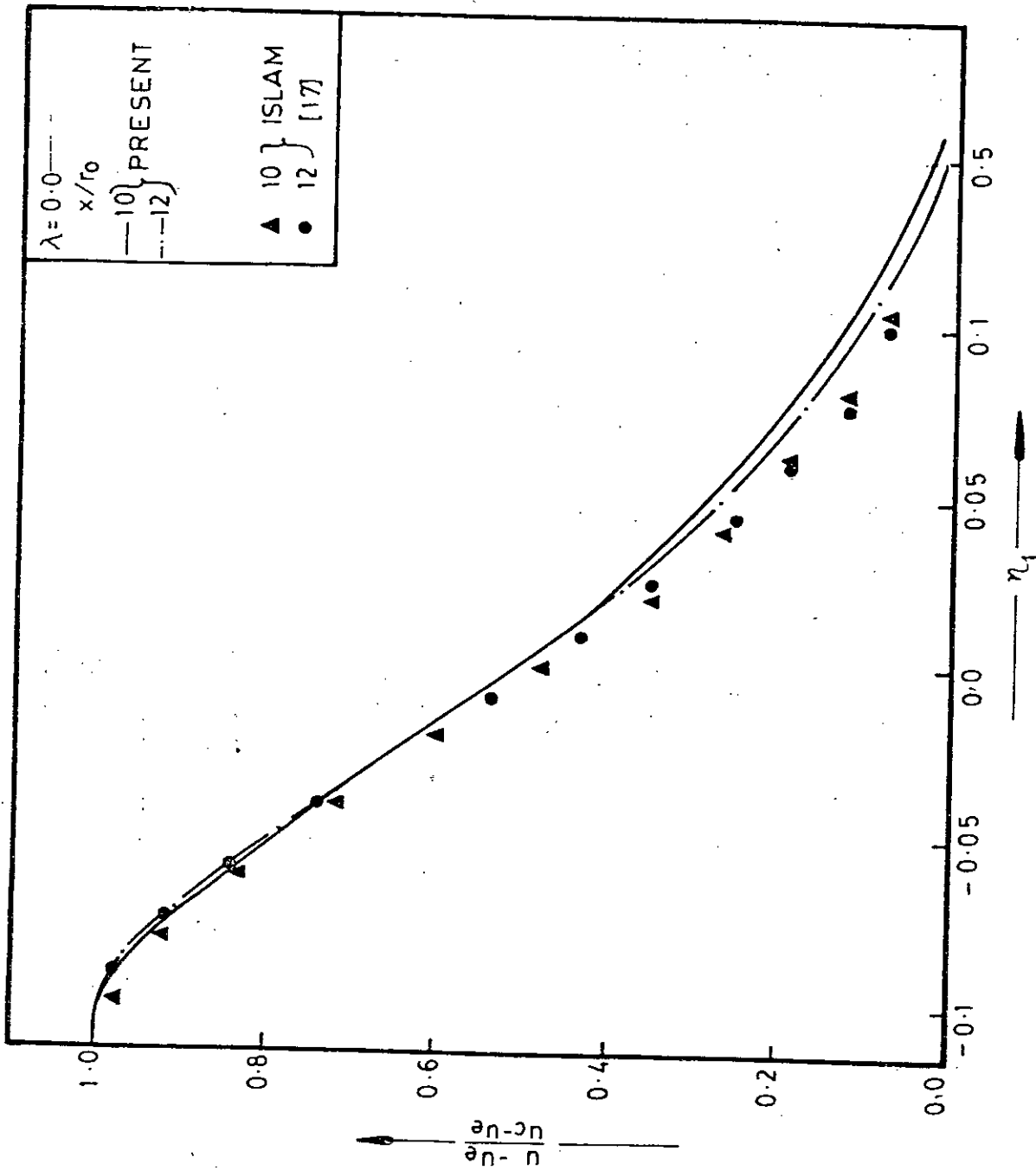


FIG. 4.8 (a) MEAN AXIAL VELOCITY DISTRIBUTION

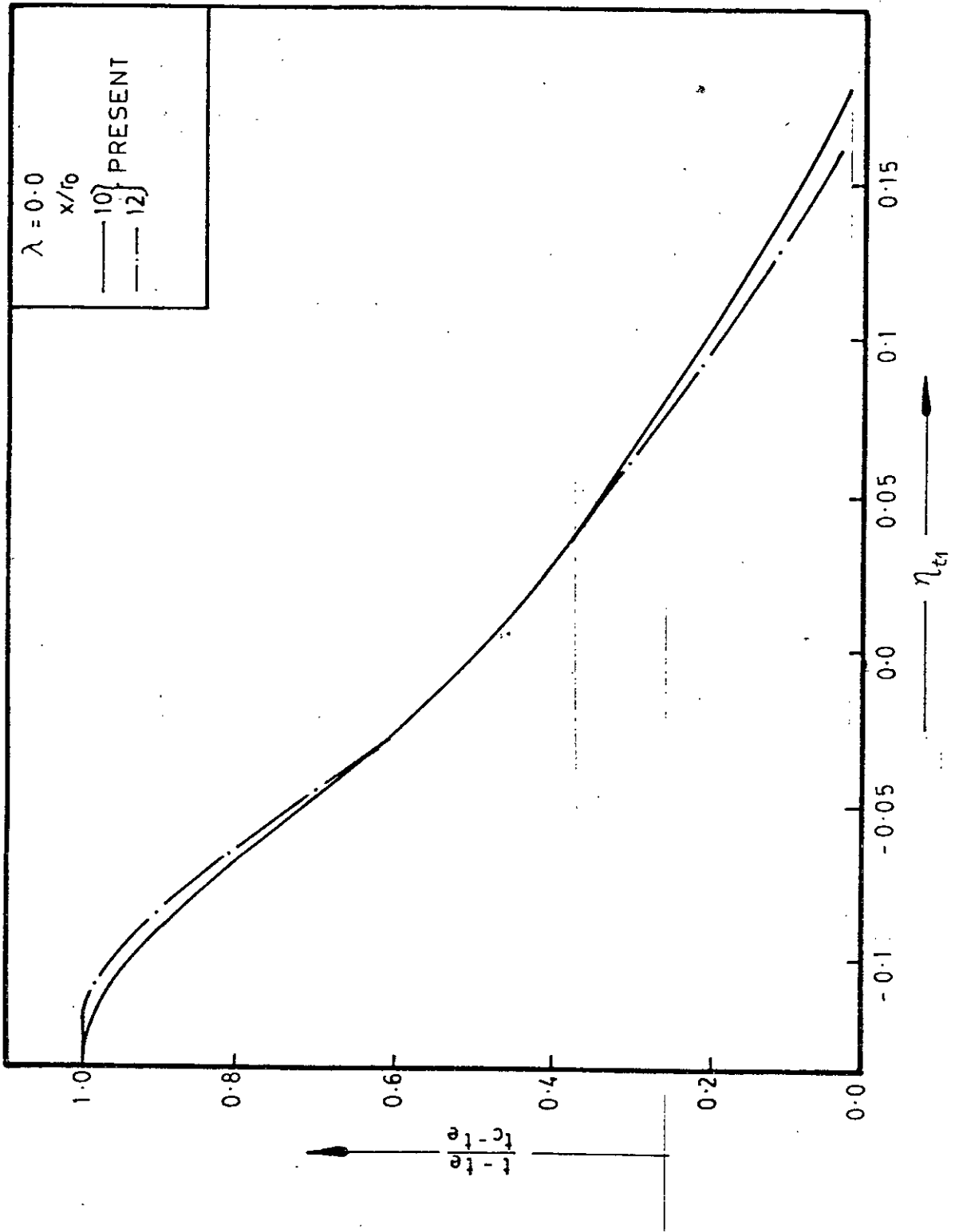


FIG. 4.8 (b) MEAN AXIAL TEMPERATURE DISTRIBUTION

62218

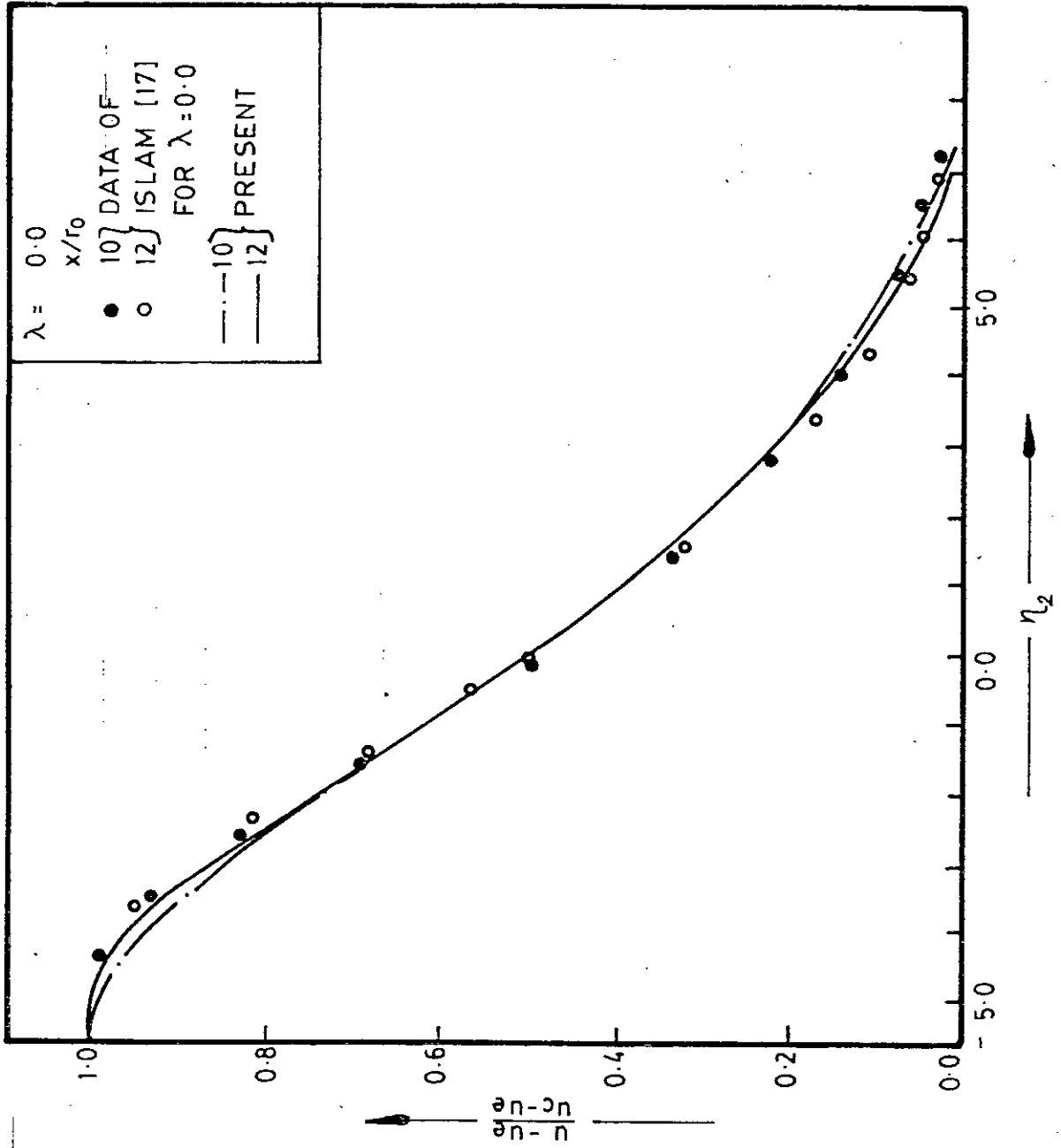


FIG. 4.9 (a) MEAN AXIAL VELOCITY DISTRIBUTION

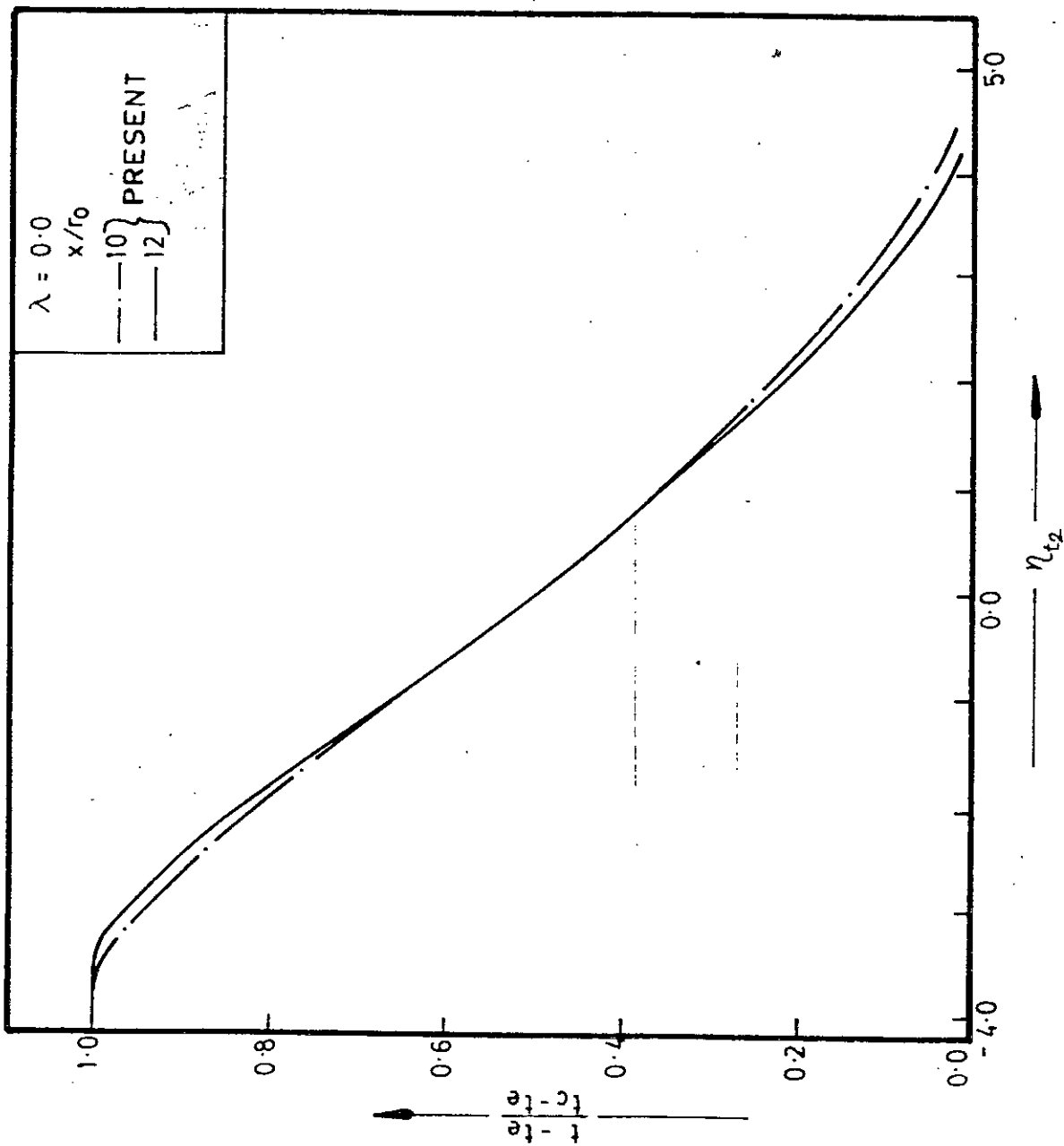


FIG. 4-9 (b). MEAN AXIAL TEMPERATURE DISTRIBUTION

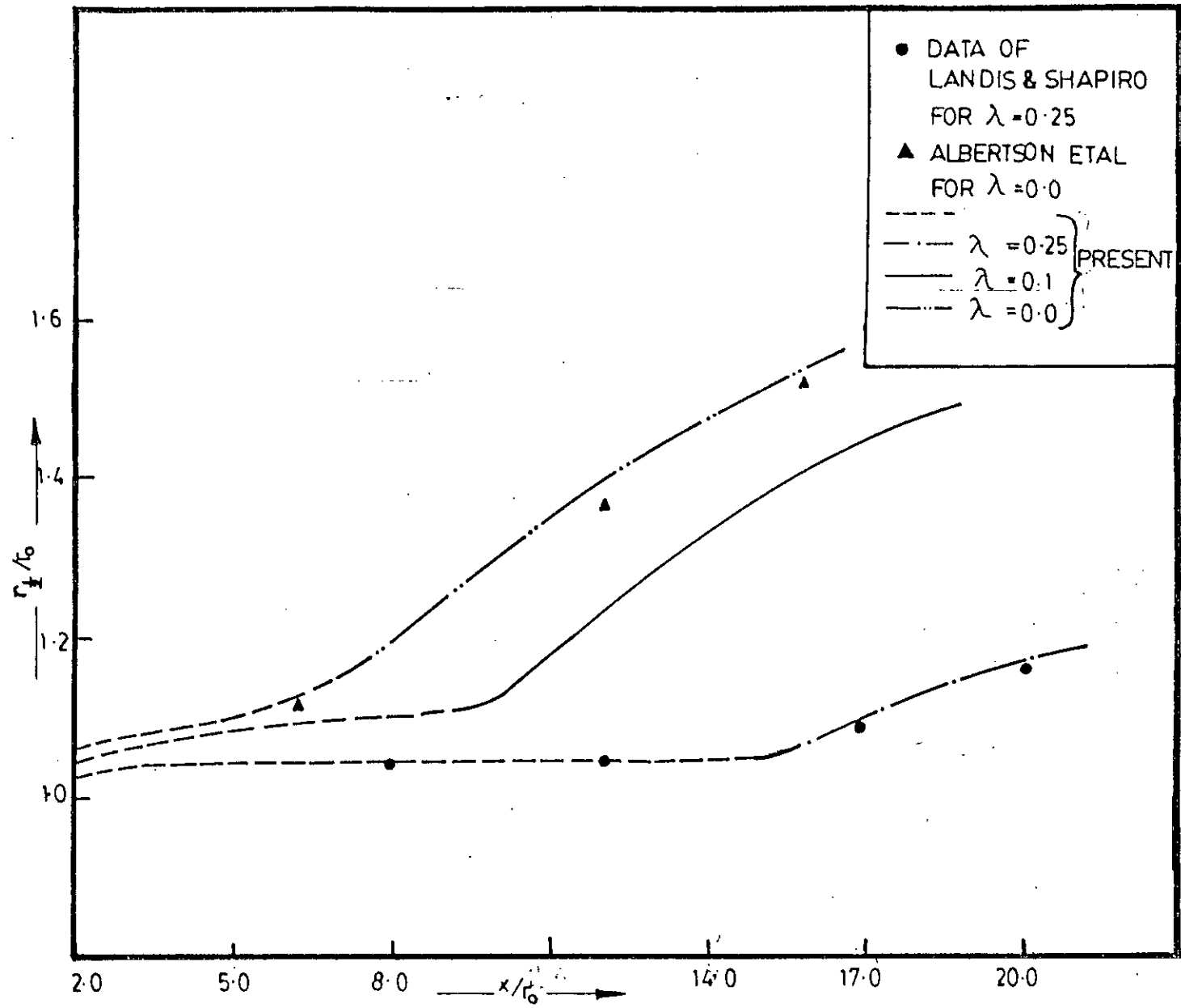


FIG. 4-10 (a) GROWTH OF HALF-RADII FOR VELOCITY



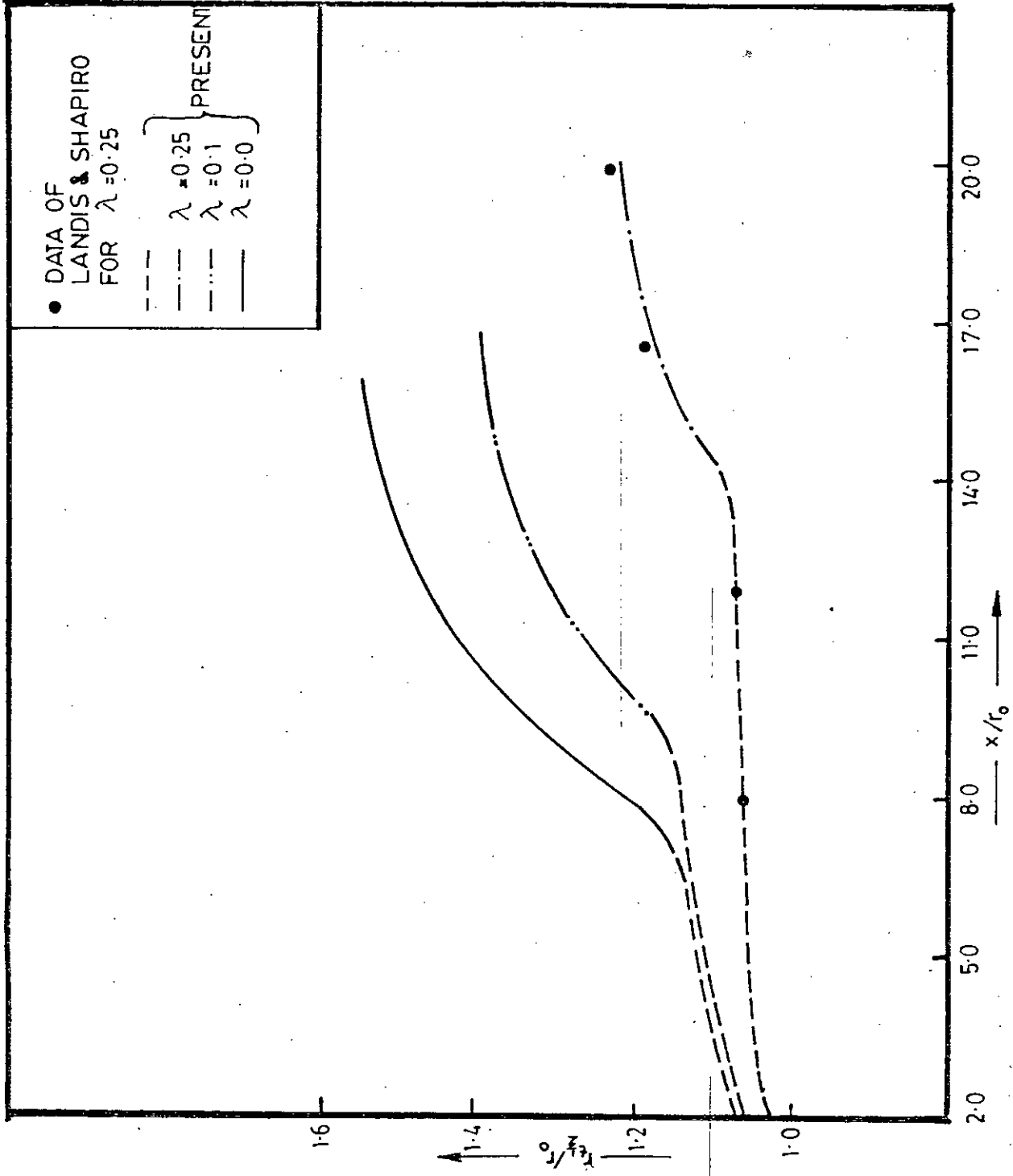


FIG. 4-10 (b) GROWTH OF HALF-RADIII FOR TEMPERATURE

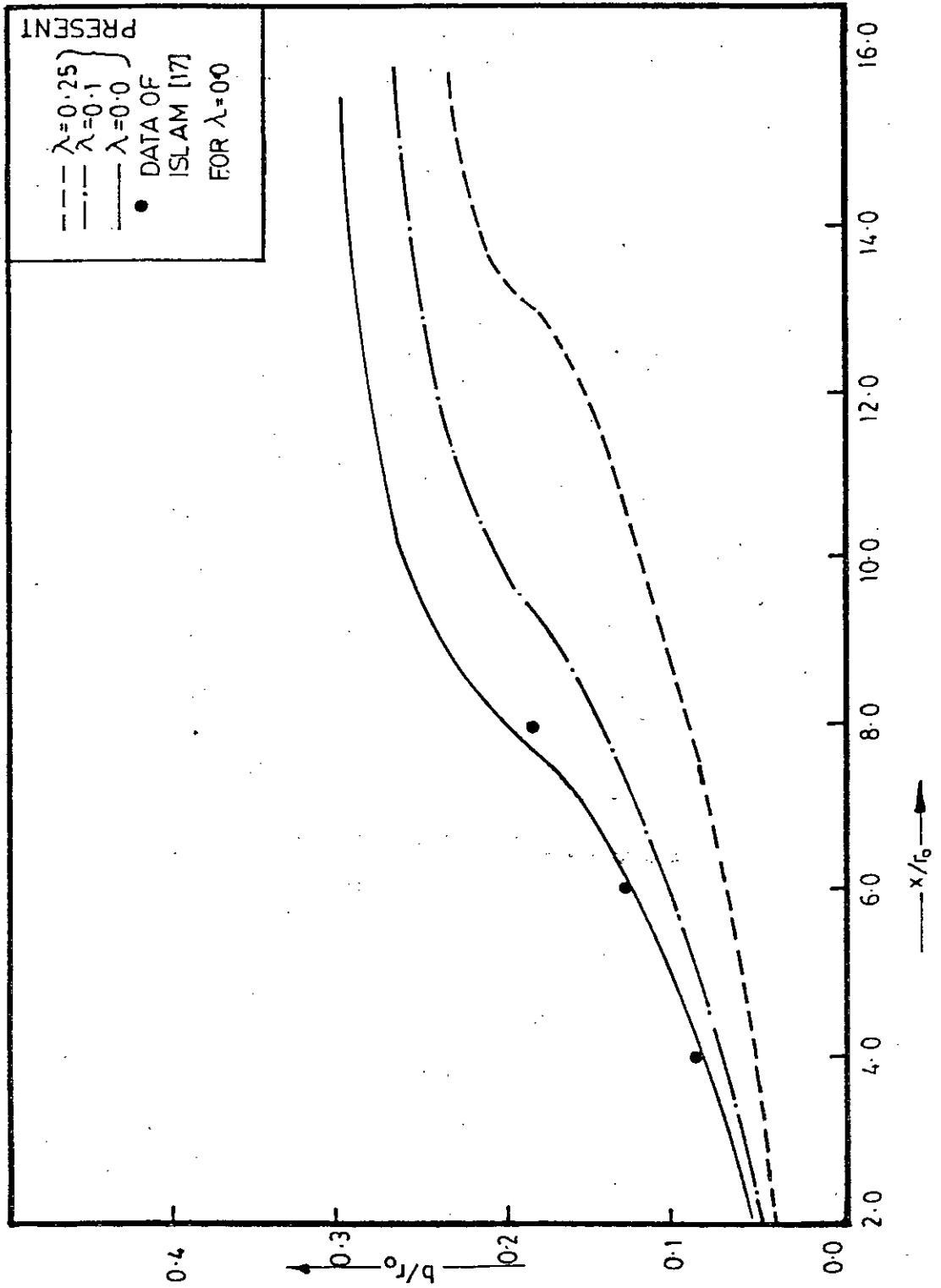


FIG. 4-11(a) LENGTH SCALE FOR VELOCITY

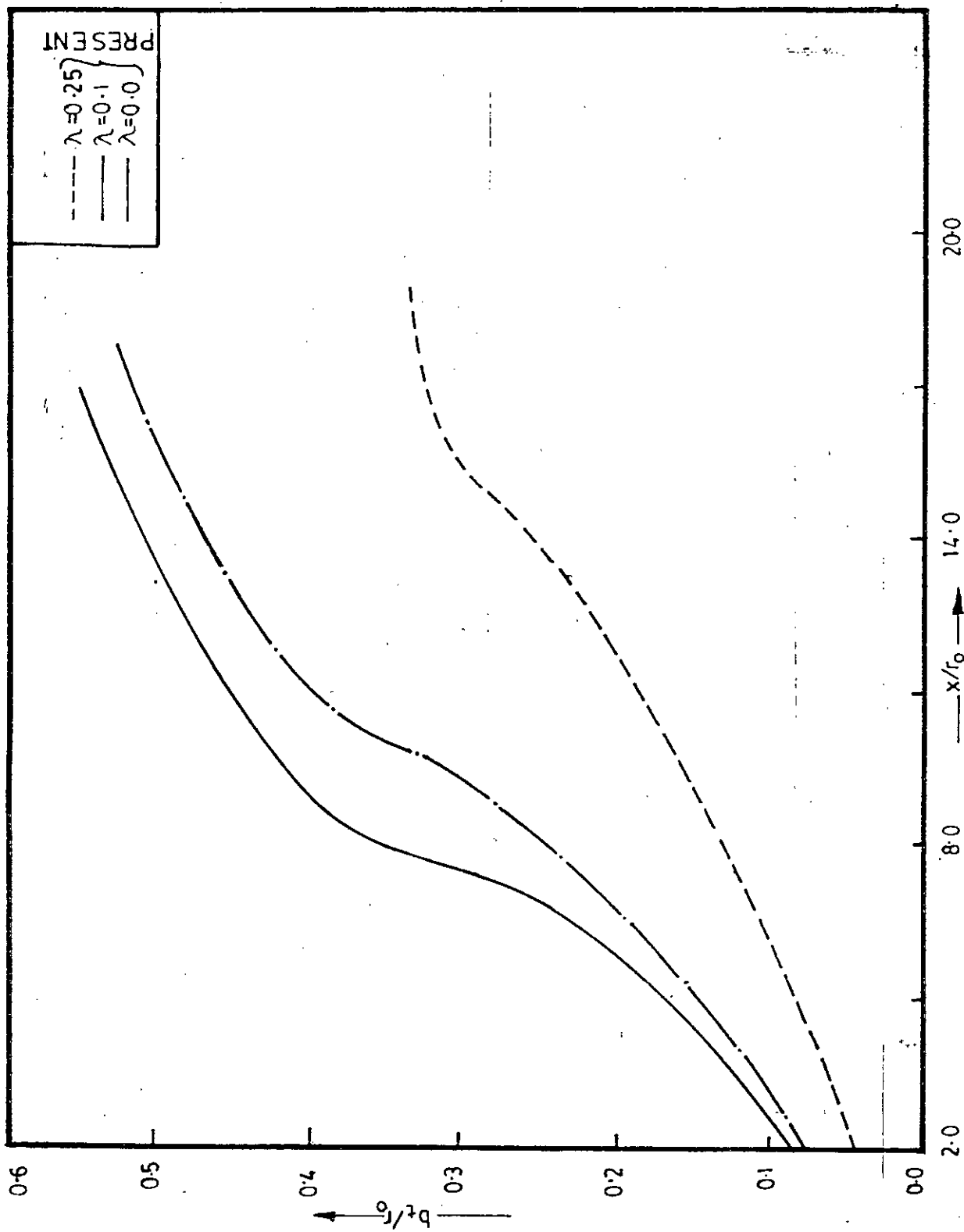


FIG. 4 II(b) LENGTH SCALE FOR TEMPERATURE

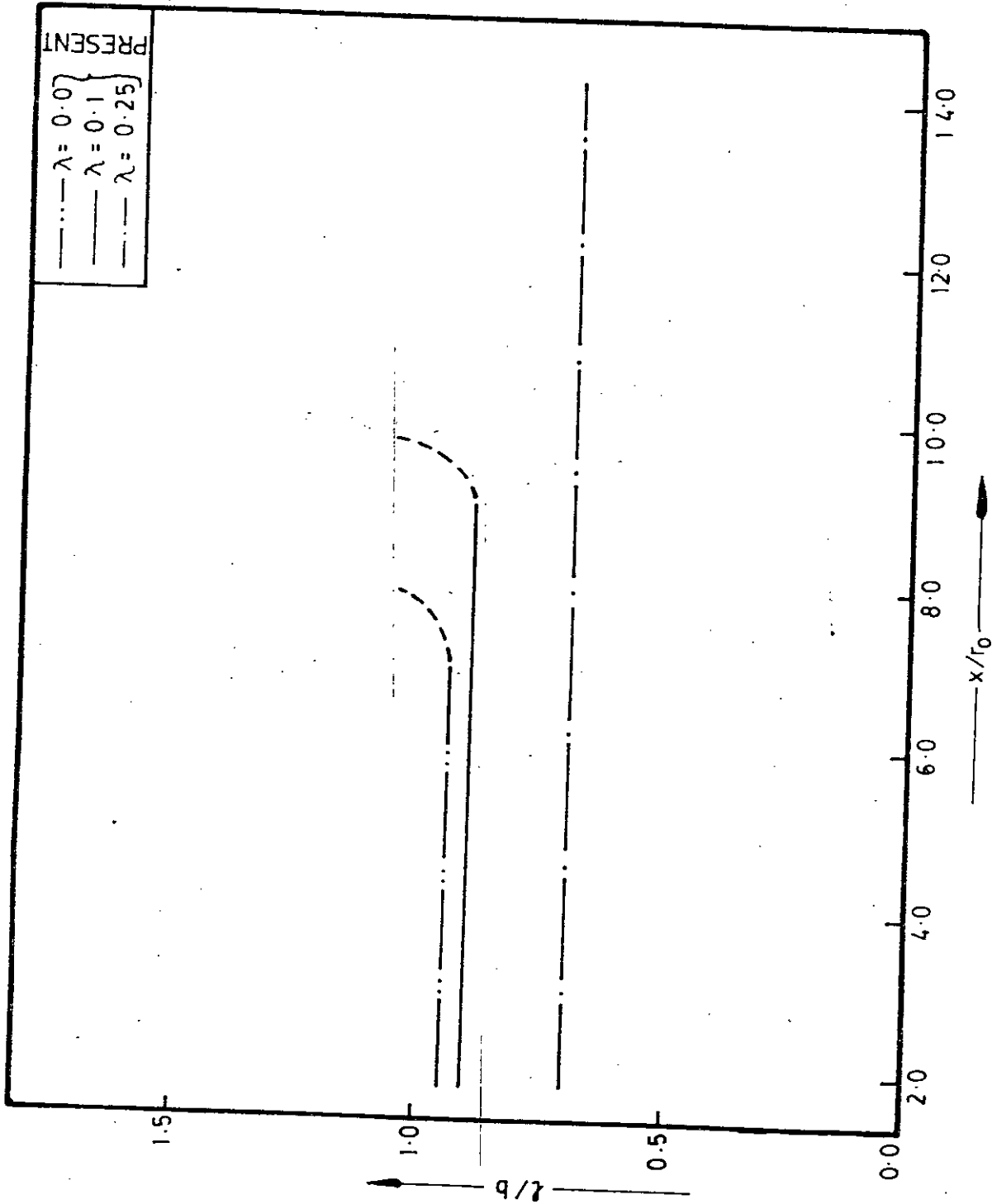


FIG. 4.12. CALCULATED VALUES OF THE RATIO,  $z/b$

APPENDICES

## APPENDIX-A

DERIVATION OF EQUATIONSDifferential Equations

Non-isothermal Turbulent flow is governed by the Continuity equation, the Navier-Stokes equations and the Energy Equation. In cylindrical co-ordinates the mass conservation equation for incompressible flow field with boundary layer assumptions is:

$$\frac{\partial \rho}{\partial t} + \frac{\partial u^0}{\partial x} + \frac{1}{r} \frac{\partial}{\partial r} (rv^0) + \frac{1}{r} \frac{\partial w^0}{\partial \theta} = 0 \quad A.1$$

The co-ordinate system is given in Fig. 3.1 and  $u^0$ ,  $v^0$  and  $w^0$  are instantaneous velocity components in  $x$ ,  $r$  and  $\theta$  directions respectively.

Reynolds equation of motion for turbulent flow, dissociates instantaneous variables into mean and fluctuating components:

$$\left. \begin{aligned} u^0 &= u + u' \\ v^0 &= v + v' \\ w^0 &= w' \\ p^0 &= p + p' \\ t^0 &= t + t' \end{aligned} \right\} \quad A.2$$

where  $u, v, p$  and  $t$  are mean components and  $u', v', w', p'$  and  $t'$  are fluctuating components. The instantaneous pressure  $p^0$  has a mean and a fluctuating component,  $p$  and  $p'$  respectively.

Introducing Equation A.2 in Equation A.1 and considering steady state:

$$\frac{\partial}{\partial x}(u+u') + \frac{1}{r} \frac{\partial}{\partial r} [r(v+v')] + \frac{1}{r} \frac{\partial w'}{\partial \theta} = 0 \quad \text{A.3}$$

Taking a time average:

$$\frac{\partial u}{\partial x} + \frac{1}{r} \frac{\partial}{\partial r} (rv) = 0 \quad \text{A.4}$$

Subtracting Equation A.4 from Equation A.3:

$$\frac{\partial u'}{\partial x} + \frac{1}{r} \frac{\partial}{\partial r} (rv') + \frac{1}{r} \frac{\partial w'}{\partial \theta} = 0 \quad \text{A.5}$$

Navier-stokes equations in cylindrical co-ordinates for incompressible flow in absence of body forces and considering constant viscosity:

x-component:

$$\frac{Du^0}{Dt} = - \frac{\partial p^0}{\partial x} + \mu \left[ \frac{1}{r} \frac{\partial}{\partial r} \left( r \frac{\partial u^0}{\partial r} \right) + \frac{1}{r^2} \frac{\partial^2 u^0}{\partial x^2} \right] \quad \text{A.6}$$

r-component:

$$\left( \frac{Dv^0}{Dt} - \frac{w^{0^2}}{r} \right) = - \frac{\partial p^0}{\partial r} + \mu \left[ \frac{\partial}{\partial r} \left( \frac{1}{r} \frac{\partial}{\partial r} (rv^0) \right) + \frac{1}{r^2} \frac{\partial^2 v^0}{\partial \theta^2} - \frac{2}{r^2} \frac{\partial u^0}{\partial \theta} + \frac{\partial^2 v^0}{\partial x^2} \right] \quad \text{A.7}$$

$$\theta\text{-component: } \left( \frac{Dw^0}{Dt} + \frac{v^0 w^0}{r} \right) = - \frac{1}{r} \frac{\partial p^0}{\partial \theta} + \mu \left[ \frac{\partial}{\partial r} \left( \frac{1}{r} \frac{\partial}{\partial r} (rw^0) \right) \right.$$

$$\left. + \frac{1}{r^2} \frac{\partial^2 w^0}{\partial \theta^2} + \frac{2}{r^2} \frac{\partial v^0}{\partial \theta} + \frac{\partial^2 w^0}{\partial x^2} \right] \quad \text{A.8}$$

Using Equation A.2 in Equation A.6:

$$\begin{aligned} & \frac{\partial(u+u')}{\partial t} + (u+u') \frac{\partial}{\partial x}(u+u') + (v+v') \frac{\partial}{\partial r}(u+u') + \frac{w'}{r} \frac{\partial}{\partial \theta}(u+u') \\ &= -\frac{1}{\rho} \frac{\partial}{\partial x}(\rho+\rho') + \left[ \frac{\partial^2}{\partial r^2}(u+u') + \frac{1}{r} \frac{\partial}{\partial r}(u+u') + \frac{1}{r^2} \frac{\partial^2}{\partial \theta^2}(u+u') \right. \\ & \qquad \qquad \qquad \left. + \frac{\partial^2}{\partial x^2}(u+u') \right] \end{aligned} \quad \text{A.9}$$

Time Averaging Equation A.9:

$$\begin{aligned} & \frac{\partial u}{\partial t} + u \frac{\partial u}{\partial x} + \overline{u' \frac{\partial u'}{\partial x}} + v \frac{\partial u}{\partial r} + \overline{v' \frac{\partial u'}{\partial r}} + \frac{w'}{r} \frac{\partial u}{\partial \theta} \\ &= -\frac{1}{\rho} \frac{\partial p}{\partial x} + \left[ \frac{\partial^2 u}{\partial r^2} + \frac{1}{r} \frac{\partial u}{\partial r} + \frac{1}{r^2} \frac{\partial^2 u}{\partial \theta^2} + \frac{\partial^2 u}{\partial x^2} \right] \end{aligned} \quad \text{A.10}$$

Multiplying Equation A.5 by  $u'$  and then time averaging:

$$\overline{u' \frac{\partial u'}{\partial x}} + \frac{1}{r} \frac{\partial}{\partial r} (\overline{r u' v'}) - \overline{v' \frac{\partial u'}{\partial r}} + \frac{1}{r} \frac{\partial}{\partial \theta} (\overline{w' u'}) - \frac{w'}{r} \frac{\partial u'}{\partial \theta} = 0 \quad \text{A.11}$$

Adding Equation A.11 and Equation A.10 and rearranging:

$$\begin{aligned} & \frac{\partial u}{\partial t} + u \frac{\partial u}{\partial x} + v \frac{\partial u}{\partial r} = -\frac{\partial}{\partial x} \left( \frac{p}{\rho} + \overline{u'^2} \right) - \frac{1}{r} \frac{\partial}{\partial r} (\overline{r u' v'}) - \frac{1}{r} \frac{\partial}{\partial \theta} (\overline{w' v'}) \\ & \qquad \qquad \qquad + \left[ \frac{\partial^2 u}{\partial r^2} + \frac{1}{r} \frac{\partial u}{\partial r} + \frac{1}{r^2} \frac{\partial^2 u}{\partial \theta^2} + \frac{\partial^2 u}{\partial x^2} \right] \end{aligned} \quad \text{A.12}$$

$\overline{u'^2}$ ,  $\overline{u'v'}$  and  $\overline{w'u'}$  are the Reynolds stresses. Miller and Comings [27] experimentally showed that  $\overline{u'^2}$  and  $p/\rho$  are approximately equal and opposite for jet flow i.e.  $(p/\rho + \overline{u'^2}) \cong 0$ . For axisymmetry,  $\frac{\partial}{\partial \theta} (\overline{w'u'}) = 0$  and  $\frac{\partial^2 u}{\partial \theta^2} = 0$ . Applying boundary



layer approximations,  $\frac{\partial^2 u}{\partial x^2}$  has been neglected. For steady flow, Equation A.12 becomes:

$$u \frac{\partial u}{\partial x} + v \frac{\partial u}{\partial r} = \frac{1}{r} \frac{\partial}{\partial r} \left[ r \left( \nu \frac{\partial u}{\partial r} - \overline{u'v'} \right) \right]$$

$$\text{or, } u \frac{\partial u}{\partial x} + v \frac{\partial u}{\partial r} = \frac{1}{r} \frac{\partial}{\partial r} \left[ r \tau / \rho \right] \quad \text{A.13}$$

$$\text{where } \tau / \rho = \nu \frac{\partial u}{\partial r} - \overline{u'v'} \quad \text{A.14}$$

Similar mathematical operations in Equations A.7 and A.8 yield that on using order of magnitude analysis the equations for mean flow vanish.

General Energy Equation for incompressible flow is:

$$\frac{D}{Dt} \left[ \rho \left( \hat{U} + \Phi + \frac{1}{2} \bar{V}^2 \right) \right] = k \nabla^2 t^0 + \left[ \rho \frac{D}{Dt} \left( \frac{1}{2} \bar{V}^2 \right) + \phi \right] \quad \text{A.15}$$

where  $\hat{U}$  is the internal energy,  $\Phi$  is the potential energy,  $\bar{V}^2$  is the kinetic energy,  $\nabla^2 t^0$  is heat addition by conduction and  $\phi$  is the dissipation.

$$\text{Considering } \rho \text{ as constant, } \frac{D(\rho \hat{U})}{Dt} = \rho \frac{D\hat{U}}{Dt} \quad \text{A.16}$$

$$\text{Let } \hat{U} = f(\hat{V}, t^0)$$

$$\begin{aligned} \text{Therefore, } d\hat{U} &= \left( \frac{\partial \hat{U}}{\partial \hat{V}} \right)_{t^0} d\hat{V} + \left( \frac{\partial \hat{U}}{\partial t^0} \right)_{\hat{V}} dt^0 \\ &= \left[ -p + t^0 \left( \frac{\partial p}{\partial t^0} \right)_{\hat{V}} \right] d\hat{V} + C_{\hat{V}} dt^0 \end{aligned}$$

Taking substantial derivative of  $\hat{U}$  :

$$\begin{aligned} \rho \frac{D\hat{U}}{Dt} &= \rho \left[ -\rho + t^0 \left( \frac{\partial \rho}{\partial t^0} \right) \hat{V} \right] \frac{D\hat{V}}{Dt} + \rho C_{\hat{V}} \frac{Dt^0}{Dt} \\ &= \left[ -\rho + t^0 \left( \frac{\partial \rho}{\partial t^0} \right) \hat{V} \right] \nabla \cdot \vec{V} + \rho C_{\hat{V}} \frac{Dt^0}{Dt} \end{aligned}$$

For incompressible fluid flow,  $\nabla \cdot \vec{V} = 0$  and then

$$\rho \frac{D\hat{U}}{Dt} = \rho C_{\hat{V}} \frac{Dt^0}{Dt}$$

$$\frac{D(\rho\hat{\phi})}{Dt} = 0, \text{ since } \hat{\phi} \text{ is independent of time.}$$

Now Equation A.15 becomes:

$$\rho C_{\hat{V}} \frac{Dt^0}{Dt} = k \nabla^2 t^0 + \hat{\phi} \quad \text{A.17}$$

If dissipation by molecular process is slow then  $\hat{\phi}$  can be neglected and Equation A.15 reduces to

$$\rho C_{\hat{V}} \frac{Dt^0}{Dt} = k \nabla^2 t^0 \quad \text{A.18}$$

In cylindrical co-ordinate Equation A.18 becomes

$$\begin{aligned} \rho C_{\hat{V}} \left( \frac{\partial t^0}{\partial t} + v^0 \frac{\partial t^0}{\partial r} + \frac{w^0}{r} \frac{\partial t^0}{\partial \theta} + u^0 \frac{\partial t^0}{\partial x} \right) \\ = k \left( \frac{\partial^2 t^0}{\partial r^2} + \frac{1}{r} \frac{\partial t^0}{\partial r} + \frac{1}{r^2} \frac{\partial^2 t^0}{\partial \theta^2} + \frac{\partial^2 t^0}{\partial x^2} \right) \end{aligned} \quad \text{A.19}$$

Using Equation A.2 in Equation A.19:

$$\begin{aligned} & \frac{\partial}{\partial t}(t+t') + (u+u') \frac{\partial(t+t')}{\partial x} + (v+v') \frac{\partial(t+t')}{\partial r} + w' \frac{\partial(t+t')}{\partial \theta} \\ &= \frac{k}{\rho C_v} \left[ \frac{\partial^2(t+t')}{\partial r^2} + \frac{1}{r} \frac{\partial(t+t')}{\partial r} + \frac{1}{r^2} \frac{\partial^2(t+t')}{\partial \theta^2} + \frac{\partial^2(t+t')}{\partial x^2} \right] \end{aligned} \quad \text{A.20}$$

Considering steady flow and then time averaging Equation A.20:

$$\begin{aligned} & u \frac{\partial t}{\partial x} + v \frac{\partial t}{\partial r} + \overline{u' \frac{\partial t'}{\partial x}} + \overline{v' \frac{\partial t'}{\partial r}} + \overline{w' \frac{\partial t'}{\partial \theta}} \\ &= \frac{k}{\rho C_v} \left[ \frac{\partial^2 t}{\partial r^2} + \frac{1}{r} \frac{\partial t}{\partial r} + \frac{1}{r^2} \frac{\partial^2 t}{\partial \theta^2} + \frac{\partial^2 t}{\partial x^2} \right] \end{aligned} \quad \text{A.21}$$

Multiplying Equation A.3 by  $t^0$  and then time averaging:

$$t \frac{\partial u}{\partial x} + \frac{t}{r} \frac{\partial}{\partial r} (rv) + \overline{t' \frac{\partial u'}{\partial x}} + \frac{t'}{r} \frac{\partial}{\partial r} (rv') + \frac{t'}{r} \frac{\partial w'}{\partial \theta} = 0 \quad \text{A.22}$$

Adding Equation A.21 and Equation A.22 and rearranging:

$$\begin{aligned} & \frac{\partial}{\partial x}(tu) + \frac{1}{r} \frac{\partial}{\partial r} (rvt) + \frac{\partial}{\partial x}(\overline{t'u'}) + \frac{\partial}{\partial r}(\overline{rv't'}) + \frac{1}{r} \frac{\partial}{\partial \theta} (\overline{t'w'}) \\ &= \frac{k}{\rho C_v} \left[ \frac{\partial^2 t}{\partial r^2} + \frac{1}{r} \frac{\partial t}{\partial r} + \frac{1}{r^2} \frac{\partial^2 t}{\partial \theta^2} + \frac{\partial^2 t}{\partial x^2} \right] \end{aligned} \quad \text{A.23}$$

For axisymmetry,  $\frac{\partial}{\partial \theta}(\overline{t'w'})=0$  and  $\frac{\partial^2 t}{\partial \theta^2}=0$ . Applying boundary layer approximations,  $\frac{\partial^2 t}{\partial x^2}$  has been neglected and then using equation A.4 in Equation A.23:

$$u \frac{\partial t}{\partial x} + v \frac{\partial t}{\partial r} + \frac{\partial}{\partial x}(\overline{t'u'}) + \frac{1}{r} \frac{\partial}{\partial r} (r \overline{v't'}) = \frac{k}{\rho C_v} \left[ \frac{\partial^2 t}{\partial r^2} + \frac{1}{r} \frac{\partial t}{\partial r} \right] \quad \text{A.24}$$

Rearranging Equation A.24:

$$u \frac{\partial t}{\partial x} + v \frac{\partial t}{\partial r} = \frac{1}{r} \frac{\partial}{\partial r} \left( \alpha r \frac{\partial t}{\partial r} - r \overline{t'v'} \right) - \frac{\partial}{\partial x} (\overline{t'u'}) \quad \text{A.25}$$

In practice  $t'$  and  $u'$  are poorly correlated so Equation A.25 becomes:

$$u \frac{\partial t}{\partial x} + v \frac{\partial t}{\partial r} = \frac{1}{r} \frac{\partial}{\partial r} \left( \alpha r \frac{\partial t}{\partial r} - r \overline{t'v'} \right) \quad \text{A.26}$$

## APPENDIX-B

FINITE-DIFFERENCE FORMULATION

A standard explicit finite-difference technique requires very small streamwise steps to satisfy the stability criterion. The Dufort-Frankel [9] method is used here. Dufort-Frankel Scheme needs information from the two previous streamwise stations. For this reason standard explicit scheme is used as a starting method for Dufort-Frankel procedure.

The finite-difference problem domain is made into a net of points as indicated in Fig. 3.1 by letting  $\Delta x$  and  $\Delta R$  be small increments of the coordinates  $X$  and  $R$ . Here the finite difference equations will be written in a format that will be applicable for uneven grid spacings with  $x$  and  $R$  directions. For this purpose, the notation  $\Delta R_+ = (R_{j+1} - R_j)$ ,  $\Delta R_- = (R_j - R_{j-1})$ ,  $\Delta x_+ = (x_{i+1} - x_i)$  and  $\Delta x_- = (x_i - x_{i-1})$  will be introduced. The dependent variables are expanded in Taylor series.

The basic variables are made non-dimensional by using the following transformation:

$$\begin{aligned} X &= \frac{x u_0}{\delta}, & R &= \frac{r u_0}{\delta}, & U &= \frac{u}{u_0}, & V &= \frac{v}{u_0} \\ N &= \frac{\delta + \delta_T}{\delta}, & T &= \frac{t}{t_0}, & N_H &= \frac{\alpha + \alpha_T}{\alpha} \end{aligned} \quad \text{B.1}$$

Replacing shear stress,  $\tau/\rho$  by  $(\delta + \delta_T) \frac{\partial U}{\partial R}$  and heat flux,  $q$  by  $-\rho C_p (\alpha + \alpha_T) \frac{\partial T}{\partial R}$  and introducing transformation B.1 in the continuity

Equation 3.1, the momentum Equation 3.2 and the energy Equation 3.3: the continuity equation is

$$\frac{\partial(Ur)}{\partial x} + \frac{\partial(Vr)}{\partial R} = 0 \quad \text{B.2}$$

the momentum equation is

$$U \frac{\partial U}{\partial x} + V \frac{\partial U}{\partial R} = \frac{1}{R} \frac{\partial}{\partial R} (Rn \frac{\partial U}{\partial R}) \quad \text{B.3}$$

and the energy equation is

$$U \frac{\partial T}{\partial x} + V \frac{\partial T}{\partial R} = \frac{1}{R} \frac{\partial}{\partial R} (Rn_H \frac{\partial T}{\partial R}) \quad \text{B.4}$$

### Finite Difference Equations for Dufort-Frankel Method

#### Continuity Equation:

Taylor's expansions about half a grid in r-direction and one grid in x-direction.

$$U_{(i+1, j+1)} = U_{(i, j+\frac{1}{2})} + \Delta x_+ U_x + \frac{\Delta R_+}{2} U_r + \frac{1}{2} \left[ (\Delta x_+)^2 U_{xx} + \Delta x_+ \Delta R_+ U_{xr} + \left( \frac{\Delta R_+}{2} \right)^2 U_{rr} \right] + O(\Delta^3) \quad \text{B.6}$$

$$U_{(i+1, j)} = U_{(i, j+\frac{1}{2})} - \Delta x_- U_x + \frac{\Delta R_+}{2} U_r + \frac{1}{2} \left[ (\Delta x_-)^2 U_{xx} - \Delta x_- \Delta R_+ U_{xr} + \left( \frac{\Delta R_+}{2} \right)^2 U_{rr} \right] + O(\Delta^3) \quad \text{B.7}$$

$$U_{(i-1, j)} = U_{(i, j+\frac{1}{2})} - \Delta x_- U_x - \frac{\Delta R_-}{2} U_r + \frac{1}{2} \left[ (\Delta x_-)^2 U_{xx} + \Delta x_- \Delta R_- U_{xr} + \left( \frac{\Delta R_-}{2} \right)^2 U_{rr} \right] + O(\Delta^3) \quad \text{B.8}$$

Subtracting B.6 from B.5:

$$U_{(i+1,j+1)} - U_{(i-1,j+1)} = (\Delta X_+ + \Delta X_-) U_x + O(\Delta^2) \quad \text{B.9}$$

Subtracting B.8 from B.7

$$U_{(i+1,j)} - U_{(i-1,j)} = (\Delta X_+ + \Delta X_-) U_x + O(\Delta^2) \quad \text{B.10}$$

Adding B.9 and B.10:

$$\left(\frac{\partial U}{\partial X}\right)_{i,j+\frac{1}{2}} = \frac{U_{(i+1,j+1)} + U_{(i+1,j)} - U_{(i-1,j+1)} - U_{(i-1,j)}}{2(\Delta X_+ + \Delta X_-)} + O(\Delta^2) \quad \text{B.11}$$

Now

$$V_{(i+1,j+1)} = V_{(i,j+\frac{1}{2})} + \Delta X_+ V_x + \frac{\Delta R_+}{2} V_r + \frac{1}{2} \left[ (\Delta X_+)^2 V_{xx} + \Delta X_+ \Delta R_+ V_{xr} + \left(\frac{\Delta R_+}{2}\right)^2 V_{rr} \right] + O(\Delta^3) \quad \text{B.12}$$

$$V_{(i+1,j)} = V_{(i,j+\frac{1}{2})} + \Delta X_+ V_x - \frac{\Delta R_-}{2} V_r + \frac{1}{2} \left[ (\Delta X_+)^2 V_{xx} - \Delta X_+ \Delta R_- V_{xr} + \left(\frac{\Delta R_-}{2}\right)^2 V_{rr} \right] + O(\Delta^3) \quad \text{B.13}$$

Subtracting B.13 from B.12:

$$\left(\frac{\partial V}{\partial R}\right)_{i,j+\frac{1}{2}} = \frac{V_{(i+1,j+1)} - V_{(i+1,j)}}{(\Delta R_+ + \Delta R_-)/2} + O(\Delta^2) \quad \text{B.14}$$

Using Equations B.11 and B.14 in Equation B.2:

$$\frac{R_{j+1} + R_j}{4(\Delta X_+ + \Delta X_-)} \left[ U_{i+1,j+1} + U_{i+1,j} - U_{i-1,j+1} - U_{i-1,j} \right] + \frac{R_{j+1} V_{i+1,j+1} - R_j V_{i+1,j}}{(\Delta R_+ + \Delta R_-)/2} = 0 \quad \text{B.15}$$

Momentum Equation:

Taylor's expansion of  $U$  about one grid in  $r$ -direction:

$$U_{(i,j+1)} = U_{(i,j)} + \Delta R_+ U_r + \left(\frac{\Delta R_+}{2}\right)^2 U_{rr} + O(\Delta^3) \quad \text{B.16}$$

$$U_{(i,j-1)} = U_{(i,j)} - \Delta R_- U_r + \left(\frac{\Delta R_-}{2}\right)^2 U_{rr} + O(\Delta^3) \quad \text{B.17}$$

Subtracting B.17 from B.16:

$$\left(\frac{\partial U}{\partial R}\right)_{i,j} = \frac{U_{(i,j+1)} - U_{(i,j-1)}}{(\Delta R_+ + \Delta R_-)} + O(\Delta^2) \quad \text{B.18}$$

Similarly expanding  $U$  about one grid in  $x$ -direction,

$$\left(\frac{\partial U}{\partial x}\right)_{i,j} = \frac{U_{(i+1,j)} - U_{(i-1,j)}}{\Delta X_+ + \Delta X_-} + O(\Delta^2) \quad \text{B.19}$$

Taylor's expansion of  $U$  about half a grid spacing in  $r$ -direction:

$$U_{(i+j+\frac{1}{2})} = U_{(i,j)} + \frac{\Delta R_+}{2} U_r + \frac{1}{2} \left(\frac{\Delta R_+}{2}\right)^2 U_{rr} + O(\Delta^3) \quad \text{B.20}$$

$$U_{(i,j-\frac{1}{2})} = U_{(i,j)} - \frac{\Delta R_-}{2} U_r + \frac{1}{2} \left(\frac{\Delta R_-}{2}\right)^2 U_{rr} + O(\Delta^3) \quad \text{B.21}$$

Subtracting Equation B.21 from Equation B.20:

$$\left(\frac{\partial U}{\partial R}\right)_{i,j} = \frac{2}{\Delta R_+ + \Delta R_-} (U_{i,j+\frac{1}{2}} - U_{i,j-\frac{1}{2}}) + O(\Delta^2) \quad \text{B.22}$$



Similarly it can be written as:

$$\begin{aligned}
 \frac{\partial}{\partial R} (RN \frac{\partial U}{\partial R})_{i,j} &= \frac{2}{\Delta R_+ + \Delta R_-} \left[ (RN \frac{\partial U}{\partial R})_{i,j+\frac{1}{2}} - (RN \frac{\partial U}{\partial R})_{i,j-\frac{1}{2}} \right] + O(\Delta^2) \\
 &= \frac{2}{\Delta R_+ + \Delta R_-} \left[ \frac{R_{j+1} + R_j}{2} \cdot \frac{N_{i,j+1} + N_{i,j}}{2} (\frac{\partial U}{\partial R})_{i,j+\frac{1}{2}} \right. \\
 &\quad \left. - \frac{R_j + R_{j-1}}{2} \cdot \frac{N_{i,j} + N_{i,j-1}}{2} (\frac{\partial U}{\partial R})_{i,j-\frac{1}{2}} \right] \quad \text{B.23}
 \end{aligned}$$

Now expanding U about half a grid in r-direction

$$U_{(i,j+1)} = U_{(i,j+\frac{1}{2})} + \frac{\Delta R_+}{2} U_r + \frac{1}{2} \left( \frac{\Delta R_+}{2} \right)^2 U_{rr} + O(\Delta^3) \quad \text{B.24}$$

$$U_{(i,j)} = U_{(i,j+\frac{1}{2})} - \frac{\Delta R_-}{2} U_r + \frac{1}{2} \left( \frac{\Delta R_-}{2} \right)^2 U_{rr} + O(\Delta^3) \quad \text{B.25}$$

Subtracting B.25 from B.24:

$$\left( \frac{\partial U}{\partial R} \right)_{i,j+\frac{1}{2}} = \frac{U_{(i,j+1)} - U_{(i,j)}}{\Delta R_+} + O(\Delta^2) \quad \text{B.26}$$

Similarly

$$\left( \frac{\partial U}{\partial R} \right)_{i,j-\frac{1}{2}} = \frac{U_{(i,j)} - U_{(i,j-1)}}{\Delta R_-} + O(\Delta^2) \quad \text{B.27}$$

Writing the following expansions for U:

$$U_{(i+1,j)} = U_{(i,j)} + \Delta X_+ U_x + \frac{\Delta X_+^2}{2} U_{xx} + O(\Delta^3) \quad \text{B.28}$$

$$U_{(i-1,j)} = U_{(i,j)} - \Delta X_- U_x + \frac{\Delta X_-^2}{2} U_{xx} + O(\Delta^3) \quad \text{B.29}$$

Adding B.28 and B.29:

$$U_{(i,j)} = 0.5 \left[ U_{(i+1,j)} + U_{(i-1,j)} \right] + O(\Delta^2) \quad \text{B.30}$$

Equation B.26 and Equation B.27 can be written as:

$$\left( \frac{\partial U}{\partial R} \right)_{i,j+\frac{1}{2}} = \frac{U_{(i,j+1)} - 0.5 \left[ U_{(i+1,j)} + U_{(i-1,j)} \right]}{\Delta R_+} + O(\Delta^2) \quad \text{B.31}$$

$$\left( \frac{\partial U}{\partial R} \right)_{i,j-\frac{1}{2}} = \frac{0.5 \left[ U_{(i+1,j)} + U_{(i-1,j)} \right] - U_{(i,j-1)}}{\Delta R_-} + O(\Delta^2) \quad \text{B.32}$$

Using Equations B.31 and B.32 in Equation B.23:

$$\begin{aligned} \frac{\partial}{\partial R} \left( R N \frac{\partial U}{\partial R} \right)_{i,j} &= \frac{2}{4R_+ + 4R_-} \left[ \frac{R_{j+1} + R_j}{2} \cdot \frac{N_{i,j+1} + N_{i,j}}{2} \cdot \right. \\ &\quad \left. \frac{U_{i,j+1} - 0.5(U_{i+1,j} + U_{i-1,j})}{\Delta R_+} \right. \\ &\quad \left. - \frac{R_j + R_{j-1}}{2} \cdot \frac{N_{i,j} + N_{i,j-1}}{2} \cdot \frac{0.5(U_{i+1,j} + U_{i-1,j}) - U_{i,j-1}}{\Delta R_-} + O(\Delta^2) \right] \end{aligned} \quad \text{B.33}$$

Using Equations B.18, B.19 and B.33 in Equation B.3, finite-difference equation for the momentum equation is:

$$\begin{aligned} U_{i,j} \left( \frac{U_{i+1,j} - U_{i-1,j}}{\Delta X_+ + \Delta X_-} \right) + V_{i,j} \left( \frac{U_{i,j+1} - U_{i,j-1}}{\Delta R_+ + \Delta R_-} \right) \\ = \frac{1}{R_j} \cdot \frac{2}{4R_+ + 4R_-} \left[ \frac{R_{j+1} + R_j}{2} \left\{ \frac{N_{i,j+1} + N_{i,j}}{24R_+} \right. \right. \end{aligned}$$

$$\left. \frac{U_{i,j+1} - 0.5(U_{i+1,j} + U_{i-1,j})}{\Delta x_+ + \Delta x_-} \right\} - \frac{R_j + R_{j-1}}{2} \left\{ \frac{N_{i,j} + N_{i,j-1}}{24R_-} \right.$$

$$\left. \frac{0.5(U_{i+1,j} + U_{i-1,j}) - U_{i,j-1}}{\Delta x_+ + \Delta x_-} \right\} + O(\Delta^2) \quad \text{B.34}$$

Energy Equation:

By similar treatment energy equation can be written as:

$$U_{i,j} \left( \frac{T_{i+1,j} - T_{i-1,j}}{\Delta x_+ + \Delta x_-} \right) + V_{i,j} \left( \frac{T_{i,j+1} - T_{i,j-1}}{\Delta R_+ + \Delta R_-} \right)$$

$$= \frac{1}{R_j} \cdot \frac{2}{\Delta R_+ + \Delta R_-} \left[ \frac{R_{j+1} + R_j}{2} \frac{N_{Hi,j+1} + N_{Hi,j}}{2\Delta R_+} \left\{ T_{i,j+1} - 0.5(T_{i+1,j} + T_{i-1,j}) \right\} \right.$$

$$\left. - \frac{R_j + R_{j-1}}{2} \frac{N_{Hi,j} + N_{Hi,j-1}}{24R_-} \left\{ 0.5(T_{i+1,j} + T_{i-1,j}) - T_{i,j-1} \right\} \right] + O(\Delta^2) \quad \text{B.35}$$

The center line derivative boundary condition was implemented using a Taylor series expansion for the velocity and temperature about the center line and using a second order approximation to the zero derivative at the center line. This permitted the calculation of the center line values of velocity and temperature according to:

$$U_{i+1,1} = \frac{4U_{i+1,2} - U_{i+1,3}}{3}, \quad T_{i+1,1} = \frac{4T_{i+1,2} - T_{i+1,3}}{3} \quad \text{B.36}$$

### Direct Explicit Scheme

The finite-difference equations for this scheme were used to start the Dufort-Frankel method. The equations can be derived by standard method [34].

The continuity equation is:

$$\frac{R_{j+1}}{4\Delta X} (U_{i+1,j} - U_{i,j} + U_{i+1,j+1} - U_{i,j+1}) + \frac{1}{\Delta R} (R_{j+1} V_{i+1,j+1} - R_j V_{i+1,j}) = 0$$

B.37

The Momentum equation is:

$$\begin{aligned} & U_{i,j} \left( \frac{U_{i+1,j} - U_{i,j}}{\Delta X} \right) + V_{i,j} \left( \frac{U_{i,j} - U_{i,j-1}}{\Delta R_+} \right) \\ &= \frac{1}{R_j} \frac{2}{\Delta R_+ + \Delta R_-} \left[ \frac{R_{j+1} + R_j}{2} \cdot \frac{N_{i,j+1} + N_{i,j}}{2} \cdot \frac{U_{i,j+1} - U_{i,j}}{\Delta R_+} \right. \\ & \quad \left. - \frac{R_j + R_{j-1}}{2} \cdot \frac{N_{i,j} + N_{i,j-1}}{2} \cdot \frac{U_{i,j} - U_{i,j-1}}{\Delta R_-} \right] \end{aligned}$$

B.38

The Energy equation is:

$$\begin{aligned} & U_{i,j} \left( \frac{T_{i+1,j} - T_{i,j}}{\Delta X} \right) + V_{i,j} \left( \frac{T_{i,j} - T_{i,j-1}}{\Delta R_-} \right) \\ &= \frac{1}{R_j} \frac{2}{\Delta R_+ + \Delta R_-} \left[ \frac{R_{j+1} + R_j}{2} \cdot \frac{N_{Hi,j+1} + N_{Hi,j}}{2} \cdot \frac{T_{i,j+1} - T_{i,j}}{\Delta R_+} \right. \\ & \quad \left. - \frac{R_j + R_{j-1}}{2} \cdot \frac{N_{Hi,j} + N_{Hi,j-1}}{2} \cdot \frac{T_{i,j} - T_{i,j-1}}{\Delta R_-} \right] \end{aligned}$$

B.39

## APPENDIX-C

STABILITY ANALYSIS OF THE MOMENTUM EQUATION

The finite difference analogue of the partial differential equation must satisfy certain conditions:

- 1) the solution being obtained should correspond the partial differential equations, at least when grid spacings is refined in a particular manner.
- 2) due to the use of particular method of solution, round of errors or errors from any source are not amplified or allowed to grow in subsequent steps in the solution.

The first point is called the consistency condition which can be studied by expanding the dependent variables in Taylor series expansions. From this expanded series, the difference between the partial differential equations and the finite difference representation can be observed [9]. This difference is known as truncation or discretization error of the equations. If this error vanishes in the limit as the grid-spacing is reduced, the finite difference representation is said to be consistent.

The second point is called the stability condition. Here Von Neuman [34] method of stability analysis is used to get an insight into how a solution of finite difference equation behaves when round off errors effect the calculations.

Unfortunately, this method can only be used to establish

necessary and sufficient conditions for stability of linear initial value problems with constant coefficients. Due to the non-linearity of momentum equation Von Neumann method is applied here locally for satisfying the conditions of the applicability of this method even though they do not satisfy over the whole solution region.

Let the error growth in  $U$  be  $\delta_i$ , and according to Neumann [34] it was expressed as:

$$\delta_i = A e^{\beta_1 R} e^{i\beta_2 x} \quad \text{C.1}$$

With the error, the velocities change to:

$$\left. \begin{aligned} U_{i,j+1} &\sim U_{i,j+1} + \delta_{i,j+1} \\ U_{i,j-1} &\sim U_{i,j+1} + \delta_{i,j-1} \\ U_{i+1,j} &\sim U_{i+1,j} + \delta_{i+1,j} \end{aligned} \right\} \quad \text{C.2}$$

and

$$\begin{aligned} \delta_{i,j+1} &= A e^{\beta_1 (R+\Delta R)} e^{i\beta_2 x} \\ \delta_{i,j-1} &= A e^{\beta_1 (R-\Delta R)} e^{i\beta_2 x} \\ \delta_{i+1,j} &= A e^{\beta_1 R} e^{i\beta_2 (x+\Delta x)} \end{aligned} \quad \text{C.3}$$

Substituting Equations C.2 in Equation B.34 and using using  $\Delta R_+ = \Delta R_- = \Delta R$  :

$$\begin{aligned}
& U_{i,j} \frac{\delta_{i+1,j} - \delta_{i-1,j}}{\Delta X_+ + \Delta X_-} + V_{i,j} \frac{\delta_{i,j+1} - \delta_{i,j-1}}{2\Delta R} \\
&= \frac{1}{2(\Delta R)^2} \left[ \left(1 + \frac{\Delta R}{2R_j}\right) (N_{i,j+1} + N_{i,j}) \left\{ \delta_{i,j+1} - 0.5(\delta_{i+1,j} + \delta_{i-1,j}) \right\} \right. \\
&\quad \left. - \left(1 - \frac{\Delta R}{2R_j}\right) (N_{i,j} + N_{i,j-1}) \left\{ 0.5(\delta_{i+1,j} + \delta_{i-1,j}) - \delta_{i,j-1} \right\} \right] \quad \text{C.4}
\end{aligned}$$

Substituting Equations C.3 in Equation C.4 and using

$$f = e^{\beta_1 \Delta R}:$$

$$f^2 + A_0 f + B_0 = 0 \quad \text{C.5}$$

$$\begin{aligned}
\text{Where } A_0 &= \frac{-U_{i,j}/(\Delta X_+ + \Delta X_-)}{\frac{V_{i,j}}{2\Delta R} - \frac{1}{2(\Delta R)^2} \left(1 + \frac{\Delta R}{2R_j}\right) (N_{i,j+1} + N_{i,j})} \\
B_0 &= \frac{\frac{V_{i,j}}{2\Delta R} + \frac{1}{2(\Delta R)^2} \left(1 - \frac{\Delta R}{R_j}\right) (N_{i,j} + N_{i,j-1})}{\frac{V_{i,j}}{2\Delta R} - \frac{1}{2(\Delta R)^2} \left(1 + \frac{\Delta R}{2R_j}\right) (N_{i,j} + N_{i,j+1})}
\end{aligned}$$

The roots of Equation C.5 are:

$$f = -\frac{A_0}{2} \pm \sqrt{\left(\frac{A_0}{2}\right)^2 - B_0} \quad \text{C.6}$$

According to Neumann stability condition;  $|f| \leq 1$

For real roots, inequality  $|\xi| \leq 1$  are:

$$-\frac{A_0}{2} + \sqrt{\left(\frac{A_0}{2}\right)^2 - B_0} \leq 1 \quad \text{C.7}$$

$$-\frac{A_0}{2} - \sqrt{\left(\frac{A_0}{2}\right)^2 - B_0} \geq -1 \quad \text{C.8}$$

Rearranging Equation C.8

$$(A_0 - B_0) \leq 1 \quad \text{C.9}$$

Using expressions for  $A_0$  and  $B_0$  in Equation C.9 and rearranging:

$$\frac{-U_{i,j}}{\Delta X_+ + \Delta X_-} \leq \left[ \frac{V_{i,j}}{\Delta R} + \frac{1}{2\Delta R} \left( \frac{N_{i,j-1} + N_{i,j+1}}{\Delta R} \right) \left( 1 - \frac{\Delta R}{2R_j} \right) \right] \quad \text{C.10}$$

Since  $U_{i,j}/(\Delta X_+ + \Delta X_-)$  is always positive,

$$\frac{U_{i,j}}{\Delta X_+ + \Delta X_-} \geq \left| \frac{V_{i,j}}{\Delta R} + \frac{1}{2\Delta R} \left( \frac{N_{i,j-1} + N_{i,j+1}}{\Delta R} \right) \left( 1 - \frac{\Delta R}{2R_j} \right) \right|$$

or,

$$\Delta X_+ + \Delta X_- \leq \frac{U_{i,j} \Delta R}{\left| \frac{V_{i,j}}{\Delta R} + \frac{N_{i,j-1} + N_{i,j+1}}{2\Delta R} \left( 1 - \frac{\Delta R}{2R_j} \right) \right|} \quad \text{C.11}$$

The stability constraint given by Equation C.11 determines the grid spacings in x-direction with uniform grid spacings in r-direction. As the radial velocity on the outside is negative, the condition C.11 satisfies automatically but it is not satisfied in the inner side where instability did not show at all.



## APPENDIX-D

## COMPUTER PROGRAM

```

C*****
C THE GOVERNING EQUATIONS - CONTINUITY, MOMENTUM AND ENERGY FOR *
C AXISYMMETRIC TURBULENT JET ARE WRITTEN IN FINITE DIFFERENCE *
C FORM. THIS PROGRAM HAS BEEN DEVELOPED TO SOLVE THOSE EQUATIONS. *
C*****
0001      DIMENSION U(7,300),V(1,300),W(1,300),TH(1,300),FVEL(1,300),
*          *R(1,300),P(1,300),PT(300),T(3,300),ITEM(1,300)
0002      U=0.0
0003      V=0.0
0004      W=0.0
0005      R=0.0
0006      P=0.0
0007      DELT=0.0010
0008      DELR=0.0010
0009      NJ1=300
0010      NJ2=NJ1-1
0011      M1=5
0012      M2=3
0013      M3=101
0014      DO 10 I=1,3
0015      DO 10 J=1,NJ1
0016          U(I,J)=UE
0017      10  T(I,J)=TE
0018          DO 20 J=1,M1
0019          U(1,J)=1.0
0020      20  T(1,J)=1.0
C
C DIRECT EXPLICIT SCHEME FOR 2ND STATION
0021      DO 30 J=2,NJ1
0022          IF(J.NE.4) GO TO 40
0023          U(2,1)=(4.0*U(2,2)-U(2,3))/3.0
0024          T(2,1)=(4.0*T(2,2)-T(2,3))/3.0
0025      40  DX1=DELTX/(2.0*DELR*U(1,J))
0026          DX2=DX1/(FLOAT(J-1)*DELR)
0027          DX3=FLOAT(2*J-1)*(U(1,J+1)-U(1,J))
0028          DX31=FLOAT(2*J-1)*1.42857*(T(1,J+1)-T(1,J))
0029          DX4=FLOAT(2*J-3)*(U(1,J)-U(1,J-1))
0030          DX41=FLOAT(2*J-3)*1.42857*(T(1,J)-T(1,J-1))
0031          DX5=DX2-(DX3-DX4)
0032          DX51=DX2*(DX31-DX41)
0033          U(2,J)=U(1,J)+DX5
0034          IF(U(2,J).LT.0.125001E-04) U(2,J)=0.125001E-04
0035          T(2,J)=T(1,J)+DX51
0036      30  CONTINUE
0037          V(1,1)=0.0
0038          P(1,1)=0.0
0039          FVEL=FLOAT(V(1,1))/FLOAT(2*J-1)
0040          W(1,1)=V(1,1)
0041          DELT=DELR*FLOAT(J-1)
0042          DELT1=DELR*FLOAT(J-1)
0043          W(1,1)=W(1,1)+DELTA*FVEL
0044          IF(W(1,1).GT.0.141421E-04) GO TO 50
0045      50  IF(J.GE.10).LT.10 GO TO 60
0046          GO TO 70
0047      60  V(1,J)=V(1,J-1)+DELTA*FVEL
0048          GO TO 50

```

```

0051      75 V(1,141)=-0.1E+00
0052      50 CONTINUE
C
C      DUFORT FRAMEWORK SUBRAME FOR MAIN PROGRAM
0053      K=2
0054      SL1=70.0
0055      DELT=RELT
0056      DO 70 J=80,143
0057      AXILD=FLOAT(I-1)*D.
0058      IF (AXILD.LT.1.5) GO TO 1
0059      IF (AXILD.LT.2.5) GO TO 2
0060      IF (AXILD.LT.3.5) GO TO 3
0061      IF (AXILD.LT.4.5) GO TO 4
0062      IF (AXILD.LT.5.5) GO TO 5
0063      IF (AXILD.LT.6.5) GO TO 6
0064      IF (AXILD.LT.7.5) GO TO 7
0065      IF (AXILD.LT.8.5) GO TO 8
0066      IF (AXILD.LT.9.5) GO TO 9
0067      IF (AXILD.LT.10.5) GO TO 10
0067      IF (AXILD.LT.11.5) GO TO 11
0067      IF (AXILD.LT.12.5) GO TO 11

```

```

DOC FORTRAN IV 360N-F0-479 3-8      MAIN/CH      DATE 15/12/84      TIME
0068      1  NK=80
0069      GO TO 12
0070      2  NK=100
0071      GO TO 13
0072      3  NK=120
0073      GO TO 13
0074      4  NK=150
0075      GO TO 13
0076      5  NK=170
0077      GO TO 13
0078      6  NK=190
0079      GO TO 13
0080      7  NK=210
0081      GO TO 13
0082      8  NK=230
0083      GO TO 13
0084      9  NK=260
0085      GO TO 13
0086      11 NK=290
0087      12 RL=FLOAT(NK)/5.0
0088      NBL=IFIX(RL)+1
0089      NN=NK+1
0090      DO 80 J=2,NN
0091      IF (J.NE.4) GO TO 90
0092      U(3,1)=(4.0*U(3,2)-U(3,3))/3.0
0093      T(3,1)=(4.0*T(3,2)-T(3,3))/3.0
0094      90  A1=(DELR-FLOAT(J-1))*12.0+RELA
0095      A2=A1*U(2,J)*U(1,J)
0096      A2T=A1*U(2,J)*T(1,J)
0097      A11=(FLOAT(J-1)+V(1,141))/2.0
0098      A22=A11*(U(2,J-1)-U(2,J+1))
0099      A22T=A11*(T(2,J-1)-T(2,J+1))
0100      B1=1.0/(4.0*DELR)
0101      B11=FLOAT(2+J-1)
0102      B22=FLOAT(2+J-3)
0103      U11=U(2,J+1)-0.5*U(1,J)
0104      T11=T(2,J+1)-0.5*T(1,J)

```

```

0105      U22=0.5*H(1,J)-H(2,J-1)
0106      T22=0.5*T(1,J)-T(2,J-1)
0107      IF(U(3,3).LT.0.999E 00) GO TO 105
0108      C=0.92917 06*(SL11+SL11)
0109      UD1=ABS(H(2,J+1)-H(2,J+1))
0110      UD2=ABS(H(2,J+1)-H(2,J))
0111      UD3=ABS(H(2,J)-H(2,J-1))
0112      C1=2.0/C*(UD1+UD2)
0113      C2=2.0/C*(UD2+UD3)
0114      C11=C1/0.7
0115      C21=C2/0.7
0116      GO TO 115
0117      105 RHINT=(FLOAT(J-1)*DR)/ZRH
0118      IF(RHINT.GT.0.9E 00) GO TO 14
0119      ENTC=1.0
0120      GO TO 17
0121      16 RE11=RHINT-0.0
0122      RE12=SQRT(RE11)
0123      RE16=RE11+RE11*RE12
0124      ENTC=0.5+*RE16
0125      17 C1=2.0+ENTC*V154
0126      C2=1.04+ENTC*V102
0127      C11=C1/0.7
0128      C21=C2/0.7
0129      115 X1=B11+C1*U11
0130      X11=B11+C11*U11
0131      X2=B22+C2*U22
0132      X21=B22+C21*U22
0133      X=A2+A22*B1+(X1-X2)
0134      XT=A21+A22*B11+(X11-X21)
0135      D1=D1+U(2,J)
0136      D2=B1/2.0
0137      Y=D1+D2*(B11+C1+B22+C2)
0138      YT=D1+D2*(B11+C11+B22+C21)
0139      U(3,J)=X/Y
0140      IF(U(3,J).LT.0.25001E-01) U(3,J)=0.25001E-01
0141      T(3,J)=XT/YT
0142      IF(J.LT.4) GO TO 135
0143      UH(1,J)=(U(3,J)-UE)/(U(3,1)-UE)
0144      IF(UH(1,J).LT.0.5E 00) GO TO 125
0145      RX=FLOAT(J-1)
DDS FORTRAN IV 3800-FO-479 3-8      MAINPOM      DATE 15/12/84      TIME
0146      125 TH(1,J)=(T(3,J)-TE)/(T(3,1)-TE)
0147      IF(TH(1,J).LT.0.5E 00) GO TO 125
0148      RY=FLOAT(J-1)
0149      135 IF(U(7,3).LT.0.999E 00) GO TO 110
0150      IF(U(3,3).LT.0.99E 00) GO TO 110
0151      FL1=FLOAT(J-1)
0152      11 IF(U(3,J).LT.0.1501E-01) GO TO 80
0153      FL2=FLOAT(J-1)
0154      80 CONTINUE
0155      RHE=RE
0156      RHI=RI+R1
0157      OUT1=SL1+D1
0158      L=IF(ABS(FL2)+1

```

```

0159      N=1+IX(KX)+4
0160      NT=1+IX(KY)+4
0161      US1=(HCA,N)-U(3,N-1)/DE
0162      US2=(US1+0.5)/U(3,1)
0163      SH1=0.17052
0164      SP=0.5*SH1
0165      TS1=(HCA,N)-1+0.5*(N-1)/DI
0166      TS2=(TS1+0.5)/U(3,1)
0167      SH2=0.17052
0168      FX=0.17052
0169      IF(U(3,1).GT.0.0)GOTO 170
0170      EN1=SL1*DM
0171      SL12=(SL1+SL2)/N1LR
0172      SL11=0.5*(SL1+SL2)
0173      VIS1=0.0
0174      VIS2=0.0
0175      CO=10.145
0176      120 VIS1=0.0
0177      VIS2=0.0
0178      DO 155 JJ=2,L
0179      V1S1=(ABS(U(3,JJ+1))+ABS(U(3,JJ)))*FLOAT(JJ)*DELR*DELR
0180      V2S1=(ABS(U(3,JJ))+ABS(U(3,JJ-1)))*FLOAT(JJ-1)*DELR*DELR
0181      V1S2=0.576E-06*V1S1
0182      V2S2=0.576E-06*V2S1
0183      IF(JJ.NE.2.OR.JJ.NE.L) GO TO 165
0184      V1S2=V1S2/2.0
0185      V2S2=V2S2/2.0
0186      165 VIS1=VIS1+V1S2
0187      VIS2=VIS2+V2S2
0188      155 CONTINUE
0189      SLT1=SL2+DELR
0190      ENTR=0.0
0191      145 V(1,1)=0.0
0192      DO 130 J1=1,NK
0193      F1=FLOAT(J1-1)/FLOAT(J1)
0194      F2=F1*V(1,J1)
0195      F11=FLOAT(2*J1-1)/FLOAT(J1)
0196      F22=F11/(8.0*DELR)
0197      F=U(3,J1+1)+U(3,J1)-U(2,J1+1)-U(2,J1)
0198      V(1,J1+1)=F2-F22+F
0199      IF(ABS(V(1,J1+1)).LT.0.1E-10) GO TO 140
0200      GO TO 130
0201      140 IF(V(1,J1+1).GT.0.0) GO TO 85
0202      GO TO 85
0203      85 V(1,J1+1)=0.1E-10
0204      GO TO 130
0205      95 V(1,J1+1)=0.1E-10
0206      GO TO 130
0207      170 CONTINUE
0208      SLT1=SLT1+DELR
0209      IF(SLT1.GT.1.0) GO TO 171
0210      WRITE(3,170) J1,ENTR,EN1,SLT1,DM,DNT,SP,OPT
0211      171 FORMAT(1,12) SLT1='F10.12',DM='F8.12',DNT='F8.12',SP='F8.12',ENTR='F8.12',
0212      *DM='F8.12',EN1='F8.12',OPT='F8.12',ENTR='F8.12',DM='F8.12',SP='F8.12',
0213      *ENTR='F8.12'
0214      WRITE(3,170) KK,KL,MM,KL,KK,KK,KK,KK,KL,KL
0215      170 FORMAT(1/5X,'U(1,14)',10X,'V(1,14)',10X,'T(1,14)',10X,

```

```

*ETA1('I4.0')'.4X.'ET1T('I4.0')'.2X.'ETA2('I4.0')'.4X.
*ETA3('I4.0')'.4X.'ET3T('I4.0')'.4X.'VEL('I4.0')'.4X.
*PIEM('I4.0')
0213      DO 180 J2=1,NM1
0214      K1=1+(J2-1)*5
0215      PV1(1,K1)=(U(3,K1)-UE)/(U(3,1)-UE)
0216      PIEM(1,K1)=(T(3,K1)-TE)/(T(3,1)-TE)
0217      K=1 DAT(K1-1)=IP
0218      ETA1=(R-RH)/AXILD
DOS FORTRAN IV 3600-FO-479 3-9          MAINPCH          DATE 15/12/84          TIME
0219      ETA2=R/INH
0220      ETA3=(R-RH)/SE

0221      ET1T=(R-RHT)/AXILD
0222      ET3T=(R-RHT)/SBT
0223      WRITE(3,190) U(3,J2),V(1,J2),T(3,J2),ETA1,ET1T,ETA2,ET2T,ET3T,
*VEL(1,J2),PIEM(1,J2)
0224      190  FORMAT(2X,3(E14.8,3X),7(E9.3,2X))
0225      180  CONTINUE
0226      K=K+1
0227      150  DO 200 J3=1,NM2
0228      P(1,J3)=U(2,J3)
0229      Q(1,J3)=U(3,J3)
0230      U(1,J3)=P(1,J3)
0231      U(2,J3)=Q(1,J3)
0232      P(1,J3)=T(2,J3)
0233      Q(1,J3)=T(3,J3)
0234      T(1,J3)=P(1,J3)
0235      200  T(2,J3)=Q(1,J3)
0236      NM=NM+1
0237      DO 300 J4=NM,NM1
0238      U(1,J4)=UE
0239      U(2,J4)=UE
0240      T(1,J4)=TE
0241      300  T(2,J4)=TE
0242      IF(U(3,1).LT.0.4E 00) GO TO 210
0243      70  CONTINUE
0244      210  STOP
0245      END
DOS FORTRAN IV 3600-FO-479 3-9          MAINPCH          DATE 15/12/84          TIME

```

